High Throughput Modules for Performance and Mechanism Assessment of Flame Retardants in Polymeric Materials

Vorgelegt von

Dipl.-Chem.

Sebastian Rabe

geb. in Berlin

Von der Fakultät II – Mathematik und Naturwissenschaften

der Technischen Universität Berlin

zur Erlangung des akademischen Grades

Doktor der Naturwissenschaften

- Dr. rer. nat. -

genehmigte Dissertation

Promotionsausschuss:

Vorsitzende: Prof. Dr. rer. nat. Karola Rück-Braun, TU Berlin

Gutachter: Priv.-Doz. Dr. rer. nat. habil. Bernhard Schartel, FU Berlin

Gutachter: Prof. Dr. rer. nat. Reinhard Schomäcker, TU Berlin

Tag der wissenschaftlichen Aussprache: 12.10.2017

Berlin 2017

Danksagung

Mein Dank gilt in erster Linie Herrn PD Dr. Bernhard Schartel und Herrn Prof. Dr. Reinhard Schomäcker für die Betreuung und Begutachtung der vorliegenden Arbeit. Insbesondere Herrn Schartel als meinem Vorgesetzten während meiner Zeit an der BAM danke ich für die hilfreichen und konstruktiven Diskussionen und Kritiken, die immer zielführend und ergebnisorientiert waren.

Ich danke meinen ehemaligen und derzeitigen Kollegen der Flammschutzgruppe des Fachbereichs 7.5 an der BAM: Dr. Kirsten Langfeld, Dr. Antje Wilke, Dr. Marie-Claire Despinasse, Dr. Karoline Täuber, Dr. Bettina Dittrich, Dr. Patrick Müller, Dr. Huajie Yin, Dr. Nora Konnertz, Dr. Daniele Frasca, Andreas Hörold, Michael Morys, Sebastian Timme, Tim Rappsilber, Lars-Henrik Dauß, Patrick Klack, Alexander Battig, Melissa Matzen, Benjamin Zirnstein, Weronika Tabaka, Martin Günther, Yuttapong Chuenban, Analice Turski-Silva Diniz und alle, die ich hier vergessen habe oder mit denen ich nur für eine kurze Zeit zusammengearbeitet habe. Sie haben mir gezeigt, dass Kollegen auch zu Freunden werden können.

Danke auch an die Werkstatt der 7.5, insbesondere Michael Schneider und Tobias Kukofka, die mir bei allen handwerklichen Arbeiten tatkräftig beiseite standen und meine Vorstellungen immer zu meiner Zufriedenheit erfüllt haben.

Ein besonderer Dank gilt meiner Familie, Stefanie und allen, die mich mental unterstützt und immer an mich geglaubt haben.

Dr. Aleksandra Sut danke ich für die emotionale Unterstützung und die endlose Geduld bei all meinen Vorhaben.

Index of abbreviations

AlPi	Aluminium diethyl phosphinate
APP	Ammonium polyphosphate
BDP	Bisphenol A bis(diphenyl phosphate)
EHC	Effective heat of combustion
EP	Epoxy resin
FAA	Federal Aviation Administration
FIGRA	Fire growth rate index
FPI	Fire performance index
FTIR	Fourier-transform infrared
HRR	Heat release rate
LOI	Limiting oxygen index
MARHE	Maximum average rate of heat emission
MCC	Microscale combustion calorimeter
MDH	Magnesium hydroxide
NIST	National Institute of Standards and Technology
PA	Polyamide
PCABS	Polycarbonate Acrylonitrile-butadiene-nitrile
PCFC	Pyrolysis combustion flow calorimeter
PEEK	Poly ether ether ketone
PER	Pentaerythritol
PHRR	Peak heat release rate
PMMA	Polymethyl methacrylate
PP	Polypropylene
PS	Polystyrene
PTFE	Polytetrafluoroethylene
RP	Red phosphorus

TGA	Thermogravimetric analysis
THE	Total heat evolved
THR	Total heat released
TPES	Styrene-based thermoplastic elastomer
UL	Underwriters Laboratories

Table of Contents

1 Background and Motivation

1.1 Flame retardancy of polymeric materials

Nowadays polymeric materials are an indispensable part of our daily lives. Their relatively low cost and high processability are reason for their ever-growing use. Unfortunately, a lot of polymers are highly flammable and have increased fire risk. Especially items of first ignition, like electronic casings or upholstery, need to be made resistant to flame and high temperatures. In the past, flame retardancy was achieved by addition of halogenated flame retardants. Those mostly brominated additives, however, were found to be hazardous to health and environment, thus increasing the demand for non-halogenated flame retardants [1, 2].

Phosphorus containing compounds were found to be promising alternatives to halogenated flame retardants. Phosphinates, phosphonates, and phosphates among others are used to achieve excellent flame retardancy performance in several polymeric materials and are easily mixed with the polymer matrix [3, 4, 5, 6]. However, they may alter the mechanical and other properties when the concentration is too high. A balance must be made between maximum flame retardant load, to achieve the desired flame retardancy performance, and the minimum concentration, at which the other important properties of the polymeric material are not altered significantly. An auspicious approach towards reducing the amount of additive is the use of multicomponent systems, in which the interactions between the additive components show synergistic effects and the total additive load can be lowered [7, 8, 9].

Flame retardants can work via different modes of action. They can work in the gas phase as well as in the condensed phase of a burning material via chemical and physical mechanisms, respectively. However, the processes occurring during the burning of a polymeric material need to be known first. They are displayed in Figure 1.

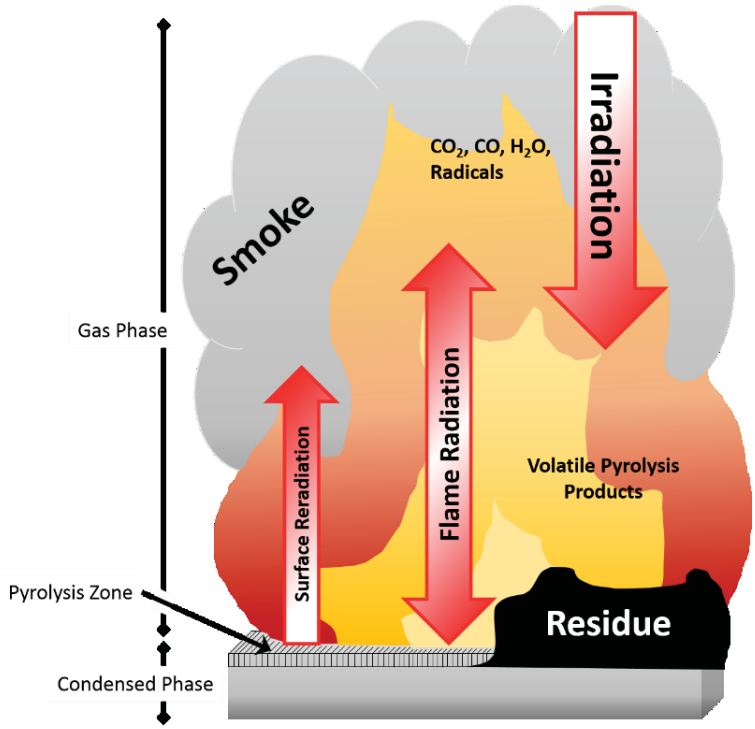

Figure 1. Schematic of processes occurring during burning of a polymeric material

After ignition of the material, the surface is pyrolyzed under predominantly anaerobic conditions. Volatile pyrolysis products are released into the gas phase and the combustible gases are oxidized, creating the flame. This leads to increased heating of the polymer surface, stronger pyrolysis and increased release of combustible gases. When all material is consumed, the flame extinguishes. This cycle can be overcome by influencing certain key features. Fuel release can be hindered by increasing the amount of produced char, radical scavengers can interfere with oxidation reactions in the gas phase and cooling effects like endothermic reactions, and flame dilution due to water release or the buildup of an intumescent heat barrier can reduce heat transfer to the pyrolysis zone. The rate at which heat is released during steady burning is defined as the product of the combustion efficiency χ, the ratio of effective heat of combustion of the fuel gases h_c^0 and the required heat for gasification h_g, the mass fraction of released fuel $(1-\mu)$ and the received effective heat flux $\dot{q}''_{net}$ according to equation (I) [10]. The effective heat flux is the sum of reradiated heat flux $\dot{q}''_{rerad}$, heat flux from an external source $\dot{q}''_{ext}$, heat flux from the flame $\dot{q}''_{flame}$, and loss of heat via conduction $\dot{q}''_{loss}$.

$$HRR = \chi(1-\mu)\frac{h_c^0}{h_g}\dot{q}''_{net} = \chi(1-\mu)\frac{h_c^0}{h_g}\left(\dot{q}''_{ext} + \dot{q}''_{flame} - \dot{q}''_{rerad} - \dot{q}''_{loss}\right) \quad \text{(I)}$$

The mode of action of a flame retardant is dependant of several factors. Besides the chemical structure of the flame retardant itself, its interaction during pyrolysis with the chemical environment plays a great role on the mechanisms by which a flame retardant is working [11, 12]. The addition of synergists and other adjuvants can influence the way a flame retardant works and can be used to optimize its efficiency by changing emphasis to a desired mode of action [8, 13].

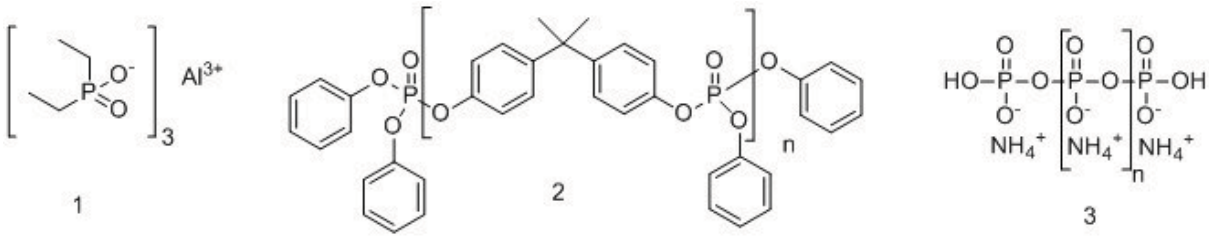

Figure 2. Chemical structures of aluminium diethyl phosphinate (1), bisphenol A-bis(diphenyl phosphate) (2) and ammonium polyphosphate (3).

Common phosphorus based flame retardants are displayed in Figure 2. Aluminium diethyl phosphinate (AlPi, 1) is an aluminium salt of the diethylphosphinic acid, which shows excellent flame retarding properties especially in the gaseous phase by reacting with OH and H radicals and thus slowing down oxidation reactions, leading to incomplete combustion and reduction of the combustion efficiency. A flame retardant which looks like an optimal precursor for a charring flame retardancy effect is bisphenol A- bis(diphenyl phosphate) (BDP, 2). It acts as an acid precursor, and undergoes esterification and dehydration in the condensed phase. Nonetheless, phosphate esters are also able to act in the gas phase via flame inhibition if their volatility is high enough and they are released during burning. Ammonium polyphosphate (APP, 3) is a great example of a flame retardant with predominant action in the condensed phase due to the formation of an intumescent protective layer. The pyrolyzing and melting material is esterified by produced acid, and released gases act as a blowing agent to form a foam-like structure, which hinders fuel and heat transport [14, 15, 16]. Past and present research still

focuses on the development of novel phosphorus-based flame retardants such as hyperbranched polyphosphates [17, 18].

Flame retardants are supposed to reduce the fire risk and the fire hazard of the items which are the first items of ignition and the origin of a fully developed room fire. That means if ignition of such items, for example a TV housing, cannot be prevented in the first place, the goal is to restrain fire growth in the early phase. Figure 3 shows the typical steps in the formation of a room fire. After the ignition of an item in the room, the fire initially grows slowly and hot pyrolysis gases accumulate underneath the ceiling. The increasing temperature leads to stronger irradiation on all objects in the room and eventually to ignition of all flammable material, the so-called flashover. This indicates the transition from a developing fire to a fully developed fire. When all fuel is consumed, the fire will decay slowly.

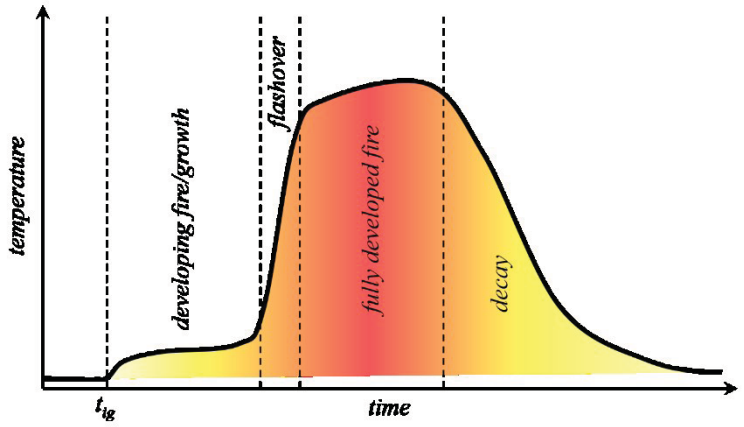

Figure 3. Temperature profile of a room fire.

The single steps of the fire formation can be divided by different length scales involved and by properties of the material. Ignition takes place in the range of centimeters and flammability (reaction to an ignition source) as well as the ability to self-extinguish are important for a material. The developing fire is defined by a length scale of decimeters to meters. Resulting irradiance ranges from 20 to 60 kW/m² and heat release rate as well as flame spread are crucial to describe the further fire behavior of a material. When the fire is considered fully developed, the focus is on the fire resistance of an item in the length scale of several meters [19]. Different test methods simulating the described conditions exist for all of these steps in the development

of a room fire. For the development of novel flame retardants or combinations of flame retardants, flammability as well as the investigation of burning behavior under forced flaming conditions in lab scale are the most important characteristics. The flammability test UL 94 (*Underwriters Laboratories 94*) allows for classification of a material depending on its reaction to a small flame; the LOI (limiting oxygen index) is used to investigate the minimal oxygen concentration needed to have a sustained flame. For the assessment of heat release rate and burning behavior under irradiation, the cone calorimeter is one of the most widely used methods.

1.2 Motivation

Nowadays, polymeric materials are combined with a variety of additives to increase their mechanical and other properties. Besides flame retardants, a range of fillers, adjuvants, plasticizers, stabilizers, antioxidants, and so on, lead to a large library of potential formulations. Additionally, the concentration, particle size distribution, morphology, and all kinds of modification of the components can be varied to achieve optimal performance in all respects. All of the above-mentioned variations possibly change the burning behavior of the system, thus generating a vast matrix of materials which ought to be screened for the best performing formulation in terms of flame retardancy. Until now, this task was tackled either with very time and material consuming methods or was accompanied by loss of information in the results. There is a strong need for methods which combine a fast and material saving approach with reliability while retaining significance and detail in the results. It is possible to apply such high throughput methods at different stages in material development. Possible application areas lie in both basic research of new flame retardants for understanding their mechanisms in different polymer matrices, and in performance screening of developed flame retardants in multicomponent polymeric systems. Therefore, two main scientific goals of this work were set and addressed:

1. For the performance screening of multicomponent flame retarded systems a new method was developed. The research on the significance of the obtained results and comparison with established fire testing methods was a crucial point in the presented work.

2. In order to screen and quantify the mode of action of phosphorus-based flame retardants in relation to phosphorus content and species, as well as their reaction to different polymer matrices, a new approach was elaborated and established.

The first part of this work was developing the rapid mass calorimeter and evaluating the results produced with this method. The use of specimens reduced in size is crucial for the significant time and material saving this work aims at. Research on the effect of reduced specimen size on the burning behavior and the validity of the results is the challenge for this part of the work. For this, a large database of various flame retarded as well as non-flame retarded materials was created, which is the foundation for the scientific discussion and comparison with the already established methods. It enables an evaluation of the flame retardancy performance on a wider range and does not only focus on specific sample series with a limited scope. In addition, investigations of specific series of samples reveal detailed coherences between sample size reduction and achieved results and allows for ranking the rapid mass calorimeter in terms of significance compared to the state of the art.

The rapid assessment of the modes of action of phosphorus-based flame retardants is covered in the second part of this work. In this approach, a systematic variation of phosphorus species, polymeric matrix, and flame retardant additive concentration is the key to a sufficient understanding of the occurring phenomena. The use of easily-preparable resins as polymeric matrices ought to reduce the effort needed for sample preparation. Quantification of the modes of action contributing to the overall fire performance of a formulation allows for easier comparison of the flame retardant-polymer-systems and faster evaluation of the prevalent mode of action.

1.3 High throughput in flame retardancy

In the last two decades there have been several approaches towards establishing high throughput techniques in fire testing. The microscale combustion calorimeter (MCC), also known as the pyrolysis combustion flow calorimeter (PCFC), was developed by the Federal Aviation Administration (FAA) in 2002 as a tool for rapid heat release rate screening of milligram-scale specimens [20, 21, 22, 23]. While the PCFC is commercially available and successful, its results lack the informative value that results from cone calorimeter measurements contain. Flame inhibiting effects cannot be detected using the PCFC because of the absence of a real flame, and the use of milligram-scale samples impedes statements about macroscopic effects like intumescence, dripping, wicking, or the formation of a protective layer [24, 25]. Published in 2006, the National Institute of Standards and Technology (NIST) as well as the Marquette University worked on a research project dealing with novel approaches for high throughput techniques for the evaluation of fire retardancy [26, 27]. A device for rapid assessment of burning time as a means for fire retardancy effectiveness was described and the coherences of burning time and total heat release were investigated. High throughput flammability characterization was examined with the use of a gradient heat flux, enabling determination of the minimal heat flux needed for sustaining flame spread. A schematic of this process is displayed in Figure 4.

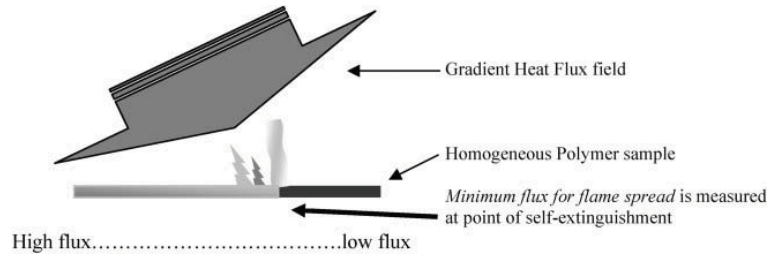

Figure 4. Schematic of the flammability assessment using a heat flux gradient. [26]

The most promising approach towards high throughput fire testing was the development of the rapid cone calorimeter. Here, a cone calorimeter was equipped with a conveyor belt in order to provide a continuous sample supply as opposed to the separate measurement of each specimen

in the standard cone calorimeter test. The use of smaller samples also contributes to the acceleration of measurements. A first test series on six flame retarded polystyrene specimens showed that a screening for the best performing formulation in terms of heat release rate could be achieved in under 20 minutes of measurement time. The heat release rate results as well as a schematic of the rapid cone calorimeter are presented in Figure 5. Unfortunately, further research on the rapid cone calorimeter, despite its interesting potential, was halted after only two sample series.

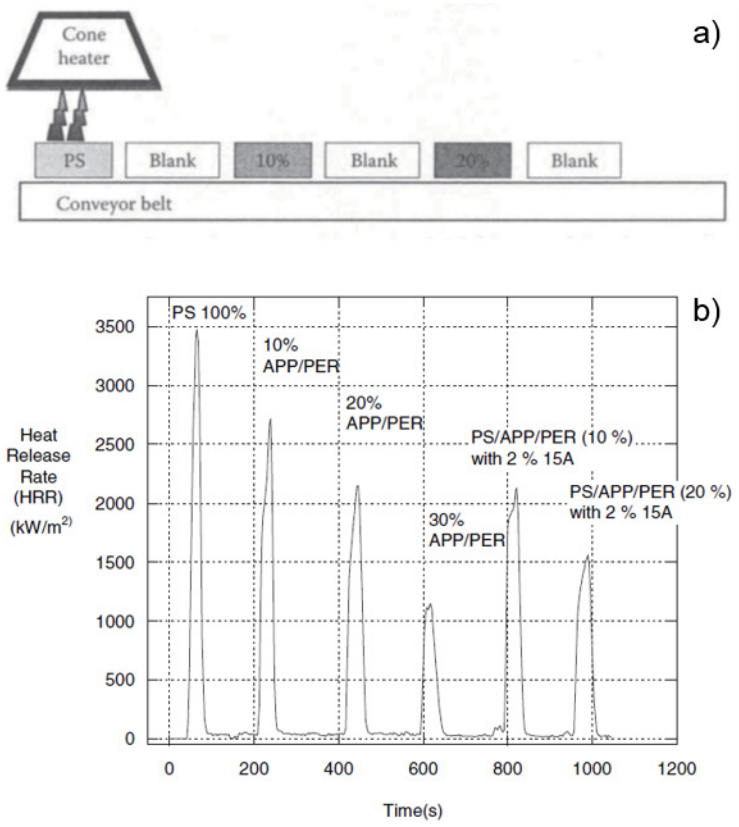

Figure 5. Schematic of the continuous sample supply in the rapid cone calorimeter (a) and heat release rate of a sample series of flame retarded polystyrene specimen (b, PS: polystyrene, APP: ammonium polyphosphate, PER: pentaerythritol, 15A: Cloisite 15A ammonium montmorillonite). [26]

The nature of a high throughput method is the fast and automated analysis and the parallel execution of process steps. The reduction of sample size plays an important role in all high throughput methods. However, since burning behavior is not able to be accelerated without changing the fire scenario, a loss of information and correlation in comparison to the cone

calorimeter test is to be expected. An automatization of the method and the parallelization of individual work steps is hardly possible due to safety regulations and the importance of the user during test procedure. Therefore, a balance must be found in those key factors for developing high throughput methods to achieve a considerable test acceleration while maintaining a relatively high grade of significance in the results.

1.4 Materials

In order to create a statistical approach towards reliability and repeatability of the results obtained with the rapid mass calorimeter, 71 different materials were investigated, which covers different material classes and flame retarded materials. Size reduction experiments in the rapid mass calorimeter were conducted on non-flame retarded polymers, namely poly(methyl methacrylate) (PMMA), polypropylene (PP), polyamide 6 (PA6), polyether ether ketone (PEEK), and pine sapwood (WOOD). They were chosen to represent different burning behaviors. The high-performance polymer PEEK, for example, has excellent thermal and mechanical properties. It is intrinsically flame retarded due to a strong charring effect caused by crosslinking reactions of the aromatic backbone structure. Around 70 % of char residue is left in a real fire scenario. Thanks to this, it was possible to make a statement about the size reduction effects on only slightly burning specimens.

The major part of measured materials consisted of halogen-free flame retarded polymeric materials. Flame retardants which work by means of flame inhibition, charring, intumescence, flame dilution, cooling, or additive and synergistic effects of multicomponent systems, were used in several polymeric matrices and at different concentrations. Furthermore, the thicknesses of the specimens were varied, which plays an important role in burning behavior. Of these 71 materials, some were chosen for detailed research based on their typical heat release rate curve in cone calorimeter measurements. Polyamide 6.6 (PA66) as well as polyamide 12 (PA12) reinforced with 30 wt% glass fiber were chosen as examples for inert filler effects. A typical

heat release rate curve for a flame inhibition effect was observed for a styrene-based thermoplastic elastomer (TPES) containing 30 wt% of AlPi. The effect of a protection layer on the heat release rate curve was investigated on different loads of exposed or encapsulated APP in PP. Magnesium hydroxide (MDH) was used in TPES as well as in PP to analyze the resulting heat release curves, and BDP and PTFE in polycarbonate/acrylonitrile butadiene styrene blend (PCABS) revealed heat release rate curves which showed combinations of charring and flame inhibiting effects.

To screen and investigate the modes of action of phosphorus-based flame retardants in a high throughput manner, four different model systems were chosen. Bisphenol A diglycidyl ether with isophorone diamine as a curing agent was chosen to represent the group of epoxy resins, whereas a PMMA resin and the polyester resin L800 cover the ranges of acrylate and polyester polymers. Polyolefins are represented by the use of paraffin as a matrix for the flame retardants. The phosphorus-based flame retardants BDP, red phosphorus (RP), as well as AlPi in two different particle size distributions were selected and incorporated in the model systems. While BDP has a phosphorus content of around 8.9 wt%, AlPi contains about 23.5 wt% of phosphorus. Red phosphorus has the highest phosphorus content with around 99 wt%. This way, a systematic sample series was created, in which the mode of action of the respective flame retardant was investigated in terms of phosphorus species, phosphorus content, particle size distribution, and polymeric matrix.

1.5 Methods

1.5.1 Pyrolysis – Thermogravimetry coupled with infrared spectroscopy

When a material is heated to a certain temperature, thermal decomposition, also known as pyrolysis, takes place. The pyrolysis happening during burning of a material with a stable flame is usually considered anaerobic. Several processes take place during thermal decomposition, such as elimination, chain scission, depolymerization, or cross-linking, which lead to volatile

as well as non-volatile compounds. The mass of non-volatile remains is investigated via thermogravimetric analysis and the nature of products released into the gas phase is detected using infrared spectroscopy. Thanks to the coupling of both methods, it is possible to assign certain gas phase species to significant steps in the mass loss rate during the pyrolysis [28, 29].

1.5.2 Pyrolysis combustion flow calorimeter

To evaluate the heat release of the combustible volatiles released during pyrolysis, the pyrolysis combustion flow calorimeter is used. The principle of the pyrolysis is the same as in the TGA, but all resulting gases are then introduced into a nitrogen/oxygen gas flow combination with a ratio of 80/20. The gas mixture is led into a combustion chamber, where it is combusted at 900 °C. The released heat, as well as the rate and temperature at which the heat was released, are then calculated by how much oxygen was consumed. Similar to the TGA, the PCFC only uses around 5 mg of a sample for a measurement [30, 20].

1.5.3 Flammability – limiting oxygen index (LOI)

The limiting oxygen index test is a vertical flammability test carried out on specimens with a size of 8 by 1 centimeters and a thickness of 4 millimeters in a gas flow mixture of oxygen and nitrogen flowing upwards through a chimney. The sample is ignited on the top and time and length of burning are recorded. A schematic of the LOI test is provided with Figure 6. The test is performed with varying oxygen concentrations, allowing assessment of the minimum oxygen concentration needed for a sustained flame. Sustained burning in this test is defined as longer than 3 minutes after removal of the ignition flame or advancing of the flame front for more than 5 centimeters downwards [31]. However, it should be noted, that the oxygen index is not a material property, since it is heavily dependent on parameters like the specimen thickness. Thus, it describes a tendency for self-extinguishment under those specific conditions.

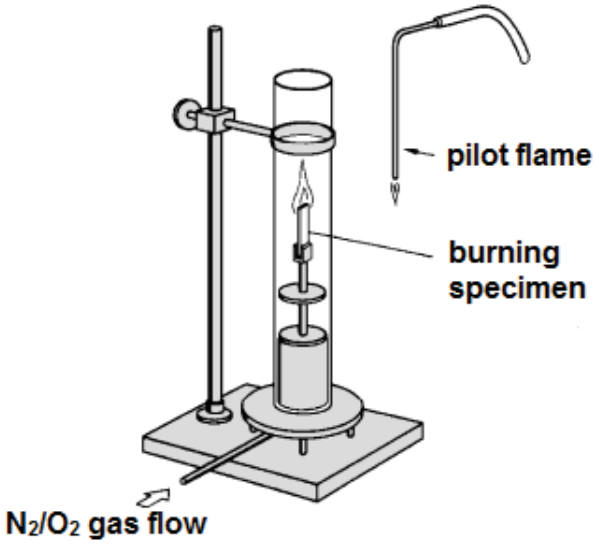

Figure 6. Schematic of the limiting oxygen index flammability test setup. [31]

1.5.4 Cone calorimeter

The most used bench-scale method for the evaluation of heat release rate is the cone calorimeter. As mentioned before, it is mainly simulating the conditions of a developing fire, thus the commonly used specimen size of 10 by 10 centimeters with a thickness of up to 1 centimeter. The sample is irradiated by a heating cone, which can generate heat fluxes up to 100 kW/m². Depending on the intumescence potential of the investigated specimen, the distance from sample to heating coil can be adjusted, however, irradiation was shown to be most regular at distances ranging from 25 to 35 millimeters. Sufficient irradiation leads to accumulation of volatile combustible gases across the surface of the sample. If the critical concentration and temperature is reached, the gases are ignited by the spark igniter. During the measurement, sample mass is constantly recorded by a load cell, smoke evolution is monitored by a laser, times needed to ignition and flameout are recorded with the press of a button, and CO, CO_2, and O_2 concentrations are analyzed by the respective gas cells. Figure 7 shows a schematic of the cone calorimeter setup [32, 33, 19].

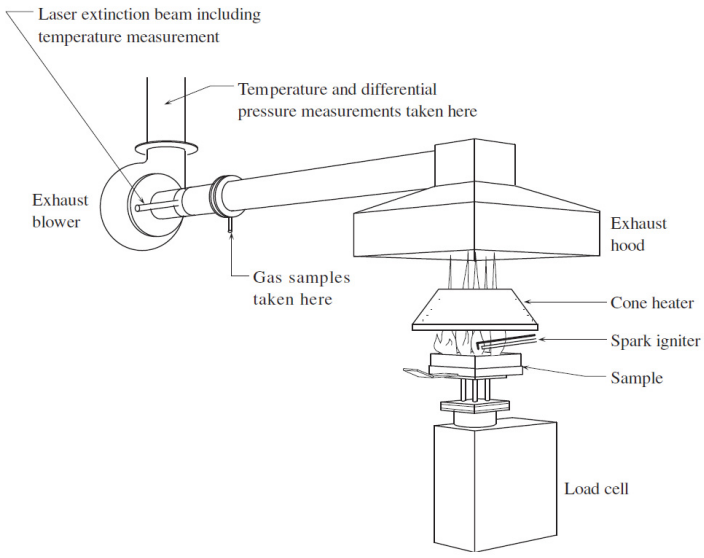

Figure 7. Setup of the cone calorimeter. [33]

The heat release rate (HRR), the single most important variable in fire hazard [34], is measured and calculated by means of oxygen consumption. Essentially, the amount of consumed oxygen during combustion is directly related to the heat of combustion. Per 1 kg of oxygen consumption, around 13.1 × 10^3 kJ of heat are released. Together with a defined exhaust gas flow rate, the HRR is calculated, following equation II.

$$\dot{Q}(t) = \left(\frac{\Delta h_c}{r_o}\right)(1.10)\, C \sqrt{\frac{\Delta P}{T_e}\frac{\left(X_{O_2}^0 - X_{O_2}(t)\right)}{1.105 - 1.5\, X_{O_2}(t)}} \quad with \quad \frac{\Delta h_c}{r_o} \approx 13.1 \times 10^3 \frac{kJ}{kg} \qquad \text{(II)}$$

$\dot{Q}(t)$: HRR, Δh_c: net heat of combustion, r_o: stoichiometric oxygen/fuel mass ratio, ΔP: orifice meter pressure differential, T_e: absolute temperature of gas at orifice meter, $X_{O_2}^0$: initial value of oxygen analyzer reading, X_{O_2}: oxygen analyzer reading, mole fraction of oxygen, C: correction factor

The correction factor C is determined via daily calibration by using a 5 kW methane flame. To acquire the heat release rate per unit area, the calculated HRR is divided by the surface of the measured sample. Taking the integral of the HRR obtains the total heat released (THR) during the measurement. A crucial value for the evaluation of burning performance is the peak of heat release rate (PHRR). The goal of a flame retardant in a polymeric material is to significantly reduce the PHRR. Many more values used for comparison of material performance can be deduced from the HRR and other measurands, such as the fire growth rate index (FIGRA), the

maximum average rate of heat emission (MARHE), the average heat release rate from time to ignition to time of flameout (HRR_{avg}), the fire performance index (FPI), and the PHRR divided by time to ignition ($PHRR/t_{ig}$) as a fire growth index.

1.5.5 Rapid mass calorimeter

The rapid mass calorimeter is based on a standard mass loss calorimeter with attached thermopile chimney for heat release rate measurement [35]. Contrary to the cone calorimeter, heat release rate is measured by means of a voltage change in the circularly arranged thermoelements. This thermopile is calibrated prior to the measurement by using a methane flame according to ISO 13927 [36]. The balance, which is normally used in the mass loss calorimeter, was replaced by a linear motion unit, on which a mount for two sample holders was constructed. This enabled for exchange of the burned sample with a new one during the measurement of the specimen on the second sample holder. Both sample holders were located at a distance of 250 mm edge to edge. Figure 8 shows a picture of the setup of the rapid mass calorimeter.

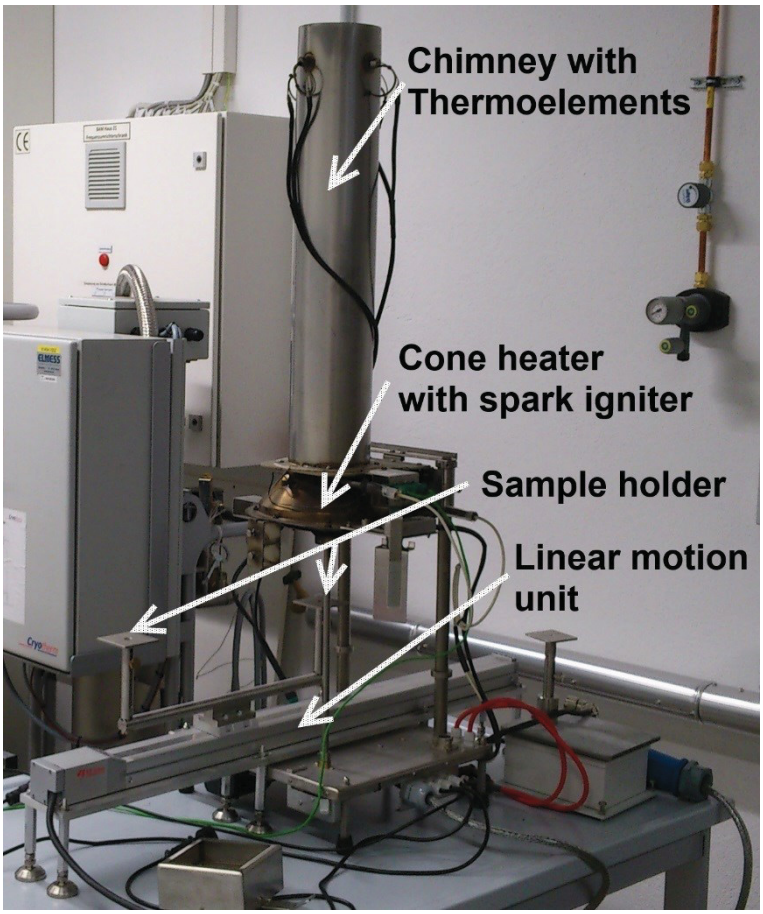

Figure 8. Setup of the rapid mass calorimeter.

The basic principle, i.e. heating up of the sample by a conical heater and ignition of the pyrolysis gases with a spark igniter, is the same as in the cone calorimeter. However, the measurements in the rapid mass calorimeter were performed in continuous tests, as opposed to the cone calorimeter, in which for each sample a new test is conducted. The linear motion unit was programmed to execute a simple loop motion, in which the wait time in between movements equals the dwell time of the specimen under the cone heater. Prior to the test, a dwell time of 80 seconds for an empty sample holder was chosen in order to allow the software to collect baseline data. After this duration, the linear motion unit changes the sample holder to provide the first specimen. The dwell time for samples to be measured depends on their burning times and the time the thermopile needs to relapse back to baseline. The dwell time must be chosen

in a way that a complete burning of the sample and a subsequent baseline collection is ensured. Concurrently, the dwell time should be chosen to result in optimal time saving.

2 Concluding discussion

2.1 Part I: screening for performance of flame retardants

2.1.1 Size reduction experiments

High throughput methods are often accompanied by a reduction in sample amount. In the rapid mass calorimeter, this was accomplished by reducing the standard cone calorimeter plates from 10 by 10 centimeters to two by two centimeters while maintaining the thickness of the specimens. To investigate the effects in heat release rate that accompany a size reduction, square specimens with edge lengths of 10, 7.5, 5, 2.5, 2 and 1 centimeters were measured in the rapid mass calorimeter. It was found, that with decreasing specimen size, the tendency for an edge burning effect, the horizontal spread of the flame over the edges of the specimen, increased. This was a problem insofar as the heat release rate is measured as a surface dependent value; its unit is kW/m². That means that when the thermocouples, which measure the heat release rate, receive a heat impact greater than the actual sample size, the surface dependent value is flawed. With decreasing sample size, the heat release rate values become unrealistically high due to the increasing ratio of sample surface area and horizontal flame spread area. Therefore, it was decided to eliminate the surface dependency by using absolute heat release rate values.

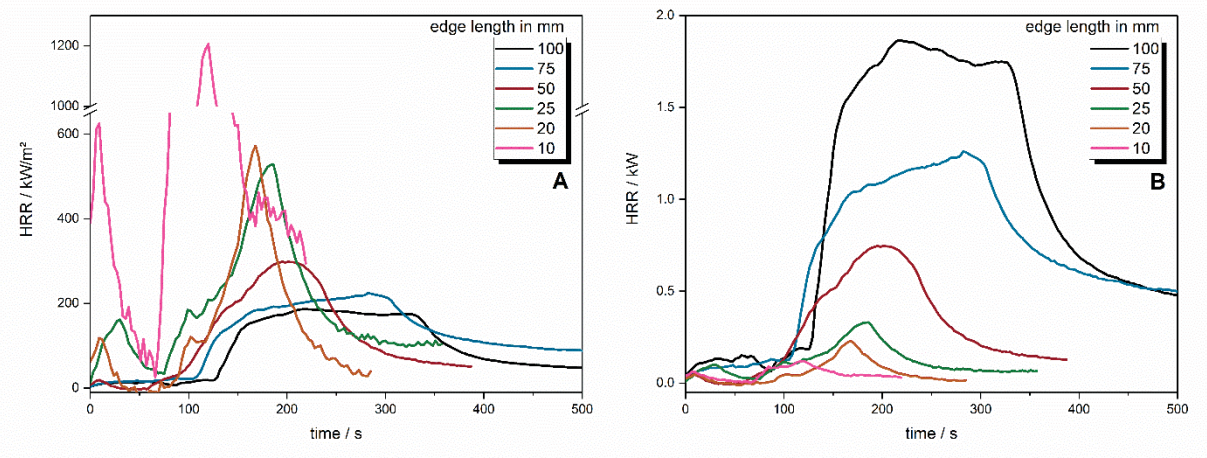

Figure 9. Surface-dependent (A) and surface-independent (B) heat release rates (HRR) for squared poly(ether ether ketone) (PEEK) specimens with varying edge lengths.

For investigation of size reduction effects on heat release rate, five different polymers were chosen, which all have differences in burning behavior and intensity. PP burns with a high PHRR while PMMA shows a steadier burning. PA66 develops a passivation layer prior to ignition but burns moderately strong. PEEK is a high-performance polymer which is intrinsically flame retarded via a strong charring mechanism and WOOD shows a low heat release rate while producing a fair amount of char residue. For all tested polymers, it was observed that the form of the heat release rate curve changed to a less characteristic peak with decreasing sample size. A standard sized peak sample, for example, showed a plateau of steady burning which lasted for around 200 seconds (Figure 9). Already with a sample the size of 7.5 times 7.5 centimeters the plateau transformed into a slope with steadily increasing heat release rate up to the PHRR due to an already appearing edge burning effect. For even smaller samples, the heat release rate took peak shape. As an example, for size reduction effects occurring in a flame retarded polymeric system, a blend of APP in PP, an intumescent system, was chosen. Standard sized specimens show interesting characteristics in the heat release rate curve shape, from which the burning behavior can be deduced. First, the HRR rises to an initial peak, after which it rapidly decreases and shows a steady burning plateau. This is due to the formation of a protective layer, which acts as a heat barrier and hinders the pyrolysis gases from feeding the flame. Eventually, the protective layer cracks and its effectiveness decreases. The HRR rises again, until the PHRR is reached and the flameout occurs. When the sample size is decreased to an edge length of 7.5 cm, these characteristics begin to merge into one peak. The former initial peak, which is now only a shoulder followed by a small plateau, is still recognizable although the difference between shoulder and PHRR becomes significantly less. Decreasing the sample size further to an edge length of 5 cm, the shoulder is now only detectable as a remnant.

Based on this finding it was hypothesized that HRR curves of smaller samples depict an average over the entire HRR curve of the standard sized sample, combining characteristics into a peak-shaped HRR curve. This hypothesis was checked by investigating correlations of cone calorimeter results with results from size-reduced samples measured in the cone calorimeter. The results of the correlation investigations are summarized in section 3.1.2. On first glance,

the characteristics of a HRR curve are lost when decreasing the sample size even more. However, in comparing studies with cone calorimeter results it was found that it is still possible to interpret burning behavior based on HRR curves obtained from samples with an edge length of only two centimeters. This is summarized in section 3.1.3 and shows that the rapid mass calorimeter is a valuable tool for the rapid assessment of the behavior of polymeric material specimens under forced flaming conditions.

2.1.2 Correlation with other fire tests

The results which were obtained with the rapid mass calorimeter were compared with cone calorimeter results. For this, the most important values of heat release rate measurements, like PHRR, THE, FIGRA, MARHE, etc., were correlated with each other in several ways. On the one hand, these indices were checked for correlation within one method, the rapid mass calorimeter, and the resulting correlation coefficients were then compared with those obtained from the other method, the cone calorimeter. For example, a correlation between the PHRR and the FIGRA of the rapid mass calorimeter resulted in a strong correlation coefficient of 0.92 (Figure 10) whereas the same values in the cone calorimeter showed a coefficient of 0.82. This is one example of a correlation which is more pronounced in the rapid mass calorimeter. This strong correlation is explained by the fact that for peak-shaped curves with a defined width, the slope of the peak is proportional to the peak height. Since cone calorimeter HRR curves exhibit more characteristics than just a peak, this correlation is weaker. In general, all the values which correlate strongly in the established cone calorimeter also show strong correlation in the rapid mass calorimeter. This proves that both tests are related to each other.

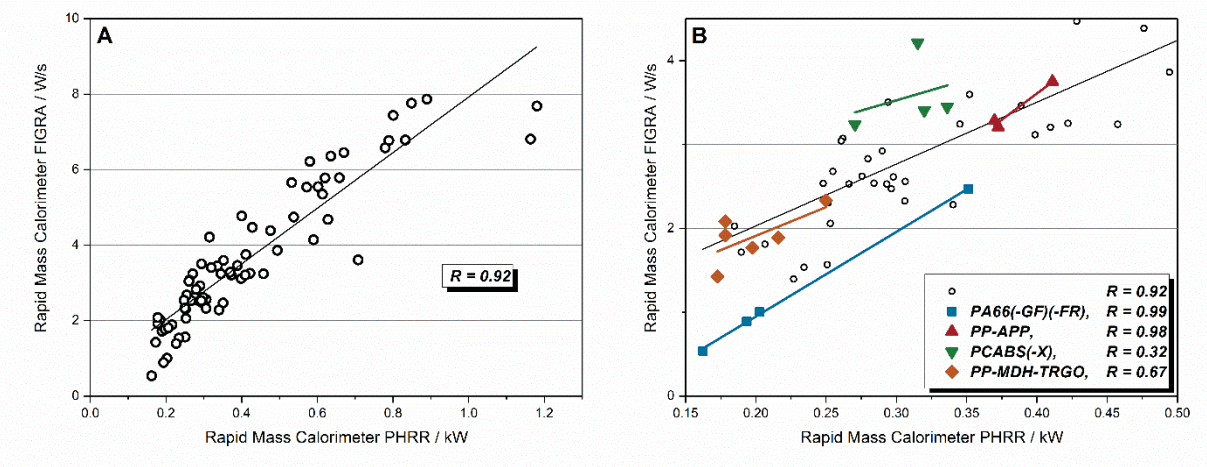

Figure 10. Correlation between rapid mass calorimeter fire growth rate index (FIGRA) and peak heat release rate (PHRR) for all specimens (A) and for specific sample series (B).

Another way of investigating the correlation of results between the rapid mass calorimeter and the cone calorimeter is the direct correlation between both methods. PHRR, THE, FIGRA and other indices from the rapid mass calorimeter were checked for their correlation coefficients with the same values obtained from cone calorimeter measurements. It was revealed, that mainly the averaging parameters, like MARHE or HRRavg, showed moderate to strong correlation. This supports the thesis, that HRR measurements on samples with reduced size tend to depict an average over all characteristics of a HRR curve of a standard-sized sample. Figure 11 displays the correlation between PHRR from rapid mass calorimeter measurements and the MARHE results from the cone calorimeter. Additionally, it was found out that besides the PHRR of both methods, the FIGRA from the rapid mass calorimeter and the PHRR from the cone calorimeter exhibited strong correlation coefficients with each other.

In conclusion, the rapid mass calorimeter was shown to exhibit equivalently good results as the cone calorimeter when focusing on the properties with the strongest correlation coefficients, namely PHRR, FIGRA, and MARHE. Considering the drastically reduced sample size to two by two centimeters and the strong dependency of burning behavior on the length scale of the specimen, the achieved results are very valuable and promising for future applications.

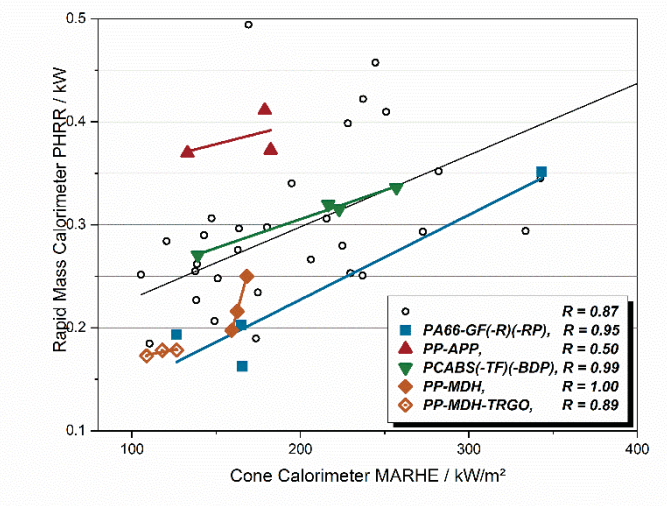

Figure 11. Correlation between PHRR of the rapid mass calorimeter and maximum average rate of heat emission (MARHE) of the cone calorimeter for specific sample series.

Results from the limiting oxygen index test were also correlated to rapid mass calorimeter as well as cone calorimeter results. Due to lack of material or results from previous works, oxygen index measurements were not existing for all 71 materials. However, for the tested materials, a strong non-linear correlation was found between the oxygen index and the PHRR of the cone calorimeter. Despite several deviant findings in literature concerning correlations between LOI and cone calorimeter [37, 38], a curve with the equation III was revealed.

$$OI = 17 + \frac{3117}{PHRR\ (\frac{kW}{m^2})} \qquad \text{(III)}$$

A similarly good correlation between the oxygen index and the PHRR of the materials in the rapid mass calorimeter further proves the reliability of this test and confirms the relation between the cone calorimeter and the rapid mass calorimeter. Equation IV was found to describe the connection between the oxygen index test and the PHRR obtained in the rapid mass calorimeter.

$$OI = 12 + \frac{3.92}{PHRR\ (kW)} \qquad \text{(IV)}$$

This correlation shows that materials which exhibit a relatively low PHRR in either method, cone calorimeter or rapid mass calorimeter, will exhibit a high limiting oxygen concentration

where self-extinguishment still occurs. This fact, that a similarly good correlation is found for both rapid mass calorimeter and cone calorimeter, further shows that they are related tests and the obtained PHRR values are comparable to a great extent.

2.1.3 In-detail analysis of heat release rate in the rapid mass calorimeter

Several materials with characteristic burning behavior and therefore characteristic heat release rate curves in the cone calorimeter were chosen to be examined in detail. In general, the flame retarded system was compared to the non-flame retarded polymer to observe the changes in heat release rate. This was done to check whether the heat release rate curves contain more information than just peak height and if some form of burning behavior interpretation is possible. The heat release rate curves obtained in the rapid mass calorimeter still contain valuable characteristics which allow for an assessment of burning behavior together with observations made during the burning test. However, there are significant differences which result from the size reduction and the accompanying edge burning effect.

In the cone calorimeter, polyamide 6.6 filled with 35 wt% of glass fibers shows a noticeable plateau of steady burning occurring after the PHRR was reached. This is explained by the consumption of polymer matrix during burning until a certain amount of inert glass fiber filler is accumulated on the surface of the pyrolysis zone to form a glass fiber mat. The deceleration of the heat release rate and the steady burning are the results of the protective effect of the glass fiber mat. In the rapid mass calorimeter, however, this plateau of steady burning occurs prior to the actual PHRR. When the edge burning effect becomes pronounced enough, the glass fiber mat is not sufficient to protect the material from irradiation and to hinder fuel transport to the flame. If polyamide 12 is reinforced with glass fiber filler, the same effect is observed also in the cone calorimeter. However, the reason here is not the edge burning effect, but simply the stronger burning of the polymer matrix.

A typical example of a heat release rate curve where a flame inhibiting effect is evident, is the incorporation of AlPi in styrene-based thermoplastic elastomers (TPES). Compared with the non-flame retarded TPES, the addition of AlPi leads to a reduction of the slope and of the PHRR in the cone calorimeter measurements. The flameout occurs right after PHRR was reached and the HRR is abruptly reduced again. Since hardly any residue is produced and heat release rate clearly shows a non-charring behavior, flame inhibition must have been the main mode of action in this system. In the rapid mass calorimeter, the same effects are observed and slope and PHRR reduction are not as pronounced as in the cone calorimeter. This shows that changes in heat release rate and burning behavior are well detectable with the rapid mass calorimeter.

Rapid mass calorimeter results were also compared with results from the established screening method, the PCFC. Heat release rate curves in the PCFC are created by subjecting the material to a heating ramp. If at a certain temperature pyrolysis gases are set free, they are introduced into an oxygen/nitrogen gas stream and completely combusted. Because of this, no real interpretation of burning behavior is possible. Additionally, the lack of a real flame as well as the milligram scale of the samples limit the detectable flame retardant effects. For example, the previously described effect occurring by incorporating glass fibers as an inert filler into polyamide 12, the shielding effect of a glass fiber mat during burning is not visible in the PCFC measurements. Merely the reduction of fuel by replacing polymer matrix with the inert filler is depicted by peak height reduction. The rapid mass calorimeter on the other hand, is able to detect such macroscopic effects and furthermore allows for an assessment of flame inhibition effects since the used samples are burning with a real flame.

Lopez-Cuesta et al. [39] described the discrepancies between the efficiency of flame retardants measured with the cone calorimeter and the PCFC by checking the correlation between PHRR reduction in the cone calorimeter and HRC reduction in PCFC. This approach was used to check whether the rapid mass calorimeter exhibits a more or less pronounced efficiency than the cone calorimeter by plotting the ratio of PHRR of flame retarded material to non-flame retarded material in the rapid mass calorimeter versus the similar ratio of PHRR in the cone calorimeter (Figure 12). If the materials would show the same efficiency in both methods, all data points

would be located on the ideal line. However, it was found that all data points were positioned above the ideal line, which means that the efficiency of a flame retardant is not as distinct in the rapid mass calorimeter than in the cone calorimeter.

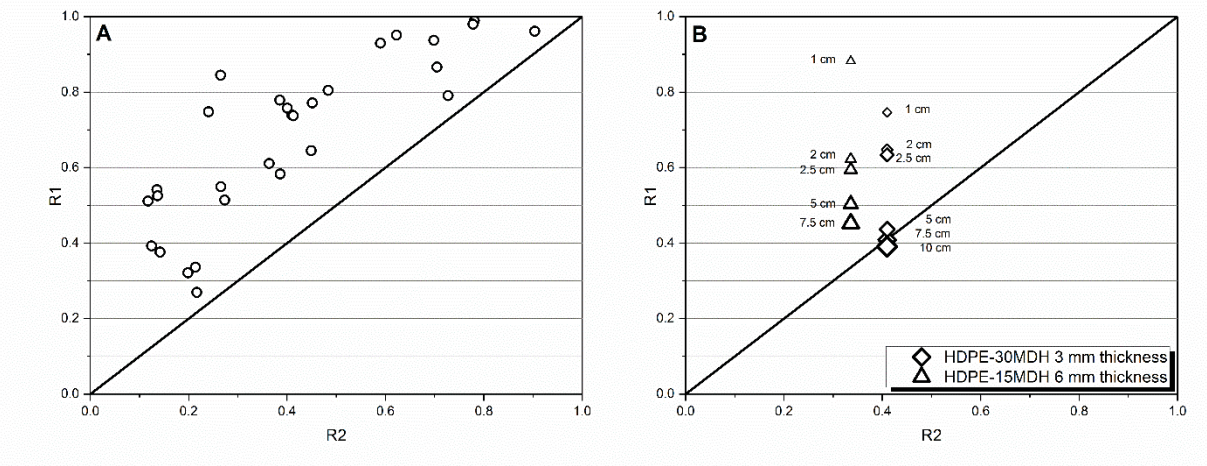

Figure 12. Correlation between the ratio PHRR of flame retarded to non-flame retarded material in the rapid mass calorimeter (R1) and the same ratio in the cone calorimeter (R2) (A) and the influence of sample size on this correlation (B).

While the lowered efficiency in the PCFC was demonstrated to be the result of the inability to detect certain flame retardant effects, it was hypothesized that the lowered efficiency in the rapid mass calorimeter is mainly due to the size reduction and the associated edge burning effect. To prove this, two polymeric systems were selected and the flame retarded and non-flame retarded formulations of those systems were varied in size and were measured in the rapid mass calorimeter. By comparing the PHRR ratio of the different sized formulations in the rapid mass calorimeter with the PHRR ratio of the constant size formulations in the cone calorimeter, it was detected that with increasing specimen size the data points approached the ideal line. This confirms that merely the size reduction of the specimens is reason for the apparent worse performance compared to the cone calorimeter. By keeping that in mind, the rapid mass calorimeter is still able to assess all kinds of effects occurring during burning of flame retarded formulations.

2.2 Part II: screening for modes of action of flame retardants

2.2.1 Dependency of flame retardant mode of action on polymeric matrix

Phosphorus-based flame retardants were incorporated in a range of model system thermosets representative for groups of thermoplastics. By means of thermogravimetric analysis it was found out that epoxy resin and polyester resin model systems are more prone to produce residue from pyrolysis than PMMA resin and paraffin model systems. AlPi incorporated in epoxy resin, for example, does not increase the amount of residue by much. However, the effects of AlPi on residue formation in the polyester system are much more different. Exolit OP935 promoted the formation of residue up to a total amount of 14 wt%.

Differences of flame retardant effects and efficiencies depending on the polymeric matrix become even clearer when measured in the cone calorimeter under forced flaming conditions. The effect of a single flame retardant was studied in all four polymer matrices by plotting the normalized effective heat of combustion (EHC) versus the phosphorus content release in the gas phase. This was done for each used flame retardant. The AlPi flame retardants Exolit OP935 and OP1230 were compared in all four polymer matrices to provide a statement about the effect of different particle size distributions (Figure 13 A and B). In both cases, the epoxy and polyester resins exhibit the most distinct EHC reduction while those flame retardants achieve only a marginal EHC reduction in PMMA resin and almost no EHC reduction in paraffin. It is also apparent that the finer-grained Exolit OP935 is most effective in epoxy resin, while the coarser-grained Exolit OP1230 shows a slightly better effectiveness in polyester resin when it comes to reduction of the effective heat of combustion.

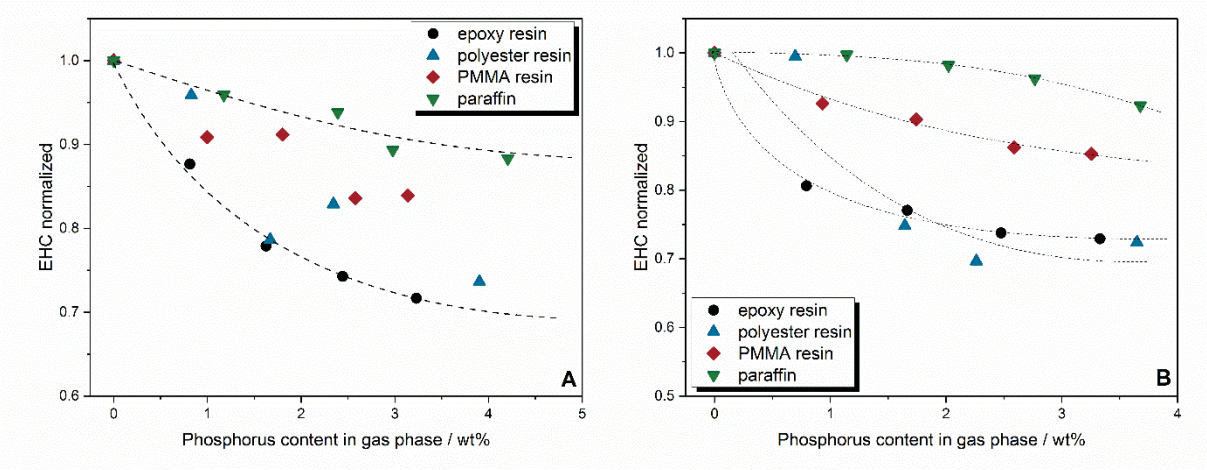

Figure 13. Effective heat of combustion in relation to the phosphorus content in the gas phase for Exolit OP935 (A) and Exolit OP1230 (B) in epoxy resin, polyester resin, PMMA resin and paraffin.

In the epoxy resin, BDP is able to induce residue formation of up to 17 wt%, whereas in the polyester resin, the amount of residue only reaches about 5 wt%. In the PMMA resin model system, almost no residue is formed. It was also observed that BDP at every loading has a much higher reduction in EHC than the AlPi flame retardants when incorporated into epoxy resin or polyester resin. In the PMMA resin, however, EHC reduction lies in the same low range for both kinds of flame retardants (Figure 14 A). Red phosphorus showed a strong reduction of EHC in epoxy resin but only a slight reduction when incorporated into paraffin. In epoxy resin, red phosphorus reduces the EHC to around 60 % whereas in paraffin the EHC reaches only around 90 % at the highest loading (Figure 14 B).

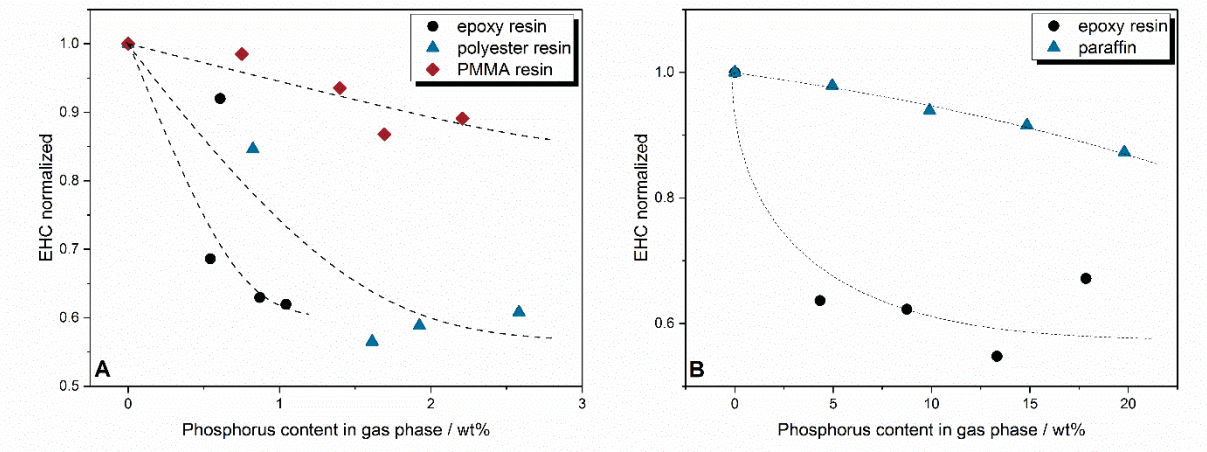

Figure 14. Effective heat of combustion in relation to the phosphorus content in the gas phase for BDP (A) and red phosphorus (B) in different matrices.

These results show that the used flame retardants are performing best in the DGEBA/IPDA epoxy resin system. The leveling off of efficiency is most noticeable in this matrix. When paraffin is used as the polymer matrix for incorporation of flame retardants, the fire retardancy performance was only marginal, making it not suitable for this kind of screening.

2.2.2 Dependency of flame retardant mode of action on phosphorus species

The mode of action of a phosphorus-based flame retardant is dependent on the phosphorus species. In general, phosphates like the used Bisphenol-A bis(diphenyl phosphate) act as precursors for the increased condensed phase mode of action, mainly charring. Furthermore, red phosphorus is known as a char inducing agent as well due to its reaction with phosphoric acid. This is especially the case in polymeric matrices with a high oxygen or nitrogen content. In hydrocarbon polymers, the formation and release of P_4 leads to gas phase activity [14].

Aluminum diethyl phosphinate was found to react mainly in the gas phase as a flame inhibiting agent in most polymer matrices. The flame retardant – polymer matrix combinations studied in this work were chosen under the premise that flame inhibition is the predominant mode of action. This way, the condensed phase actions of the flame retardants become more noticeable when the amount of incorporated flame retardant is increased. In fact, it was found out, that BDP in epoxy resin exhibited the largest increase in residue formation while having the lowest phosphorus content of all tested flame retardants. Moreover, BDP was the only flame retardant whose incorporation in epoxy resin led to the formation of a protective layer. This was additionally concluded by the nature of the formed residue. The surface of the residue of sample EP-25-BDP, for example, exhibited a very closed and compact texture while the residues of other formulations featured a brittle and loose structure. A calculation of the amount of protective layer effect contributing to the overall flame retardant performance concluded that up to 35 % of the PHRR reduction is attributed to this protective layer effect. In conclusion, the assessment of different flame retardants in polymeric matrices revealed their preferred mode of

action and the novel way of quantification enabled a statement about the contribution to the overall fire retardancy performance in the respective matrix.

2.2.3 Dependency of flame retardant mode of action on phosphorus content

Flame retardancy performance is strongly dependent on the amount of phosphorus content incorporated into the polymer matrix. Several effects come into play when the flame retardant load, and thus the phosphorus content, is increased. The ability to release phosphorus into the gas phase as well as the effectiveness of a flame retardant in gas phase and condensed phase changes heavily. For investigations of dependencies of phosphorus content in the gas phase on flame inhibition performance, the EHC was monitored in the cone calorimeter. It was observed that with higher phosphorus concentration in the gas phase, the decrease in EHC follows a non-linear decay, up to a leveling off. This means that an increase in flame retardant load and therefore phosphorus content is of no advantage after a critical concentration. It might even be detrimental for the effectiveness since additionally released phosphorus species which do not take part in flame inhibition may increase the EHC again (Figure 15 B III). For epoxy resin and polyester resin, all the flame retardants exhibit this leveling off phenomenon (Figure 15 A). In PMMA resin, a tendency towards leveling off is still noticeable, whereas the EHC of the flame retarded paraffin model system formulations follow a linear behavior.

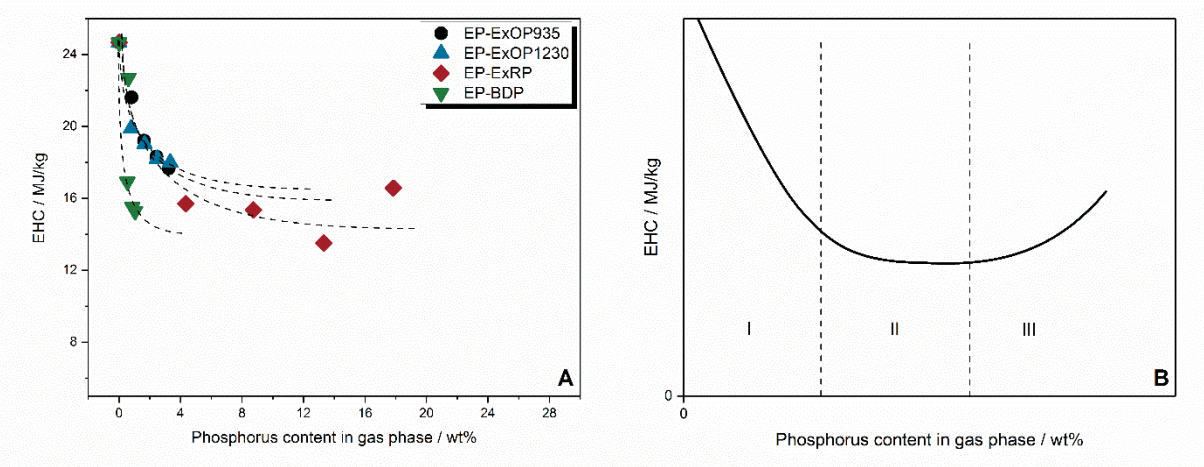

Figure 15. Effective heat of combustion in relation to the phosphorus content in the gas phase for the four different flame retardants in epoxy resin (A) and a schematic of the proposed curve progression (B).

In the same way, the condensed phase activity, monitored by residue formation, was investigated. An increase in flame retardant load, and therefore in phosphorus content, leads to an increase in residue amount and in remaining phosphorus in the residue. But this relation is only valid up to a certain concentration of phosphorus in the residue. In the cases of BDP incorporated into epoxy resin and polyester resin, this concentration lies at around 6 and 8 wt% respectively. By increasing the phosphorus concentration further, the amount of residue increases rapidly, exhibiting a sigmoidal curve behavior. This effect is displayed in Figure 16. The reason for that is the tendency of BDP, or other flame retardants, to build up a protective layer, shielding the material from heat and hindering fuel transport to the flame. Because of this, the amount of incompletely pyrolyzed material in the residue increased and caused the jump in the curve. If the phosphorus concentration in the residue increases even further, the curve adopts a linear behavior again.

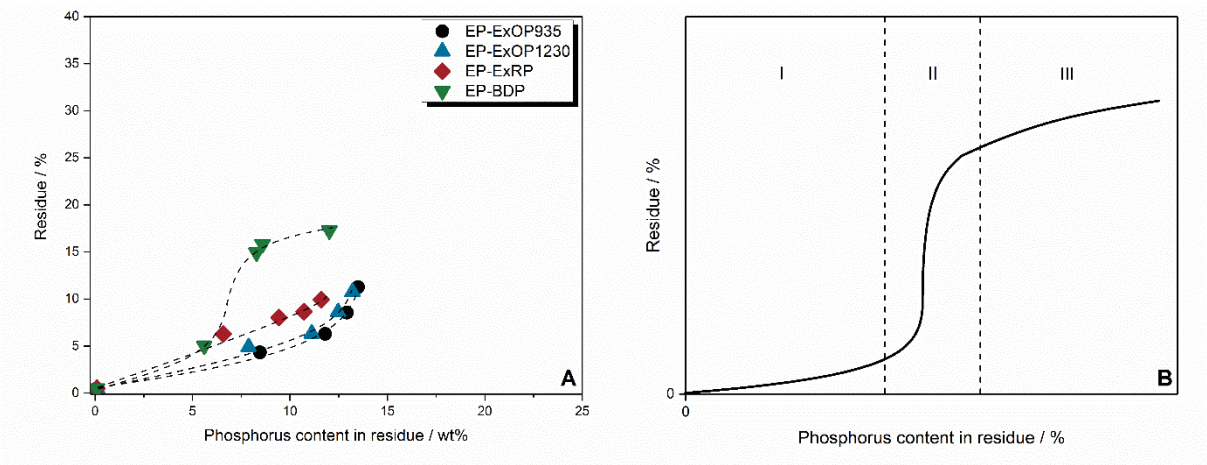

Figure 16. Residue formation in relation to the phosphorus content in the residue for flame retardants in epoxy resin (A) and a model curve progression for some of the investigated formulations showing a nearly linear increase of residue with phosphorus content (I), a step in residue formation (II) and a relapse back to linear curve progression (III).

The nature of the formed residues allowed to further prove this conclusion. It was observed that the residue which resulted from burning the epoxy-BDP-system exhibited a more closed and even surface (Figure 17 B), whereas formulations with AlPi or RP as flame retardants in epoxy resin produce a more brittle and rough char (Figure 17 A). In the polyester resin system, the amount of residue from the formulation with a load of 25 wt% of BDP only lies at 3.5 wt%. This is evidence that the main effect of BDP in the polyester resin system must be a flame inhibiting effect in the gas phase.

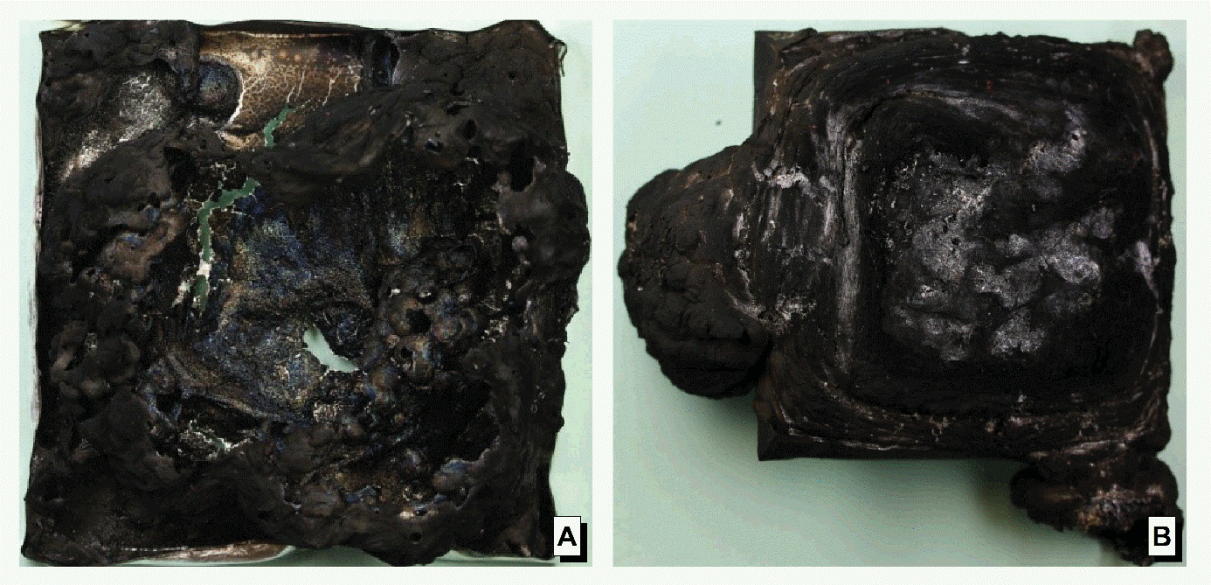

Figure 17. Photographs of residues of EP-15-ExOP935 (A) and EP-25-BDP (B).

The investigation of the dependencies of flame retardant performance on the phosphorus content in the gas phase and condensed phase, respectively, brought new insight into the behavior of the different phosphorus-based flame retardants. Separate observation of gas phase and condensed phase performance allowed for the discovery of the predominant mode of action of a flame retardant in a specific polymeric matrix. Increasing phosphorus content in the gas phase as well as in the residue revealed the levelling off of flame inhibition effectiveness and the step-like change in residue amount. These findings contribute to the overall understanding of phosphorus-based flame retardant behavior in different polymeric matrices and provide a basis for future development of flame retarded polymeric systems.

3 Publications

3.1 The rapid mass calorimeter: A route to high throughput fire testing

Sebastian Rabe, Bernhard Schartel, *Fire and Materials* **2017**, 41, 834-847.

https://doi.org/10.1002/fam.2420

This article was accepted and published.

First author contribution:

- Conceptualizing the working packages
- Setting up the rapid mass calorimeter
- Choosing the materials for statistical and detailed approaches
- Development of the rapid mass calorimeter method
- Cone calorimeter, rapid mass calorimeter, PCFC and all other measurements
- Analysis and interpretation of the data
- Scientific discussion and conclusions
- Conceptualizing and writing the manuscript

Contributions from other authors:

- Bernhard Schartel:
    - Conceptualizing and writing of funding application
    - Contribution to the scientific discussion
    - Contribution to the concept of the manuscript

Abstract: The rapid mass calorimeter based on reduced-size specimens is proposed for accelerated fire testing and put up for discussion, particularly for flame retarded polymeric materials. A mass loss calorimeter is combined with a semiautomatic sample changer. Experiments on specimens of reduced size were conducted on poly(methyl methacrylate), poly(propylene), polyamide 66, poly(ether ether ketone), and pine sapwood square samples with edge lengths of 100, 75, 50, 25, 20, and 10 mm. Specimens of 20 × 20 mm^2 were selected to achieve a crucial reduction in specimen size and a measuring protocol developed. A total of 71 different polymeric materials were investigated in the rapid mass calorimeter and cone calorimeter for comparison and several materials known to have different heat release rate characteristics in the pyrolysis combustion flow calorimeter were used to test this additional screening method as well. The important fire properties obtained in the rapid mass calorimeter show reasonable correlation with the cone calorimeter results and also with the oxygen index. All in all, the rapid mass calorimeter produces reliable and meaningful results and, despite acceleration and size reduction, still allows for a certain degree of burning behavior interpretation. Material savings of 96% and time savings of around 60%-70% are achieved compared to cone calorimeter measurements.

Received: 10 June 2016 | Revised: 2 December 2016 | Accepted: 2 December 2016

DOI 10.1002/fam.2420

WILEY

RESEARCH ARTICLE

The rapid mass calorimeter: A route to high throughput fire testing

Sebastian Rabe | **Bernhard Schartel**

Bundesanstalt für Materialforschung und –prüfung (BAM), Unter den Eichen 87, 12205 Berlin, Germany

Correspondence
Bernhard Schartel, Bundesanstalt für Materialforschung und –prüfung (BAM), Unter den Eichen 87, 12205 Berlin, Germany.
Email: bernhard.schartel@bam.de

Summary

The rapid mass calorimeter based on reduced-size specimens is proposed for accelerated fire testing and put up for discussion, particularly for flame retarded polymeric materials. A mass loss calorimeter is combined with a semiautomatic sample changer. Experiments on specimens of reduced size were conducted on poly(methyl methacrylate), poly(propylene), polyamide 66, poly(ether ether ketone), and pine sapwood square samples with edge lengths of 100, 75, 50, 25, 20, and 10 mm. Specimens of 20 × 20 mm^2 were selected to achieve a crucial reduction in specimen size and a measuring protocol developed. A total of 71 different polymeric materials were investigated in the rapid mass calorimeter and cone calorimeter for comparison and several materials with different heat release rate characteristics in the pyrolysis combustion flow calorimeter to test this additional screening method as well. The important fire properties obtained in the rapid mass calorimeter show reasonable correlation with the cone calorimeter results but also with the oxygen index. All in all, the rapid mass calorimeter produces reliable and meaningful results and, despite acceleration and size reduction, still allows for a certain degree of burning behavior interpretation. Material savings of 96% and time savings of around 60%-70% are achieved compared to measure cone calorimeter.

KEYWORDS

cone calorimeter, fire testing, high throughput, mass loss calorimeter, rapid mass calorimeter

1 | INTRODUCTION

Modern flame-retardant polymeric materials contain a variety of additives that make them multicomponent systems. Flame retardants, flame-retardant combinations, fillers, adjuvants, and synergists, as well as their concentration, particle size distribution, and so forth have an influence on burning behavior. Thus, accelerated screening methods are needed to find the best formulation in terms of fire performance for this large and complex multidimensional matrix. Because of limitations in time, materials, and therefore costs, no complete comprehensive elucidation of all possible formulations is possible. In the last decade the NIST (National Institute of Standards and Technology) worked on a larger project from which several ideas for high throughput fire tests emerged,[1–4] eg, fire testing based on a gradient heat flux and reduced specimen size, so that the fire performance of several formulations can be evaluated at once. Moreover, the rapid cone calorimeter was developed. For this, a cone calorimeter was equipped with a conveyor belt to provide a constant supply of reduced-size samples. Despite the great research potential illuminated in this project, the topic has not been pursued to a significant extent.

The same holds for other high-throughput approaches dealing successfully with large number of materials but stick to a singular work.[5] The pyrolysis combustion flow calorimeter (PCFC, also called the microscale combustion calorimeter) is the only method commercially available today that provides small-scale fast heat release rate (HRR) measurement via oxygen consumption.[6] However, its measuring principle and the nature of the milligram specimens limit the significance of the results obtained and thus the PCFC's field of application with respect to flame-retarded polymeric materials.[7,8] Certain important modes of action by flame retardants, like flame inhibition, changed dripping behavior, protection layer effects, and so on are not covered because of the combustion conditions, the milligram scale specimens, and the lack of a real flame.

Thus the task is to preserve the conditions of a fire test, such as diffusion flame, forced flaming conditions, and pyrolysis of a macroscopic specimen and transfer them to reduced-scale and accelerated testing without losing a good correlation. The basic principle of the rapid cone calorimeter was adopted and the rapid mass calorimeter developed and proposed to function as an accelerated kind of cone calorimeter testing. Moreover, the potential of the rapid mass

calorimeter as a high-throughput fire test is discussed for flame-retarded polymeric materials by investigating in detail the fire behavior of reduced-size specimens and a large variety of different materials.

2 | EXPERIMENTAL

2.1 | Rapid mass calorimeter

The principle of the rapid cone calorimeter is adopted, but to further reduce the time and effort demanded for steps such as maintenance and calibration, the rapid mass calorimeter was built, using a mass loss calorimeter (Fire Testing Technologies, UK) with a thermopile chimney attached according to ISO 13927.[9] Heat release rate is measured, but the balance was exchanged by a linear motion unit (Oriental motor, JP) with mounts for 2 sample holders located at a distance of 350 mm from each other from center to center and 250 mm edge to edge. This ensured a safe exchange of residues with new specimens while also preventing heat radiation from reaching the subsequent sample. The setup is illustrated in Figure 1A. The linear motion unit can be programmed for various purposes. For this research, a basic loop program was used to make measuring semiautomatic. A dwell time of 60 seconds for an empty specimen holder is used to record the HRR baseline, followed by a simple loop motion with certain dwell times in each position. While the automation is not the key factor when it comes to reducing the fire testing time, it certainly adds a level of comfort and improves repeatability. The main factor reducing fire testing time is the specimen size reduction. A specimen size of 20 mm × 20 mm and a dwell time of 200 seconds under the cone heater were chosen, as discussed in detail in Section 3 of this study. The measurements were done in triplicate. The user was responsible for exchanging the burned sample with a new specimen. Additionally, observation plays a significant role in describing the burning behavior of polymeric materials.

For safety reasons, the rapid mass calorimeter was enclosed in a housing. A box was built of 5-mm thick Isoplan 1100 ceramic fiber plates, able to withstand temperatures of up to 1100°C, as shown in Figure 1B. Built-in windows on each side allow for safe and easy sample handling as well as observation of the burning process, while additional ventilation holes ensure optimal air circulation. A detailed scheme of the sample holder linear motion unit is displayed in Figure 1C.

2.2 | Mass loss calorimeter and cone calorimeter

A mass loss calorimeter (Fire Testing Technologies, UK) with an attached thermopile chimney was used according to ISO 13927.[9] Square specimens of different sizes (edge length = 100, 75, 50, 25,

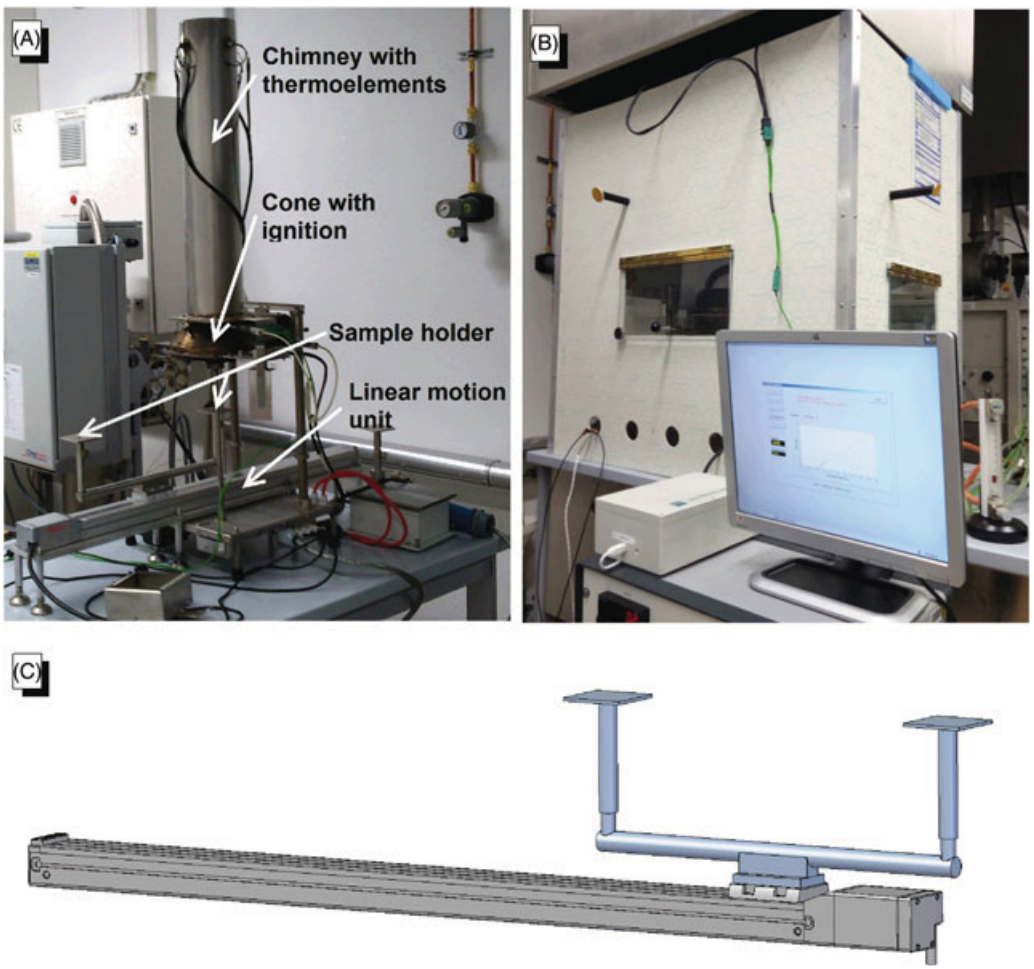

FIGURE 1 The rapid mass calorimeter; A, Setup with linear motion unit underneath mass loss calorimeter, B, Rapid mass calorimeter housing and data acquisition, and C, Construction schematics of the dual sample holder on the linear motion unit [Colour figure can be viewed at wileyonlinelibrary.com]

20, and 10 mm) were investigated. Cone calorimeter (FTT, UK) measurements were performed on specimens 100 × 100 mm in size with thicknesses between 3 and 10 mm according[10] to ISO 5660. The specimens, wrapped in an aluminum tray, were placed 25 mm under the cone heater and irradiated with a heat flux of 50 kW/m^2. All measurements took place without a retainer frame. The measurements were usually performed only in duplicate but in triplicate whenever any fire property showed a deviation between the first 2 measurements greater than 10%.

2.3 | Pyrolysis combustion flow calorimeter

All measurements with the PCFC were performed with a combustor temperature of 900°C and a pyrolyzer temperature gradient ranging from 150°C to 750°C, at a heating rate of 1 K/s. The specimen mass amounted to 5.00 ± 0.05 mg. For data analysis, a Gauss fit was performed on the obtained peak HRR (PHRR) to determine the heat release capacity (HRC = peak of the Gauss fit of the HRR/heating rate). In the case of multiple peaks, the values were summed up to obtain the HRC sum.[8,11] All PCFC measurements were done in triplicate, and the results averaged.

2.4 | Materials

A large number of different polymeric materials were tested, 71 in total (Table 1), including different polymers, woods, and halogen-free flame-retarded polymeric materials to provide maximum variety. Most of them were taken from former studies[8,12–23]; thus the attention of readers interested in more details on the individual materials and their processing is directed to these original studies. All of the investigated polymeric materials and corresponding test specimens were provided by partners with high competence in compounding and processing and showed sufficiently high quality. Certain formulations were examined in detail with the rapid mass calorimeter, PCFC, and cone calorimeter to reveal more about burning behavior and assist in the interpretation of the results. These materials were chosen for their characteristic HRR curve shapes in cone calorimeter tests,[24] which depend on their fire behavior and on the mode of action of the flame retardants used. For experiments on reduced-size specimens and method development, 5 polymers with different burning behaviors and performances were used, ranging from highly flammable polymers like poly(propylene) (PP) and poly(methyl methacrylate) (PMMA) over polyamide 66 (PA66) to intrinsically flame-retarded charring poly(ether ether ketone) (PEEK), and pine sapwood (WOOD).

2.5 | Correlation determination

Correlations were ascertained using a linear fit function. The Pearson correlation coefficient was used to measure the linear relationship between parameters, which can range from −1 to +1 for an exact negative or exact positive linear dependence, respectively.[25] Correlation coefficient strengths are defined in Table 2.

3 | RESULTS AND DISCUSSION

3.1 | Reducing specimen size

Size reduction of the specimen is the most crucial premise to accelerate testing. Unfortunately, since burning behavior is always the response of a defined specimen in a specific fire scenario, it changes with specimen size.[26,27] Thus, every development of a fire test featuring high throughput not only faces the dilemma that reducing specimen size is mandatory for speeding up testing but also gives rise to serious limitations. For scale reduction experiments, PMMA, PP, PA66, PEEK, and WOOD square plates with 6 different surface areas between 100 and 10 000 mm^2 were measured in the mass loss calorimeter. The results of this, depicted in Figures 2, 3, and 4, show that with decreasing specimen size, both the HRR per unit area and the absolute HRR reach much higher values than expected when the surface area is decreased. Because of an edge burning effect and the horizontal spread of the flame across the surface of the entire sample, the thermopile encounters much greater thermal impact than expected for the corresponding surface area of the top of the specimen. In fact, the ratio of flame size to specimen size increases with smaller samples, leading to very high peaks for the smallest specimen, with a surface of 10 × 10 mm^2. This effect is depicted in Figure 5, where PHRR and total heat evolved (THE) are plotted versus the surface area of the top of the specimen. With decreasing specimen size, the deviations rise. This is more distinct for strongly burning materials like PP than for more intrinsically flame-retarded materials such as WOOD and PEEK. In Figures 2, 3, and 4, the HRR curves are depicted as HRR per unit area as well as in absolute values. This way, the obtained results clearly show the change in burning intensity, the basic HRR curve shape, and thus the change in burning behavior with different specimen sizes.

Experiments on PEEK specimens of varying sizes in the mass loss calorimeter show an interesting change in HRR curve shape (Figure 2). Standard-sized specimens with an edge length of 100 mm show a distinct, steadily burning plateau in which the rates of char formation and fuel release are in equilibrium. Decreasing the specimen size shifts this equilibrium in favor of fuel release. Because of the edge burning effect, char formation is no longer sufficient to provide this balance. With a specimen size of 50 × 50 mm, the steady-burning plateau changed into a shoulder still indicating this effect, whereas this did not occur in smaller specimens. Nevertheless, the good fire performance of PEEK is still exhibited in smaller specimens and can be evaluated. Polyamide 66 (Figure 3) and PMMA (Figure 4) show simpler curve shapes, which remain more or less unchanged with decreasing specimen size.

To increase the significance of burning behavior results and their interpretation, we conducted experiments on reduced-size specimens not only on pure polymers and nonflame–retarded materials but also on an intumescent flame-retarded system. The HRR curve behavior shows a characteristic initial peak followed by a minimum (Figure 6). The material burns until a protective layer is formed, which hinders the fuel from reaching the flame. After a while, the protective layer cracks and the flame is again provided with fuel until depletion. This is shown in the HRR by a maximum. When specimen size is decreased, those characteristics are lost. With an edge length of

TABLE 1 Polymeric materials and their thicknesses used for the investigation of reduced-size specimens, to develop the measuring protocol for the rapid mass calorimeter, comparison between rapid mass calorimeter, the PCFC and cone calorimeter, and materials measured in the rapid mass calorimeter and the cone calorimeter

Material	Label	Thickness, mm
Experiments on Reduced-Size Specimens		
Poly(methyl methacrylate)	PMMA	3
Poly(propylene)	PP	3
Polyamide 66 (Ultramid® A3)	PA66	3
Poly(ether-ether ketone)	PEEK	4
Pine sapwood	WOOD	5
Comparing rapid mass calorimeter with cone calorimeter and PCFC		
PA66/35 wt.-% glass fiber	PA66-35GF	3
PA66/35 wt.-% GF + red phosphorus	PA66-35GF-RP	3
Bisphenol A polycarbonate/acrylonitrile butadiene styrene/Polytetrafluoroethylene	PCABS/TF	3
PC/ABS/TF + resorcinol bis(diphenyl phosphate)	PCABS/TF-RDP	3
PC/ABS/TF + triphenyl phosphate	PCABS/TF-TPP	3
Styrene Ethylene Butylene Styrene/PP/mineral oil/antioxidant	TPES	5.8
TPES +30 wt.-% aluminum diethyl phosphinate	TPES-30AlPi	5.8
Polyamide 12	PA12	4
PA12 + 30 wt.-% GF	PA12-30GF	4
Poly(butylene terephthalate)	PBT	5
PBT + 30 wt.-% GF	PBT-30GF	5
PP + 25 wt.-% ammonium polyphosphate	PP-25APP	3
PP + 25 wt.-% coated APP	PP-25APP*	3
PP + 20 wt.-% APP*	PP-20APP*	3
PP + 30 wt.-% flax	PP-30FLAX	4
PP + 30 wt.-% flax 25 wt% APP	PP-30FLAX-25APP	4
Cone calorimeter and rapid mass calorimeter		
PP + 30 wt.-% flax +25 wt.-% expandable graphite	PP-30FLAX-25GR	4
PP + 30 wt.-% Flax +15 wt.-% EG	PP-30FLAX-15EG	4
PA66 + 25 wt.-% GF + RP	PA66-25GF-RP	3
PA66 + 25 wt.-% GF + RP + rubber	PA66-25GF-FR-Rubber	3
PC/ABS/TF + 5 wt.-% Talk + BDP	PCABS-TF-5 T-BDP	3
PC/ABS/TF + 20 wt.-% Talk + BDP	PCABS-TF-20 T-BDP	3
PC/ABS/TF + 10 wt-% Talk + zinc borate + BDP	PCABS-TF-10 T-ZnB-BDP	3
PC/ABS/TF + BDP	PCABS-TF-BDP	3
PA66 + 20 wt.-% Sidistar® T 120	PA66-20SID	4
PA12 + 20 wt.-% SID	PA12-20SID	4
High-density poly(ethylene) (Hostalen® GM 5050)	HDPE3mm	3
HDPE	HDPE6mm	6
HDPE +15 wt.-% $Mg(OH)_2$	HDPE3mm-15MDH	3
HDPE +15MDH	HDPE6mm-15MDH	6
HDPE +30 wt.-% MDH	HDPE3mm-30MDH	3
Pine	PINE	10
Beech Belmadur	BELMA	10
Pinus radiata	PINUS	10
Accoya	ACCO	10
Flame retarded PCABS (Bayblend® FR 3005)	BayblendFR3005	4
Flame retarded PCABS (Bayblend® FR 2000)	BayblendFR2000	4
Flame retarded PCABS (Bayblend® FR 3000)	BayblendFR3000	4
Flame retarded PCABS (Bayblend® FR 3030)	BayblendFR3030	4
Flame retarded PCABS (Bayblend® KU 2–1514)	BayblendKU2–1514	4
Epoxy resin (Araldite® GY 250/Aradur® 250, 2:1)	EP	5

(*Continues*)

TABLE 1 (Continued)

Material	Label	Thickness, mm
EP + 5 wt.-% layered silicate (Nanomer® I.30E)	EP-5NANO	5
EP + 5 wt.-% layered silicate +7 wt.-% SID	EP-5NANO-7SID	5
Poly(vinyl chloride) + 5 wt.-% ZnS	PVC-5ZnS	4
PBT + AlPi	PBT-AlPi	5
PBT + 30 wt.-% GF	PBT-30GF	4
Low density poly(ethylene) (LD 615BA)	LDPE	4
Polystyrene (Lacqrene 1810)	PS	4
Impact-resistant PP (Moplen) + 5 wt.-% expanded graphite	EP300K-5EG60	3
EP300K + 5 wt.-% multilayer graphene (BET =350 $m^2 g^{-1}$)	EP300K-5MLG350	3
PC/ABS	PCABS	3
PC/ABS + BDP	PCABS-BDP	3
PC/ABS + TF	PCABS-TF	3
PC/ABS + TF + 1 wt.-% boehmite + BDP	PCABS-TF-1Al-BDP	3
PP + 53 wt.-% $Mg(OH)_2$	PP-53MDH	3
PP + 53 wt.-% $Mg(OH)_2$ + 1 wt.-% thermally reduced graphite oxide	PP-53MDH-1TRGO	3
PP + 54 wt.-% $Mg(OH)_2$	PP-54MDH	3
PP + 54 wt.-% $Mg(OH)_2$ + 1 wt.-% TRGO	PP-54MDH-1TRGO	3
PP + 59 wt.-% $Mg(OH)_2$	PP-59MDH	3
PP + 59 wt.-% $Mg(OH)_2$ + 1 wt.-% TRGO	PP-59MDH-1TRGO	3
Flame retarded polystyrene (FR 3180)	PS4	3
Shorea bracteolata	MERANTI	10
Chipboard	CHIP	10
TPE-S + 30 wt.-% APP	TPES-APP	5.8
TPE-S + 30 wt.-% AlPi	TPES-AlPi	5.8
TPE-S + 7.5 wt.-% APP +22.5 wt.-% EG	TPES-APP-EG	5.8
TPE-S + 50 wt.-% $Mg(OH)_2$	TPES-MDH	5.8
TPE-S + 15 wt.-% APP +7.5 wt.-% AlPi +7.5 wt.-% dipentaerythritol	TPES-APP-AlPi-DiPer	5.8
TPE-S + 6.2 wt.-% APP* + 18.7 wt.-% EG + 5 wt.-% AlPi	TPES-APP*-EG-AlPi	5.8
TPE-S + 6.2 wt.-% APP +18.7 wt.-% EG + 5 wt.-% AlPi	TPES-APP-EG-AlPi	5.8
TPE-S + 30 wt.-% $Mg(OH)_2$ + 2.5 wt.-% ZnB + 2.5 wt.-% glass frits +10 wt.-% EG + 5 wt.-% APP	TPES-MDH-ZB-GF-EG-APP	5.8

Abbreviation: PCFC, pyrolysis combustion flow calorimeter.

TABLE 2 Pearson correlation coefficient R definition

Correlation Strength	Pearson R
Strong	$0.85 \leq \lvert R \rvert$
Moderate	$0.70 \leq \lvert R \rvert < 0.85$
Marginal	$0.55 \leq \lvert R \rvert < 0.70$
Weak	$0.40 \leq \lvert R \rvert < 0.55$
Poor	$\lvert R \rvert < 0.40$

75 mm, an initial peak due to the protective layer formation is visible in the form of a shoulder. For smaller specimen sizes, only 1 broad peak is observable. Because of the edge burning effect, the protective layer is not capable of creating a sufficient barrier between fuel and flame, which leads to continuous fuel support. Nevertheless, the intumescent flame retardant still broadens and thus decreases the HRR in smaller samples.

A specimen size of 20 mm × 20 mm was proposed to be used as the standard size for rapid mass calorimeter testing. It is proposed to achieve crucial reduction in materials needed for testing and burning time but still offer repeatability and reliability of the results. Obviously, larger samples, such as 50 mm × 50 mm, offer a burning behavior more similar to cone calorimeter test results but would lack with respect to the goal of the publication. At the end of the day, it is a compromise between loosing similarities with the cone calorimeter results and gaining a benefit of accelerated testing. Going for 20 mm × 20 mm seems to max out the limits in the investigated samples (Figures 2–6) and is a clear alternative to standard-sized cone calorimeter testing. Only 4% of a standard cone calorimeter test specimen is used, providing significant savings in material.

3.2 | Rapid mass calorimeter

To develop the method and measurement procedure, the same set of 5 materials were used as for the experiments on reduced-size specimens. The method had to be developed to ensure complete burning of the specimen and optimal time savings. For this, the linear motion unit was programmed for different dwell times under the cone heating unit. These times depended strongly on the burning time of the material to be tested. Figure 7 shows HRR curves and residues for sample series with different dwell times under the cone heater. With a dwell time of

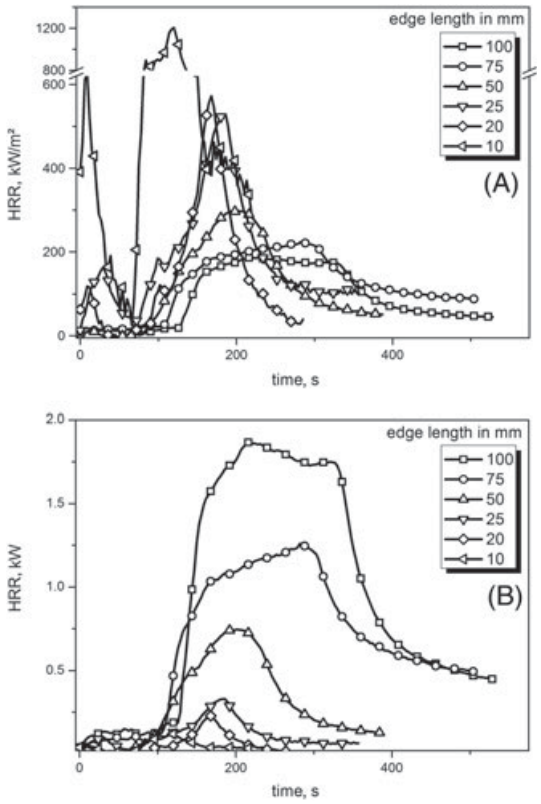

FIGURE 2 A, HRR per unit area in kW/m^2 and B, HRR in kW for various sizes of PEEK specimens. HRR, heat release rate; PEEK, poly(ether ether ketone)

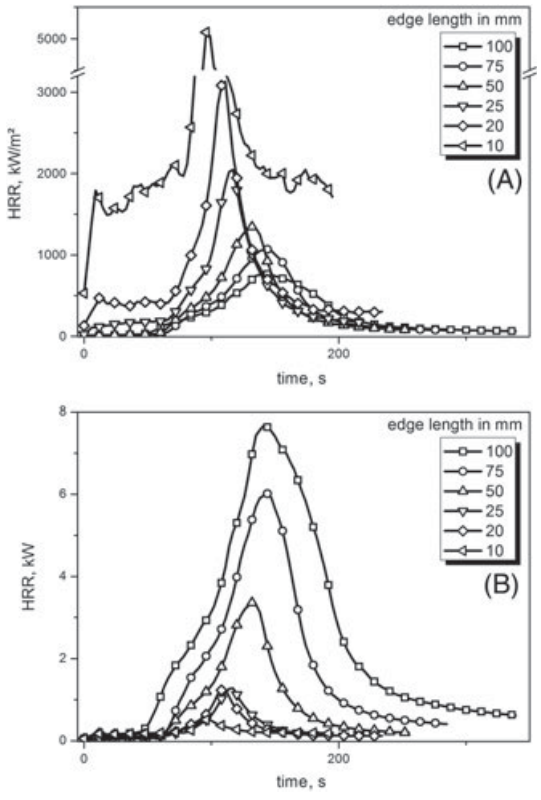

FIGURE 3 A, HRR per unit area in kW/m^2 and B, HRR in kW for various sizes of PA66 specimens. HRR, heat release rate; PA, Polyamide 66

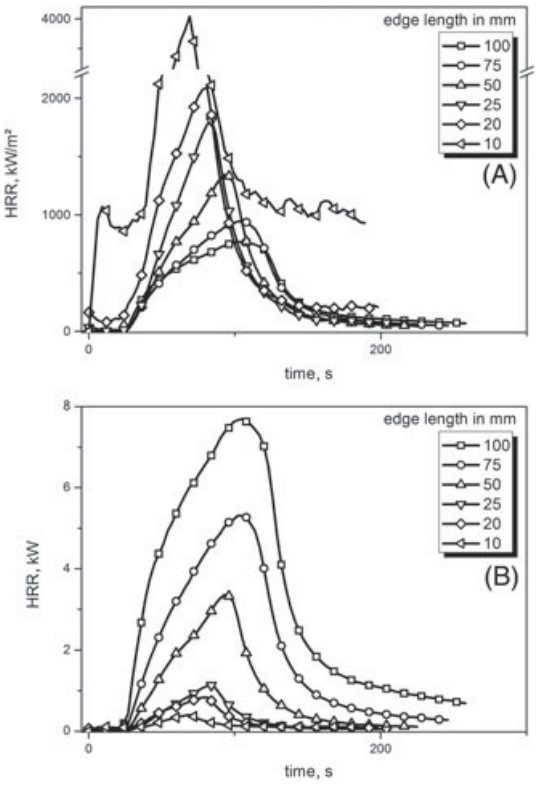

FIGURE 4 A, HRR per unit area in kW/m^2 and B, HRR in kW for various sizes of PMMA specimens. HRR, heat release rate; PMMA, poly(methyl methacrylate)

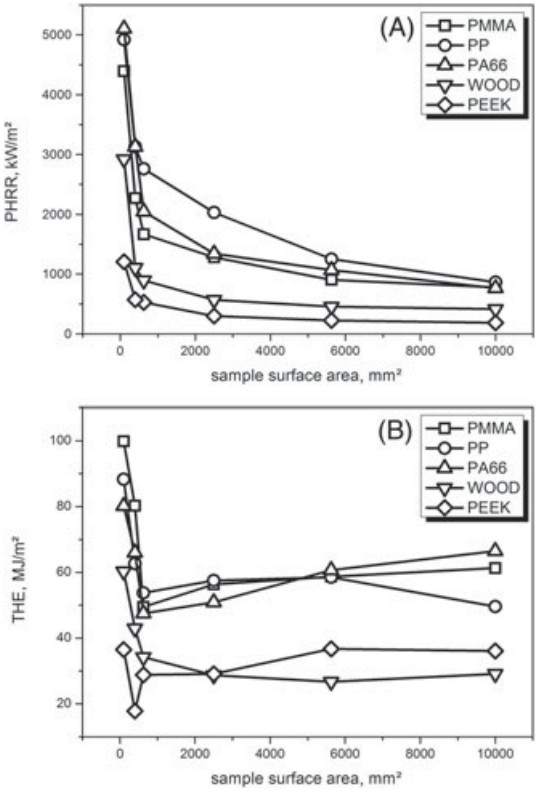

FIGURE 5 A, PHRR and B, THE of PMMA, PP, PA, WOOD, and PEEK plotted versus specimen size. PA, Polyamide; PEEK, poly(ether ether ketone); PHRR, peak heat release rate; PMMA, poly(methyl methacrylate); PP, poly(propylene); THE, total heat evolved; WOOD, pine sapwood

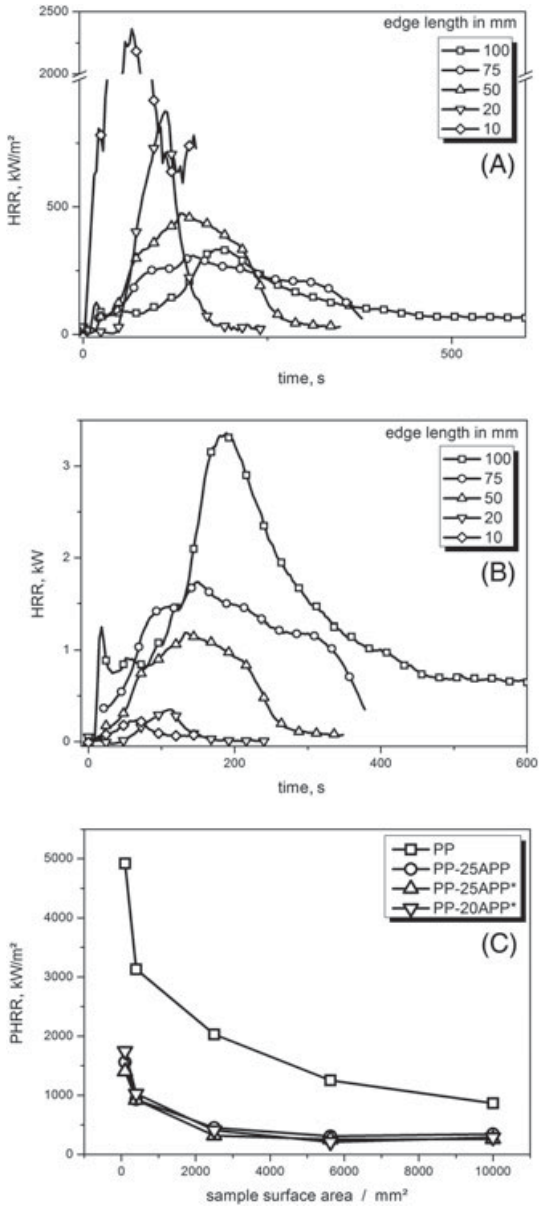

FIGURE 6 A, HRR per unit area in kW/m^2, B, HRR in kW of the intumescent flame-retarded PP-25APP specimen in various sizes, and C, PHRR plotted versus specimen size for 3 different intumescent PP-25APP, PP-25APP*, and PP-20APP* compared to PP. HRR, heat release rate, PHRR, peak heat release rate

100 seconds complete burning of PA66 is not ensured, which is apparent in the residue picture as well as in the low HRR peak. Since PEEK has a long time to ignition, a dwell time of 100 seconds is much too short even to show a change in HRR. By extending the dwell time to 150 seconds, both PA66 and PEEK are allowed to burn completely. However, the time is not long enough to allow the HRR to revert back to the baseline. Thus, a dwell time of 200 seconds was concluded to be optimal for this set and order of samples. A longer dwell time of 250 seconds was deemed unnecessary because it needlessly increased testing time.

Because repeatability was good, the rapid mass loss calorimeter seems to be a suitable tool to clearly rank the fire risks of different polymers (Figure 8). Uncertainty was below 6% for the PHRR and less than 5 seconds for time to ignition. Analogous to cone calorimeter, for several kinds of materials measuring in duplicate may be enough.

At first glance, the HRR curves produced (Figure 8) are similar to results obtained from PCFC,[28] but upon close examination, they are not. Most polymers measured in PCFC result in only 1 peak, which is then evaluated using a peak fit function. Multicomponent systems usually show more than 1 peak in PCFC, a result of the diverse decomposition temperatures of the different components. Evaluation becomes more complicated, especially when peaks overlap. At the end of the day, the HRR curve measured in PCFC is controlled by the pyrolysis steps.[8] In contrast, HRR curves from rapid mass calorimeter measurements show characteristics that are connected to their burning behavior under forced flaming combustion. As depicted in Figure 8, the HRR curve of PMMA shows a shoulder prior to reaching the PHRR. This is the result of the pyrolysis front moving, similar to fire behavior in the cone calorimeter. For thicker samples, HRR reaches a steady burning plateau until a specific thermal thickness is reached. Other characteristics like peak broadening for PEEK or prolonged decay are also observed in the rapid mass calorimeter, just as in the cone calorimeter.

As a consequence, the rapid mass calorimeter harbors the potential to screen not only polymers such as PP, PA66, PMMA, PEEK, and WOOD but also flame-retarded polymeric materials with less simple burning behavior. A first test series of flame-retarded polymeric materials was investigated, consisting of 3 different intumescent PP/ammonium polyphosphate (APP) formulations, PA12, PA12-30GF, and PVC-5ZnS (Figure 9). The PHRR, THE, and other parameters of the HRR curve showed tendencies similar to those reported for the cone calorimeter results and clear differences in pyrolysis.[13,21] The PHRR

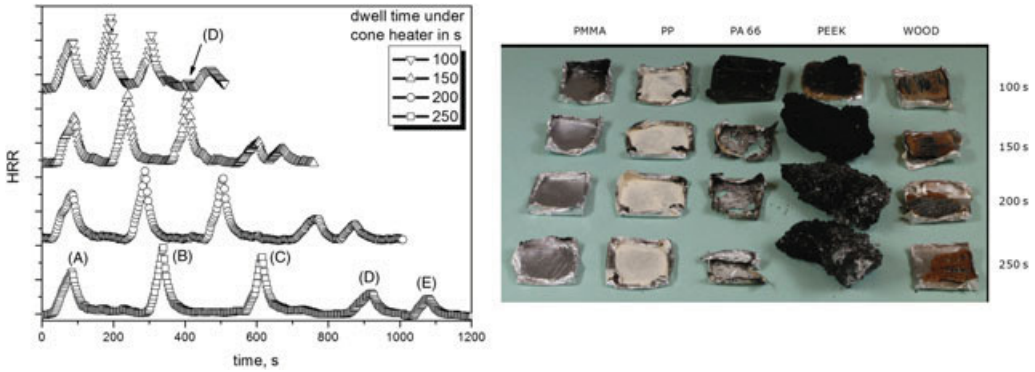

FIGURE 7 The HRR curves and residues of a sample series consisting of A, PMMA, B, PP, C, PA66, D, PEEK, and E, WOOD measured in the rapid mass calorimeter with the linear sample changer set to different dwell times. HRR, heat release rate; PA, Polyamide 66; PEEK, poly(ether ether ketone); PMMA, poly(methyl methacrylate); PP, poly(propylene); WOOD, pine sapwood [Colour figure can be viewed at wileyonlinelibrary.com]

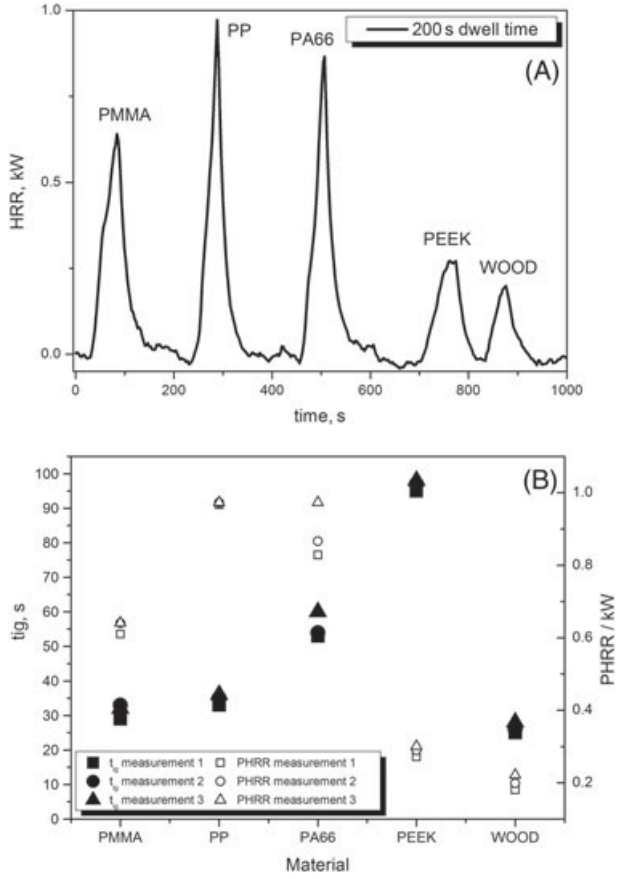

FIGURE 8 A, Rapid mass calorimeter sample series of selected pure polymers and B, Repeatability for PHRR and t_{ig} of this series. PHRR, peak heat release rate; HRR, heat release rate; PA, Polyamide 66; PEEK, poly(ether ether ketone); PMMA, poly(methyl methacrylate); PP, poly(propylene); WOOD, pine sapwood

of PA12 and PA12-GF were greater than that of the others; PA12-GF showed a shoulder. The PHRR of PP-25APP was a little bit higher than that of PP-25APP* but less than that of PP-20APP*, while PVC-5ZnS produced the smallest but broadest peak. These characteristics

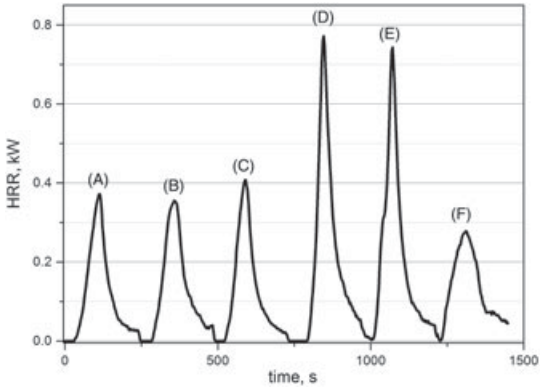

FIGURE 9 The HRR measured with the rapid mass calorimeter for a series of filled and flame retarded polymers: A, PP-25APP, B, PP-25APP*, C, PP-20APP*, D, PA12, E, PA12-30GF, and F, PVC-5ZnS. HRR, heat release rate

TABLE 3 Pyrolysis combustion flow calorimeter results

Sample	T@PHRR, °C	HR, kJ/g	HRC, J/g-K	Residue, wt.-%
PA66	465 ± 5	30 ± 1	655 ± 19	1
PA66-GF35	455 ± 3	18 ± 1	363 ± 1	36
PA66-GF35-FR	390 ± 11	18 ± 1	286 ± 11	36
PA12	475 ± 5	35 ± 1	902 ± 30	0
PA12-GF	477 ± 3	31 ± 1	858 ± 12	10
PBT	419 ± 1	22 ± 1	607 ± 8	5
PBT-30GF	420 ± 3	16 ± 1	415 ± 1	34
TPES	447 ± 1	43 ± 1	548 ± 25	0
TPES-30AlPi	440 ± 10	37 ± 1	493 ± 20	3
PP	473 ± 1	43 ± 1	1114 ± 11	0
PP-25APP	480 ± 2	33 ± 1	861 ± 10	11
PP-25APP*	480 ± 1	33 ± 1	860 ± 20	11
PP-20APP*	480 ± 1	34 ± 1	900 ± 30	9
PP-30FLAX	477 ± 7	33 ± 1	863 ± 16	5
PP-30FLAX-25APP	482 ± 4	18 ± 1	514 ± 7	23

TABLE 4 Cone calorimeter and rapid mass calorimeter test results

	Cone Calorimeter			Rapid Mass Calorimeter		
Sample	PHRR, kW/m^2	THE, MJ/m^2	Residue, wt.-%	PHRR, W	THE, kJ	Residue, wt.-%
PA66	1509 ± 10	100 ± 2	0	1102 ± 27	35 ± 1	0
PA66-GF35	582 ± 3	80 ± 1	34	377 ± 25	15 ± 1	28
PA66-GF35-FR	299 ± 10	66 ± 2	43	233 ± 15	12 ± 1	35
PA12	2205 ± 70	164 ± 1	0	832 ± 60	31 ± 2	0
PA12-GF	1992 ± 50	153 ± 2	10	800 ± 40	33 ± 2	11
PBT	2523 ± 37	112 ± 1	1	571 ± 30	16 ± 1	2
PBT-30GF	690 ± 10	84 ± 1	30	294 ± 25	23 ± 1	27
TPES	2346 ± 140	215 ± 4	0	779 ± 6	29 ± 1	0
TPES-30AlPi	1048 ± 35	160 ± 2	1	623 ± 5	38 ± 3	0
PP	2349 ± 90	123 ± 2	0	1252 ± 90	63 ± 2	0
PP-25APP	345 ± 14	95 ± 2	16	373 ± 34	20 ± 1	17
PP-25APP*	260 ± 20	93 ± 4	16	370 ± 34	24 ± 2	17
PP-20APP*	288 ± 4	101 ± 1	8	411 ± 38	22 ± 1	17
PP-30FLAX	809 ± 40	138 ± 10	2	389 ± 36	28 ± 2	5
PP-30FLAX-25APP	363 ± 14	99 ± 3	21	251 ± 23	25 ± 2	33

indicate the potential of this method to be used in screening various flame-retarded polymeric materials. This point is discussed in detail in the following.

3.3 | Comparison of rapid mass calorimeter, PCFC, and cone calorimeter results

To clarify the differences between the rapid mass calorimeter and PCFC, we compared the results of both methods with the state-of-the-art cone calorimeter fire testing method. For this comparison, the compounds listed in Tables 1, 3, and 4 were used, with the premise of providing variety in the HRR curve shapes from cone calorimeter experiments. The HRR behavior is conditional on the underlying mode of action of the flame retardant incorporated in the respective compound. Hence, the gas phase inhibiting effect of the flame-retardant aluminum diethyl phosphinate (AlPi) in styrene based thermoplastic elastomer (TPES) will show a different characteristic HRR curve than, for instance, a flame retardant inducing intumescence like APP in PP.

Inert fillers like glass fibers often show a characteristic HRR curve in the cone calorimeter (Figure 10). The PA66-30GF shows a PHRR at the beginning of burning, where the polymer matrix burns until a glass fiber mat builds up a kind of protective layer at the top of the burning specimen. The protective effect of this fiber mat reduces fuel transport to the flame, which shows as a plateau in the HRR. Compared to PA66, the PHRR of PA66-30GF is reduced by more than 50%. When the char-inducing flame-retardant red phosphorus is added, PHRR is again reduced to around 50% and the HRR curve shape shows characteristic behavior for a charring material.[12]

Although the same formulations measured with the rapid mass calorimeter show similar PHRR reductions, their curve shapes differ

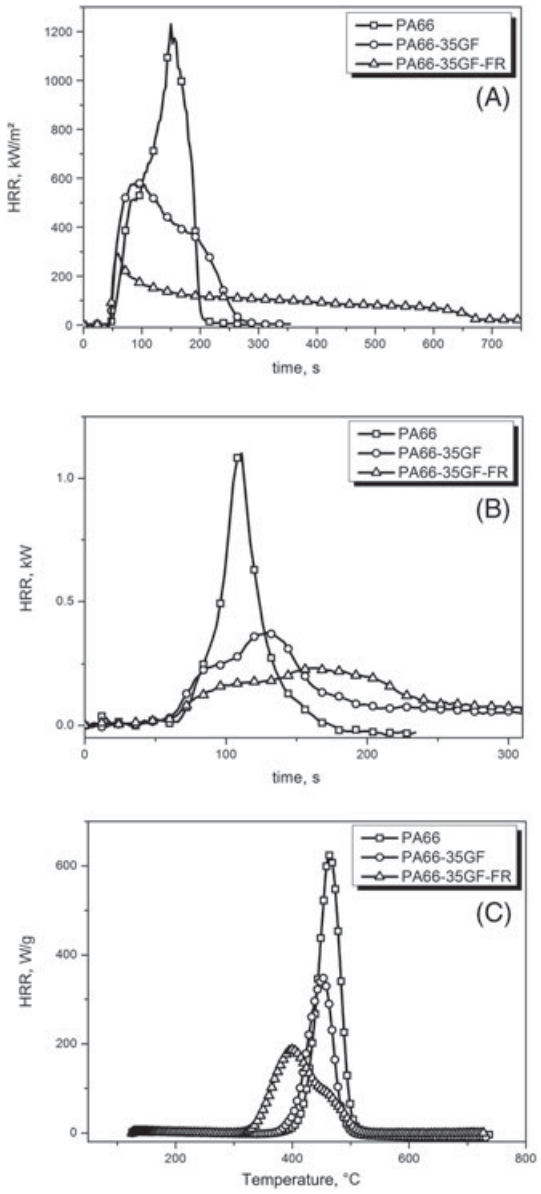

FIGURE 10 A, Cone calorimeter, B, Rapid mass calorimeter, and C, PCFC HRR curves for flame-retarded and nonflame–retarded glass fiber reinforced polyamide 66. PCFC, pyrolysis combustion flow calorimeter; HRR, heat release rate

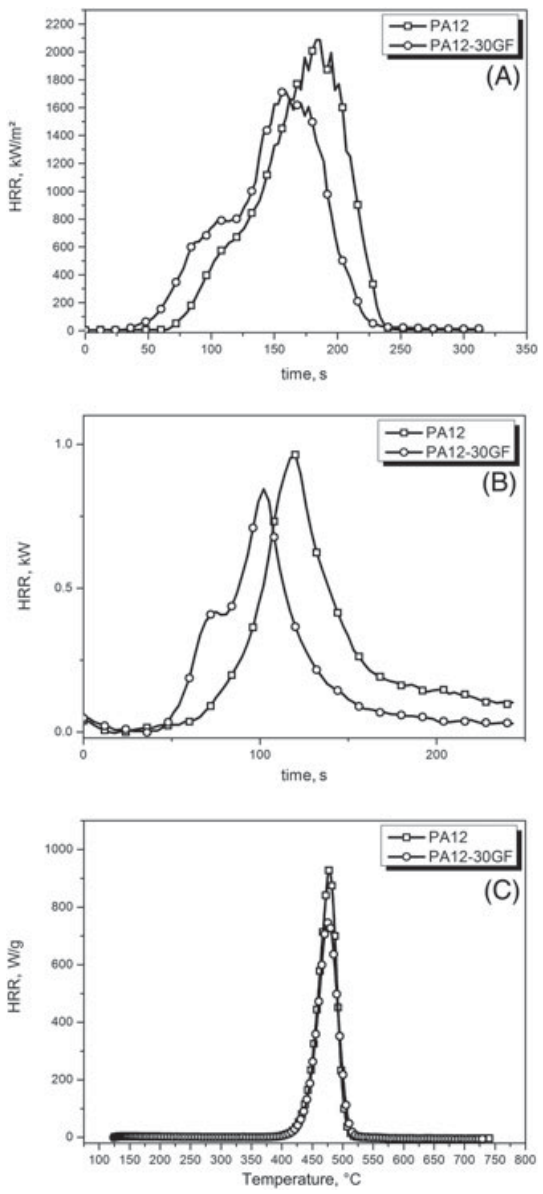

FIGURE 11 The HRR curves of PA12 and PA12 reinforced with 30% glass fiber derived from A, Cone calorimeter, B, Rapid mass calorimeter, and C, PCFC. PCFC, pyrolysis combustion flow calorimeter; HRR, heat release rate

somewhat from cone calorimeter measurements. Nevertheless, they still have the ability to display the different flame-retardancy effects. The addition of inert glass fiber filler results in a HRR curve that shows a shoulder prior to its PHRR. The glass fiber mat produced during burning is not as efficient at preventing fuel supply to the flame as it was in the cone calorimeter test. Because of the edge burning effect, fuel provided by the polymer matrix evades the protective glass fiber mat and produces the peak in HRR at the end of the curve. The addition of red phosphorus leads to a general reduction in HRR. In comparison to cone calorimeter results, the increased charring has less influence on the burning behavior due to the edge burning effect.

The PCFC showed a reduction in HRR for PA66-35GF and PA66-35GF-FR but does not allow burning behavior to be interpreted. The PA66 and PA66-35GF showed 1 peak according to their pyrolysis; the reduction for PA66-35GF is due to the replacement of fuel. Since the PCFC monitors the HRR per specimen mass, 35GF resulted in a 35% reduction, a level found in hardly any fire test. Adding red phosphorus to PA66 has been reported to separate the different pyrolysis steps and result in a 2-step decomposition pathway.[12] The change in pyrolysis controlled the change in HRR monitored by the PCFC.

In the cases of PA12 and PA12-30GF, the HRR curves observed in the cone calorimeter and rapid mass calorimeter are very similar (Figure 11). The PA12-30GF shows a shortened time to ignition, a shoulder prior to the maximum, and a reduced PHRR compared to PA12. The glass fiber mat produced is less efficient in PA12 than in the PA66 discussed above and shows the same effect on the HRR curve in the cone calorimeter as it does in the rapid mass calorimeter. Besides the slight reduction in PHRR, a plateau prior to the peak was introduced. Thus, the protective layer effect is overshadowed and the HRR increases again until all material is consumed.

An HRC decrease from pure PA12 to glass fiber–reinforced PA12 is evident in PCFC and in the same range as the PHRR decreases in the

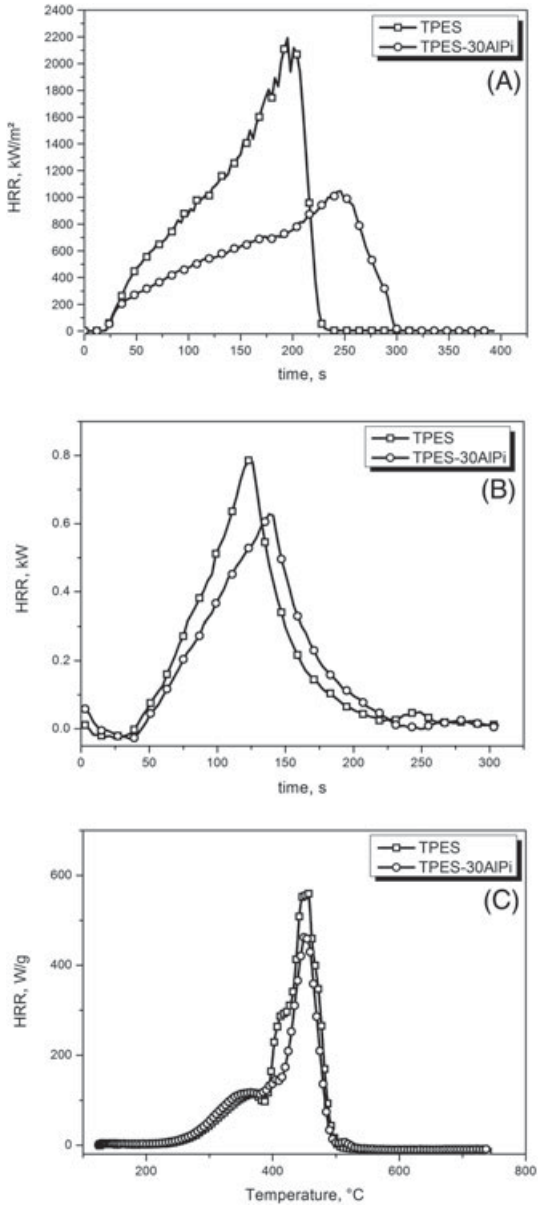

FIGURE 12 A, Cone calorimeter, B, Rapid mass calorimeter, and C, PCFC HRR curves of TPES and 30% AlPi flame-retarded TPES. HRR, heat release rate; PCFC, pyrolysis combustion flow calorimeter; TPES, thermoplastic elastomers

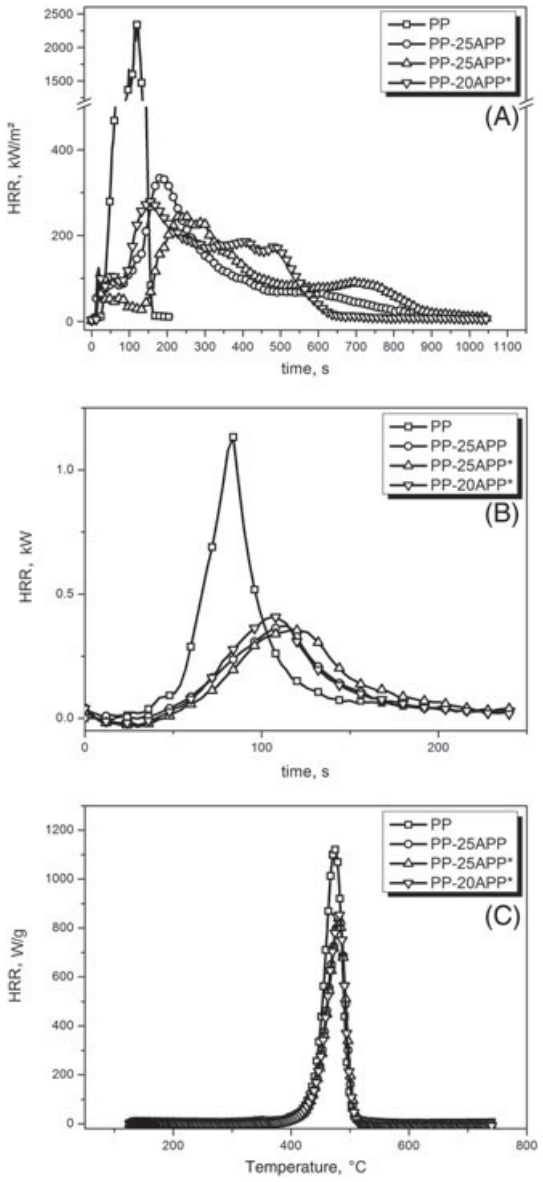

FIGURE 13 The HRR curves of intumescent PP-APP formulations from A, Cone calorimeter, B, Rapid mass calorimeter, and C, PCFC. HRR, heat release rate; PCFC, pyrolysis combustion flow calorimeter

rapid mass calorimeter. In PCFC, this effect is attributed solely to the replacement of fuel with inert filler. No flame-retardant mechanism is identifiable. Neither did an earlier heat release occur nor was there a change to a more structured HRR curve.

A typical HRR curve for a flame-inhibiting mode of action is found in the system TPES/30AlPi.[20] In cone calorimeter experiments, the most obvious difference, besides the lowered PHRR, is the decrease in slope and the corresponding prolonged time until flameout (Figure 12). The basic shape of the HRR curve is not changed, since only combustion efficiency is reduced in the gas phase. The AlPi flame retardant did not show any activity in the solid phase since no significant residue was formed. Rapid mass calorimeter experiments show a similar curve progression. The PHRR reduction, slope reduction, and prolonged time to flameout are not as distinct as in the cone calorimeter; nevertheless, the effect of the flame retardant is observed. Since the change in curve behavior is the same as in the cone calorimeter tests, the mode of action of the flame retardant is deducible even without knowledge of the standard scale results.

In contrast, PCFC results showed complex HRR curves that are rather difficult to interpret. The multicomponent TPES showed several decomposition steps with increasing temperature, which exhibit differences in intensity and width. Introducing AlPi increased the complexity of the HRR curve and decreased the overall HRC. The second main decomposition step is decreased and an additional decomposition step introduced after the main decomposition.

Different PP/APP formulations were examined with regard to their characteristic HRR curve progressions (Figure 13). The different stages of the burning process in cone calorimeter experiments have already been explained in Section 3.1. Compared to PP, great improvement in burning performance was achieved. The PHRR was reduced by up to 90% when loaded with 25 wt.-% APP*. Simultaneously, time to flameout was increased many times over. Additionally, one is able to describe the differences in HRR progression occurring because of encapsulation of APP or reduction of load by 5 wt.-%. It is obvious that encapsulation not only reduces PHRR and THE but is also capable of extending the time until the protective layer suffers cracks, thus prolonging the plateau at the minimum of the HRR curve. Furthermore, the decay of HRR is prolonged as well. Comparing 25 wt.-% APP with 20 wt.-% of encapsulated APP* shows a reduction of PHRR caused by encapsulation but a shorter time to flameout. The THE is higher with lower APP load.

Compared to the cone calorimeter, rapid mass calorimeter measurements allow for similar conclusions despite some differences in HRR. Compared to PP, a pronounced reduction in PHRR occurred because of the protective layer effect. The time to PHRR is prolonged as well. There is no significant reduction in PHRR between 25% nonencapsulated and encapsulated APP. Nevertheless, the HRR curve of PP-25APP* is broader and shows a longer decay than that of PP-25APP. Decreasing the load from 25% APP* to 20% APP* leads to an increased PHRR and a shortened burning time.

The PCFC test results do not contain much valuable information. Compared to PP, the HRC was reduced but only by around 20% and 25%. Because the PCFC measures the HRR per specimen mass, the replacement of fuel was monitored well, whereas the protective layer effect did not occur on the milligram scale. The time to PHRR was not prolonged as in the cone calorimeter and the rapid mass calorimeter. The 3 flame-retarded formulations show almost no difference at all in HRC and heat release per specimen mass (HR). The PCFC allows pyrolysis to be analyzed but cannot account for residue properties, which affect a flaming combustion. It is not possible to find the best performing formulation using the PCFC alone.

Another example of a characteristic HRR curve is exhibited in PP-30FLAX (Figure 14). The addition of 30 wt.-% flax leads to a lowering of the PHRR to about 30% that of PP; THE was not significantly changed, and 5 wt.-% residue was formed. What is most remarkable is the change in the HRR curve shape from 1 high peak to 2 peaks with a local minimum in between. Since 30 wt.-% of noncharring PP was replaced by flax, a residue was formed, leading to a reduction in PHRR at the beginning of burning. Since flax is not an inert filler, it still contributes to oxygen consumption during burning. Cracking of the char during later stages of combustion

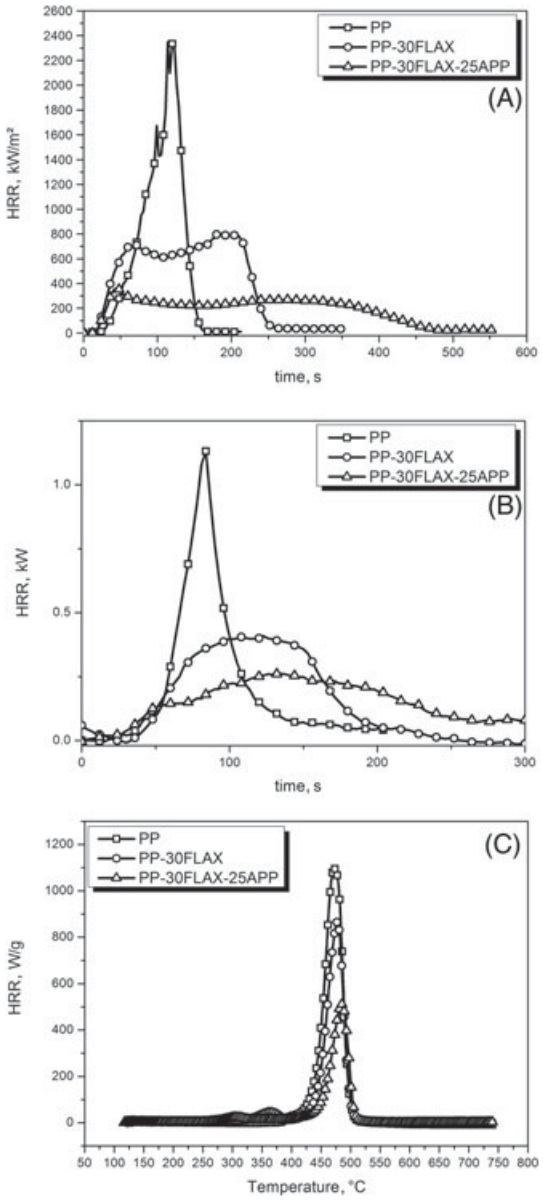

FIGURE 14 The HRR curves of PP, PP-30FLAX, and PP-30FLAX-25APP derived from A, Cone calorimeter, B, Rapid mass calorimeter, and C, PCFC. HRR, heat release rate; PCFC, pyrolysis combustion flow calorimeter

explains the formation of the second peak. Inclusion of the intumescent flame-retardant APP reduces the PHRR to around 40% than that of PP-30FLAX and changes the HRR curve yet again. As typical for intumescent systems, the curve shows an initial rise in HRR, after which the protective layer is formed. In contrast to the previously observed PP-APP systems, no second peak occurs in the system PP-30FLAX-25APP. This plateau of steady burning results from a compact intumescent layer, which is not prone to cracking. Because of this flame-retardancy effect, fuel can reach the flame only on the area of transition from pyrolyzing material to combusted material around the edges of the specimen.

The rapid mass calorimeter shows similar fire behavior under forced flaming combustion conditions. However, neither the 2 peaks for PP-30FLAX nor the sharp initial peak from PP-30FLAX-25APP is found in the HRR curves. Instead, added flax filler leads to a broadening of the peak, perhaps averaging and scaling down the HRR curve monitored in the cone calorimeter. The same applies to the intumescent system, in which instead of the initial peak and the relatively low steady-burning plateau, an even broader peak results with the remnant of the initial peak in the form of a small shoulder with a subsequent plateau around the 60- to 70-second mark.

The PCFC measurements show a reduction of 23% in HRC as well as HR from pure PP to PP-30FLAX. Addition of 25% APP leads to further HRC reduction of 40% and HR reduction of 45%. The reductions are mainly the result of the replacement of PP with additive. Flax fibers alone were shown to decompose under equal conditions at a temperature of around 350°C.[29] This decomposition step appears in the PCFC HRR curve for PP-30FLAX, whereas in PP-30FLAX-25APP, it is shifted to lower temperatures and results in an elevation of the baseline until decomposition of PP starts. The PCFC measurements alone do not provide significant representation of the flame-retarding potential of flax incorporated in a polymer like PP. Addition of the intumescence-inducing flame-retardant APP increases performance in the PCFC, but results do not allow for conclusions about the underlying mode of action.

All the comparisons discussed demonstrate that using 20 mm × 20 mm specimen, the rapid mass calorimeter still monitors the macroscopic burning behavior of a plate specimen but deteriorated particular by edge burning effects.

3.4 | Correlation between rapid mass calorimeter and cone calorimeter

Correlation coefficients between parameters (Table 5) derived from rapid mass calorimeter and state-of-the-art cone calorimeter were analyzed to yield insight into the significance and reliability of the results and allow to detect and explain coherencies and differences between the 2 methods. They also show which parameters are most suited for comparison in a screening with the rapid mass calorimeter.

Since all parameters are derived over all of the 71 samples, many different flame retardants and additives and their modes of action were taken into consideration and provide a large variation. The correlation coefficients provide a more statistical and general statement about the significance and the reliability of reduced-scale rapid mass calorimeter results. This leads to a generalization of the method and shows that the higher the correlation coefficient of a pair of parameters, the greater the probability that the rapid mass calorimeter parameter is suitable for screening.

The PHRR in both methods, cone calorimeter and rapid mass calorimeter, correlates strongly with each other over all specimens (R = 0.88), flame retarded and nonflame retarded. In contrast, the PCFC was shown to have a strong correlation between the HRC and PHRR of the cone calorimeter only for pure polymers.[28] Flame-retarded polymers, however, were not able to show even a marginal correlation coefficient in the case of PCFC.[31,32] An even stronger correlation exists between the PHRR of cone calorimeter and fire growth rate index (FIGRA) obtained by rapid mass calorimeter (R = 0.89), because of the fact that the signals mostly occur in the shape of peaks. Higher peaks will show a steeper rise, thus resulting in a higher FIGRA. The times to ignition of both methods correlate strongly with each other, showing proportionality in t_{ig} and specimen size. Cone calorimeter THE and the maximum average rate of heat emission from rapid mass calorimeter give a correlation coefficient of moderate strength (R = 0.82). Nevertheless, this correlation is stronger than that between the THE in the 2 methods (R = 0.75).

The averaging parameters maximum average rate of heat emission and HRRavg derived from the cone calorimeter (Figure 15) show strong-to-moderate correlation with the PHRR (R = 0.87 and 0.84)

TABLE 5 Pearson correlation coefficients between rapid mass calorimeter and cone calorimeter

		RAPID MASS CALORIMETER										
		PHRR	t_{ig}	THE	FIGRA	PHRR/t_{ig}	FPI	MARHE	t_b	HRR_{avg}	b	Mass Loss
Cone calorimetrer	PHRR	**0.88**	0.43	0.41	**0.89**	0.27	-0.43	0.68	-0.47	0.79	-0.34	0.55
	t_{ig}	0.37	**0.88**	0.02	0.31	-0.46	0.32	0.12	-0.47	0.42	-0.72	0.31
	THE	0.75	0.04	0.75	0.61	0.64	-0.62	0.82	0.02	0.74	0.23	0.16
	FIGRA	0.63	0.17	0.4	0.72	0.31	-0.47	0.56	-0.34	0.58	-0.2	0.53
	PHRR/t_{ig}	0.71	-0.01	0.43	0.76	0.57	-0.61	0.68	-0.3	0.58	0.01	0.45
	FPI	-0.63	0.1	-0.58	-0.63	-0.6	0.72	-0.68	0.11	-0.59	-0.16	-0.37
	MARHE	**0.87**	0.34	0.5	**0.88**	0.37	-0.52	0.77	-0.44	0.81	-0.24	0.53
	t_b	-0.49	-0.57	-0.07	-0.55	0.2	0.05	-0.36	0.56	-0.5	0.53	-0.59
	HRR_{avg}	0.84	0.41	0.47	0.83	0.28	-0.45	0.72	-0.42	0.8	-0.29	0.52
	b	0.84	0.39	0.48	0.83	0.3	-0.46	0.73	-0.41	0.79	-0.27	0.51
	Mass Loss	0.65	0.13	0.25	0.7	0.34	-0.56	0.51	-0.54	0.55	-0.25	0.77

Abbreviations: t_{ig}: time to ignition, FPI: Fire Performance Index, t_b: time of burning, HRR_{avg}: average HRR from t_{ig} to flameout, b: b-parameter.[30]

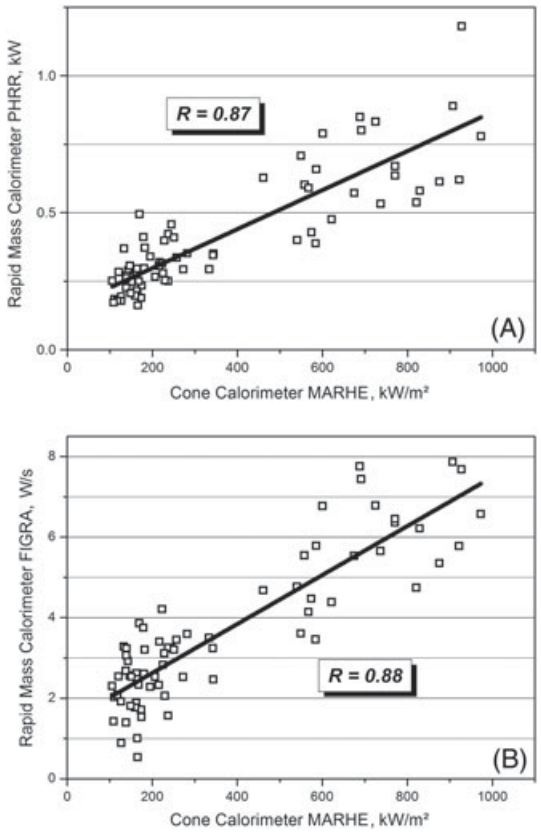

FIGURE 15 Correlations between MARHE from A, Cone calorimeter and PHRR and FIGRA from B, Rapid mass calorimeter, respectively. FIGRA, fire growth rate index; MARHE, maximum average rate of heat emission; PHRR, peak heat release rate

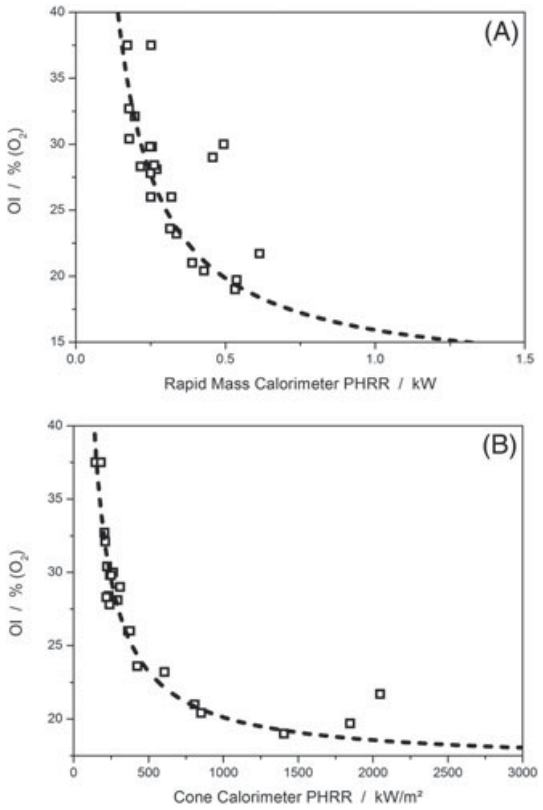

FIGURE 16 Correlation between OI and PHRR derived from A, Rapid mass calorimeter and B, cone calorimeterPHRR, peak heat release rate

and FIGRA (R = 0.88 and 0.83). This supports the assumption that the small-scale rapid mass calorimeter results depict an average over the standard-scale burning behavior and merge particular features from the cone calorimeter HRR into a more generic curve shape.

3.5 | Correlation with oxygen index

Correlations with other fire tests were checked exemplarily to yield insight into the relation between reduced-scale fire tests under forced flaming conditions and flammability tested against a small flame. Oxygen index (OI) was chosen because of the availability of the data. Previous work has shown different results regarding the correlation between the PHRR measured in the cone calorimeter and the OI.[33,34] Overall, the OI of 22 of the materials investigated was available, including the polycarbonate acrylonitrile butadiene styrene and TPES formulations, PP/30FLAX with various flame retardants, EP/Nanomer, and EP300K materials. Nonlinear fitting of the data points led to a good accordance with the curve function of Equation 1:

$$OI = 17 + \frac{3117}{PHRR}; \qquad R2 = 0.92 \tag{1}$$

Apart from slight deviations due to melt flow effects in OI experiments, the results show surprisingly great correlation with R^2 = 0.92 (Figure 16). A similar and good correlation was found between OI and PHRR from the rapid mass calorimeter. Deviations are visible, but most data points are located on and around the correlation curve with the Equation 2 and an R^2 of 0.89. Therefore rapid mass calorimeter may be used not only for estimating the performance in the cone calorimeter test but also even for a more general assessment.

$$OI = 12 + \frac{3.92}{PHRR}; \qquad R2 = 0.89 \tag{2}$$

4 | CONCLUSION

In this work, the rapid mass calorimeter was introduced as a high-throughput screening method under forced flaming combustion and put up for discussion. The effects of reducing specimen scale were investigated especially with regard to key factors to ensure accelerated testing with acceptable deterioration of the results. It was shown that results obtained with the rapid mass calorimeter and a specimen size of 20 × 20 mm^2 as a compromise between those 2 key factors allow for interpretation in a similar fashion as standard-sized samples measured with the cone calorimeter. Different approaches and modes of action of flame retardants and additives were considered to provide large coverage over burning behavior scenarios.

The rapid mass calorimeter was proven to be an interesting and promising tool for the assessment of high-throughput screening of flame-retardant polymeric materials. Because of the reduction of the specimens to 1/25th of a standard scale cone calorimeter specimen, material savings of 96% were achieved. Reduction of the measurement time yielded around 60%-70% savings in time, not

including the additional time savings because of the reduced calibration efforts.

ACKNOWLEDGEMENTS

Thanks go to everyone helping to build the rapid mass calorimeter, P. Klack and T. Kukofka. Thanks to P. Klack also for his support at the PCFC and cone calorimeter. Several companies and research institutes are acknowledged for supporting us with samples, including ELKEM, Bayer MaterialScience (now Convestro), BASF, University Freiburg, TITK (Rudolstadt), and SKZ (Würzburg).

REFERENCES

1. Gilman JW, Bourbigot S, Shields JR, et al. High throughput methods for polymer nanocomposites research: extrusion, NMR characterization and flammability property screening. *J Mater Sci* 2003;38:4451–4460.
2. Wilkie CA, Chigwada G, Gilman JW, Lyon RE. High-throughput techniques for the evaluation of fire retardancy. *J Mater Chem* 2006;16:2023–2029.
3. Davis RD, Lyon RE, Takemori MT, Eidelman N. High throughput techniques for fire resistant materials development. In: Wilkie CA, Morgan AB, eds. *Fire Retardancy of Polymeric Materials*. Second ed. Boca Raton, FL, USA: CRC press; 2010:421–451.
4. Gilman JW, Brassell LD, Davis RD, et al. Evaluation of iron carbonate as a flame retardant for polyolefins. In: Schartel B, ed. *Advances in the Flame Retardancy of Polymeric Materials: Current perspectives presented at FRPM'05*. Germany: Books on Demand; 2007:131–140.
5. Chigwada G, Wilkie CA. Synergy between conventional phosphorus fire retardants and organically-modified clays can lead to fire retardancy of styrenics. *Polym Degrad Stab* 2003;80:551–557.
6. Lyon RE, Walters RN. Pyrolysis combustion flow calorimetry. *J Anal Appl Pyrolysis* 2004;71:27–46.
7. Lyon RE, Walters RN, Stoliarov SI. Screening flame retardants for plastics using microscale combustion calorimetry. *Polym Eng Sci* 2007;47:1501–1510.
8. Schartel B, Pawlowski KH, Lyon RE. Pyrolysis combustion flow calorimeter: a tool to assess flame retarded PC/ABS materials? *Thermochim Acta* 2007;462:1–14.
9. Plastics—simple heat release test using a conical radiant heater and a thermopile detector. 1st ed. ISO 13927; 2001.
10. Reaction-to-fire tests—heat release, smoke production and mass loss rate. 3rd ed. ISO 5660-1, 2015-03.
11. Standard test method for determining flammability characteristics of plastics and other solid materials using microscale combustion calorimetry. ASTM D 7309; 2011.
12. Schartel B, Kunze R, Neubert D. Red phosphorus-controlled decomposition for fire retardant PA 66. *J Appl Polym Sci* 2002;83:2060–2071.
13. Schartel B, Kunze R, Neubert D, Tidjani A. ZnS as fire retardant in plasticized PVC. *Polym Int* 2002;51:213–222.
14. Schartel B, Braun U, Schwarz U, Reinemann S. Fire retardancy of polypropylene/flax blends. *Polymer* 2003;44:6241–6250.
15. Pawlowski KH, Schartel B. Flame retardancy mechanism of triphenyl phosphate, resorcinol bis(diphenyl phosphate) and bisphenol A bis(diphenyl phosphate) in polycarbonate/acrylonitrile-butadiene-styrene blends. *Polym Int* 2007;56:1404–1414.
16. Braun U, Schartel B. Flame retardancy mechanisms of aluminium phosphinate in combination with melamine cyanurate in glass-fibre-reinforced poly(1,4-butylene terephthalate). *Macromol Mater Eng* 2008;293:206–217.
17. Schartel B, Richter KH, Böhning M. Synergistic Use of Talc in Halogen-free Flame Retarded Polycarbonate/Acrylonitrile-Butadiene-Styrene Blends. In: Morgan AB, Wilkie CA, Nelson GL, eds. *Fire and Polymers VI: New Advances in Flame Retardant Chamistry and Science. ACS symposium series 1118*. Washington, DC, USA: ACS; 2012 :15–36.chap. 2
18. Dittrich B, Wartig K-A, Hofmann D, Mülhaupt R, Schartel B. Flame retardancy through carbon nanomaterials: carbon black, multiwall nanotubes, expanded graphite, multi-layer grapheme and grapheme in polypropylene. *Polym Degrad Stab* 2013;98:1495–1505.
19. Dittrich B, Wartig K-A, Mülhaupt R, Schartel B. Flame-retardancy properties of intumescent ammonium poly(phosphate) and mineral filler magnesium hydroxide in combination with graphene. *Polymers* 2014;6:2875–2895.
20. Langfeld K, Wilke A, Sut A, et al. Halogen-free fire retardant styrene-ethylene-butylene-styrene-based thermoplastic elastomers using synergistic aluminum diethylphosphinate-based combinations. *J Fire Sci* 2015;33:157–177.
21. Braun U, Wachtendorf V, Geburtig A, Bahr H, Schartel B. Weathering resistance of halogen-free flame retardance in thermoplastics. *Polym Degrad Stab* 2010;95:2421–2429.
22. Gallo E, Schartel B, Braun U, Russo P, Acierno D. Fire retardant synergisms between nanometric Fe2O3 and aluminium phosphinate in poly(butylene terephthalate). *Polym Adv Technol* 2011;22:2382–2391.
23. Schartel B, Schmaucks G. Flame retardancy synergism in polymers through different inert fillers' geometry. *Polym Eng Sci* 2017; doi: 10.1002/pen.24485
24. Schartel B, Hull TR. Development of fire-retarded materials—interpretation of cone calorimeter data. *Fire Mater* 2007;31:327–354.
25. Havlicek LL, Crane RD. *Practical Statistics for the Physical Sciences*. Washington, DC: American Chemical Society; 1988.
26. Lindolm J, Brink A, Hupa M. Influence of decreased sample size on cone calorimeter results. *Fire Mater* 2012;36:63–73.
27. Janssens M, Huczek J, Faw A. Effect of specimen size on test results obtained in the cone calorimeter. FLAME 2008 conf. proceedings, Stamford, CT, USA.
28. Lyon RE, Walters RN, Stoliarov SI. Thermal analysis of flammability. *J Therm Anal Calorim* 2007;89:441–448.
29. Sonnier R, Otazaghine B, Viretto A, Apolinario G, Ienny P. Improving the flame retardancy of flax fabrics by radiation grafting of phosphorus compounds. *Eur Polym J* 2015;68:313–325.
30. Cleary TG, Fire Retardant Chemicals Association. Technical and marketing issues impacting the fire safety of building and construction and home furnishings applications. Spring Conference. March 29-April 1, 1992, Orlando, FL, Lancaster, PA, USA: Technomic Publishing Co.; 1992.
31. Lin TS, Cogen JM, Lyon RE. Correlations between microscale combustion calorimetry and conventional flammability tests for flame retardant wire and cable compounds. 56th International Wire & Cable Symposium. Lake Buena Vista (Orlando), FL, USA; 2007.
32. Cogen JM, Lin TS, Lyon RE. Correlations between pyrolysis combustion flow calorimetry and conventional flammability tests with halogen-free flame retardant polyolefin compounds. *Fire Mater* 2009;33:33–50.
33. Weil ED, Hirschler MM, Patel NG, Said MM, Shakir S. Oxygen index: correlations to other fire tests. *Fire Mater* 1992;16:159–167.
34. Schartel B. Uses of Fire Tests in Materials Flammability Development. In: Wilkie CA, Morgan AB, eds. *Fire Retardancy of Polymeric Materials*. 2nd ed. Boca Raton, FL, USA: CRC press; 2010:421–451.

How to cite this article: Rabe S, Schartel B. The rapid mass calorimeter: A route to high throughput fire testing. *Fire and Materials*. 2017;0:1–14. https://doi.org/10.1002/fam.2420

3.2 The rapid mass calorimeter: Understanding reduced-scale fire test results

Sebastian Rabe, Bernhard Schartel, *Polymer Testing* **2017**, 57, 165-174.

https://doi.org/10.1016/j.polymertesting.2016.11.027

This article was accepted and published.

First author contribution:

- Conceptualization of the working plan
- Cone calorimeter and rapid mass calorimeter measurements
- Collection, analysis and interpretation of the data
- Generation of correlation coefficient matrices
- Scientific discussion and conclusion
- Writing of the outline and the final manuscript

Contributions from other authors:

- Bernhard Schartel:
    - Conceptualizing and writing of funding application
    - Contribution to the scientific discussion
    - Contribution to the concept of the manuscript

Abstract: The effects of reducing specimen size on the fire behavior of polymeric materials were investigated by means of the rapid mass calorimeter, a high-throughput screening instrument. Results from the rapid mass calorimeter were compared with those from the cone calorimeter. Correlation coefficients between the different measures of each method and between the two methods are discussed to elucidate the differences and similarities in the two methods. Materials with characteristic heat release rate (HRR) curves in the cone calorimeter were evaluated in detail. The rapid mass calorimeter produces valuable and interpretable results with HRR curve characteristics similar to cone calorimeter results. Compared to cone calorimeter measurements, material savings of 96% are achieved, while maintaining the advantages of a macroscopic fire test.

Polymer Testing 57 (2017) 165–174

Contents lists available at ScienceDirect

Polymer Testing

journal homepage: www.elsevier.com/locate/polytest

Test Method

The rapid mass calorimeter: Understanding reduced-scale fire test results

Sebastian Rabe, Bernhard Schartel*

Bundesanstalt für Materialforschung und –prüfung (BAM), Unter den Eichen 87, 12205 Berlin, Germany

ARTICLE INFO

Article history:
Received 18 October 2016
Accepted 21 November 2016
Available online 23 November 2016

Keywords:
Rapid mass calorimeter
High throughput
Cone calorimeter
Flame retardancy

ABSTRACT

The effects of reducing specimen size on the fire behavior of polymeric materials were investigated by means of the rapid mass calorimeter, a high-throughput screening instrument. Results from the rapid mass calorimeter were compared with those from the cone calorimeter. Correlation coefficients between the different measures of each method and between the two methods are discussed to elucidate the differences and similarities in the two methods. Materials with characteristic heat release rate (HRR) curves in the cone calorimeter were evaluated in detail. The rapid mass calorimeter produces valuable and interpretable results with HRR curve characteristics similar to cone calorimeter results. Compared to cone calorimeter measurements, material savings of 96% are achieved, while maintaining the advantages of a macroscopic fire test.

1. Introduction

Modern polymeric materials are multicomponent systems. Many variables must be considered during the development of a novel material. Additives, plasticizers [1–3], adjuvants, synergists [4,5] and so forth can be varied in kind, concentration, particle size distribution [6,7] and other parameters, yielding an extensive matrix of possible systems. To assess the fire performance of these formulations and to find the best performing material, high throughput screening methods are essential. Until now, the performance of such materials in terms of fire behavior under flaming conditions has been evaluated with the cone calorimeter. For fast evaluation of fire performance, the pyrolysis combustion flow calorimeter (PCFC, or microscale combustion calorimeter, MCC) has been proposed [8]. While the cone calorimeter is a fire test using 100 mm × 100 mm plates, the latter performs fast screening of the pyrolysis of specimens on the milligram scale. Macroscopic modes of action like the formation of protective layers, dripping, wicking and so forth, as well as flame inhibition, cannot be observed in the PCFC [9]. There is a pronounced dilemma between proper fire testing based on macroscopic specimen and accelerated testing demanding reduction of the specimen size. The rapid mass calorimeter aims to reduce specimen size while maintaining fire testing of a macroscopic specimen. The rapid mass calorimeter has been proposed and discussed in a previous publication [10]. Selected according to their characteristic heat release rate (HRR) curve shapes in the cone calorimeter, various sets of materials were evaluated in the rapid mass calorimeter, and the results compared with those from the cone calorimeter to assess the value of rapid mass calorimeter testing.

Scale reduction is crucial if the forced-flaming combustion test is to be accelerated [11]. The rapid mass calorimeter should still be operated on a macroscopic scale, limiting the minimum size to which the specimens can be reduced. Changes in length scale and thickness of specimens alter the obtained fire properties dramatically [12–15]. Modes of action like heat and fuel transport barriers created from inert filler or from an intumescent system also showed different performance [10]. Further flame retarding effects were not as distinct in the rapid mass calorimeter as in the cone calorimeter. Therefore, the task is to reveal and understand the reasons for this divergent behavior. For this, correlation coefficients derived from the heat release rate (HRR) of the rapid mass calorimeter and cone calorimeter results are elucidated; as well as the correlation coefficients of the results within each method. The differences in correlation strength between the methods are discussed, explaining effects that occur when specimen size is reduced to 20 mm × 20 mm. A set of 73 different materials was used, including a large number of flame retarded materials. Several characteristic materials were selected to discuss the reduced size effect in detail, particularly with respect to flame retardancy.

* Corresponding author.
E-mail address: bernhard.schartel@bam.de (B. Schartel).

http://dx.doi.org/10.1016/j.polymertesting.2016.11.027
0142-9418/

2. Experimental

2.1. Rapid mass calorimeter

The rapid mass calorimeter consists of a mass loss calorimeter (Fire Testing Technology, UK) equipped with a chimney with thermoelements to record the heat release rate (HRR) according to ISO 13927 [16]. The balance has been replaced with a linear motion unit (Oriental Motor, JP) to facilitate semi-automatic sample exchange. The 20 mm × 20 mm samples were wrapped in an aluminum tray and placed on the center of the sample holder. The distance from sample surface to cone heater was 25 mm and the heat flux was 50 kW/m^2. The setup and method were described in detail in a previous publication [10].

2.2. Cone calorimeter

Forced-flaming combustion tests were performed with a cone calorimeter (FTT, UK). Specimens 100 mm × 100 mm in size and encased in an aluminum tray were irradiated with a heat flux of 50 kW/m^2 at a distance of 25 mm. Thicknesses of the samples ranged from 3 mm to 10 mm. No retainer frame was used [17].

2.3. Correlation analysis

The results from both methods, rapid mass calorimeter and cone calorimeter, were checked for their Pearson R correlation coefficients, within each method and also between the two methods. Pearson R values can range from ±1 for perfect linear correlation to 0 for no correlation at all, as seen in Table 1 [18].

2.4. Materials

In total, 73 different polymeric materials (Table 2) were measured in the cone calorimeter and the rapid mass calorimeter. From those materials certain systematic series were selected for further evaluation and comparison. All investigated systems originate from earlier projects and were provided by partners with high compounding and processing competence [9,19–30].

3. Results and discussion

3.1. Comparison of correlation coefficients within each method

The rapid mass calorimeter allows for accelerated screening of flame retarded polymeric materials. The HRR is measured via the voltage difference in the thermopile, and mass is recorded before and after the test with a separate balance. The test yields similar measures as the cone calorimeter test. To compare the character of both methods, correlation coefficients are evaluated either between the measures of each method or between the measures of both methods.

Tables 3 and 4 clarify the similarity of both methods by providing correlation coefficients of the HRR measurement results.

Table 1
Correlation strength definition for the Pearson correlation coefficient R.

Correlation Strength	Pearson R
Poor	$\|R\| < 0.40$
Weak	$0.40 \leq \|R\| < 0.55$
Marginal	$0.55 \leq \|R\| < 0.70$
Moderate	$0.70 \leq \|R\| < 0.85$
Strong	$0.85 \leq \|R\|$

Results that correlate strongly in the cone calorimeter also show strong correlation in the rapid mass calorimeter. In general, all of the tendencies of the correlation coefficients are the same. This similar correlation pattern proves that the rapid mass calorimeter and cone calorimeter are strongly related tests. The time to ignition shows no significant correlation at all, no matter the method with which the results were obtained, because t_{ig} is not directly related to any of the other fire properties. A flame retardant can achieve a reduction of, e.g. PHRR or THE and prolong the time of burning, but must not necessarily prolong the time to ignition of the material.

At first glance, rapid mass calorimeter HRR curves show a slope, a peak and a decay. The most important characteristic of a peak is its peak height. Flame retardants incorporated in a polymeric material serve to lower the peak height. PHRR and THE do not correlate well with each other, which leads to the conclusion that added flame retardants change more than just the peak height of the HRR curve. In fact, HRR curves obtained with the rapid mass calorimeter show the same or similar characteristics as HRR curves from the cone calorimeter and thus can be interpreted similarly.

Values that show about the same correlation in both methods are MARHE ↔ THE, PHRR ↔ HRRavg and MARHE ↔ FIGRA. The relation between MARHE and HRRavg shows strong correlation with a coefficient of R = 0.90 in the rapid mass calorimeter (Fig. 1), and is about the same strength in the cone calorimeter (R = 0.97). This similarity shows that MARHE and HRRavg proportions are mainly unaffected by specimen size and method variation. Specimen size does not seem to alter the relation between these two measures very much.

Those averaged measures are also among the few that show any moderate to strong correlation in the rapid mass calorimeter. They correlate well mainly with PHRR, FIGRA and with each other. When HRRavg is calculated from rapid mass calorimeter HRR data, it will always result in a value dependent on burning duration and PHRR. This explains the strong correlation coefficient values with PHRR (R = 0.90) and FIGRA (R = 0.83). These measures are also among the values that change most obviously in the rapid mass calorimeter results when a flame retardant is integrated or its content varied in a polymeric material. Averaging the value of the HRR from the time of ignition to flameout (HRRavg) is a tool to combine the complete burning behavior into a single value (see Fig. 2).

Correlations between FIGRA and PHRR as well as FIGRA and HRRavg are among the strongest when comparing measures derived from the rapid mass calorimeter. Increasing peak height due to heavily burning specimens often results in a steeper slope of the recorded HRR curve. If a sample shows high flame retardant performance, resulting in a low PHRR, the slope of the curve will also be less steep. However, if the burning behavior of the investigated specimen results in a HRR curve that shows not a distinctive peak, but a rather wide plateau, this relation no longer applies. A good correlation of HRR results over all tested materials is statistical evidence for the significance of measurements with the rapid mass calorimeter. Correlation between measurement results of specific, coherent specimens are stronger, and show more clearly that changes in HRR values are consistent among sample series with similar characteristic curve shapes. Such stronger correlations due to structure-property relationships are depicted for four different sample series in Fig. 3. The sample sequence consisting of glass fiber reinforced PA66 with and without red phosphorus as a char-inducing flame retardant shows the strongest correlation between FIGRA and PHRR, exhibiting a correlation coefficient of R = 0.99. Formulations with APP in PP also show a strong dependence of both values, while specimens with MDH and TRGO in PP correlate only marginally for the FIGRA and PHRR. The correlation in the PCABS sample series is weak at R = 0.32. The single outlier that lowers the correlation between FIGRA and PHRR was PCABS-

Table 2
Investigated materials.

Abbreviations	Material	Thickness in mm
Materials for Comparison of Cone Calorimeter with Rapid Mass Calorimeter		
PA66	Polyamide 66 (Ultramid® A3)	3
PA66-35 GF	PA66 + 35 wt.-% glass fiber	3
PA66-25 GF-RP	PA66 + 25 wt.-% glass fiber + red phosphorus	3
PA66-35 GF-RP	PA66 + 35 wt.-% glass fiber + red phosphorus	3
PA66-25 GF-R-RP	PA66 + 25 wt.-% glass fiber + rubber + red phosphorus	3
PP	Poly(propylene)	3
PP-25APP	PP + 25 wt.-% Ammonium polyphosphate	3
PP-25APP*	PP + 25 wt.-% encapsulated APP (APP*)	3
PP-20APP*	PP + 20 wt.-% APP*	3
PP-53MDH	PP + 53 wt.-% $Mg(OH)_2$	3
PP-53MDH-1TRGO	PP + 53 wt.-% $Mg(OH)_2$ + 1% thermally reduced graphene oxide	3
PP-54MDH	PP + 54 wt.-% $Mg(OH)_2$	3
PP-54MDH-1TRGO	PP + 54 wt.-% $Mg(OH)_2$ + 1% TRGO	3
PP-59MDH	PP + 59 wt.-% $Mg(OH)_2$	3
PP-59MDH-1TRGO	PP + 59 wt.-% $Mg(OH)_2$ + 1% TRGO	3
TPES	Styrene-ethylene-butylene-styrene/PP/mineral oil/antioxidant	5.8
TPES-30MDH	TPES + 50 wt.-% $Mg(OH)_2$	5.8
PCABS	Bisphenol A polycarbonate/acrylonitrile butadiene styrene/Polytetrafluoroethylene	3
PCABS-BDP	PCABS + 12.5 wt.-% Bisphenol-A bis(diphenyl phosphate) (BDP)	3
PCABS-PTFE	PCABS + 0.45 wt.-% Teflon	3
PCABS-PTFE-BDP	PCABS + 0.45 wt.-% Teflon + 12.5 wt.-% BDP	3
Further Materials for Correlation Elucidation		
PMMA	Poly(methyl methacrylate)	3
PEEK	Poly(ether-ether ketone)	4
PP-30FLAX	PP + 30 wt.-% flax	4
PP-30FLAX-APP	PP + 30 wt.-% flax + APP	4
PP-30FLAX-25GR	PP + 30 wt.-% flax + 25 wt.-% expandable graphite	4
PP-30FLAX-15EG	PP + 30 wt.-% flax + 15 wt.-% EG	4
PCABS-PTFE-RDP	PCABS-PTFE + resorcinol bis(diphenyl phosphate)	3
PCABS-PTFE-TPP	PCABS-PTFE + triphenyl phosphate	3
PCABS-PTFE-5T-BDP	PCABS-PTFE + 5 wt.-% talc + BDP	3
PCABS-PTFE-20T-BDP	PCABS-PTFE + 20 wt.-% talc + BDP	3
PCABS-PTFE-10T-ZnB-BDP	PCABS-PTFE + 10 wt-% talc + zinc borate + BDP	3
PCABS-PTFE-1Al-BDP	PCABS-PTFE + 1 wt.-% boehmite + BDP	3
PA12	Polyamide 12	4
PA12-30 GF	PA12 + 30 wt.-% GF	4
PBT	Poly(butylene terephthalate)	5
PBT-30GF	PBT + 30 wt.-% GF	5
PBT-AlPi	PBT + AlPi	5
PBT-30GF	PBT + 30 wt.-% GF	4
TPES-AlPi	TPES + 30 wt.-% aluminum diethyl phosphinate	5.8
TPES-APP	TPES + 30 wt.-% APP	5.8
TPES-APP-EG	TPES + 7.5 wt.-% APP + 22.5 wt.-% EG	5.8
TPES-MDH	TPES + 50 wt.-% $Mg(OH)_2$	5.8
TPES-APP-AlPi-DiPer	TPES + 15 wt.-% APP + 7.5 wt.-% AlPi + 7.5 wt.-% dipentaerythritol	5.8
TPES-APP*-EG-AlPi	TPES + 6.2 wt.-% APP* + 18.7 wt.-% EG + 5 wt.-% AlPi	5.8
TPES-APP-EG-AlPi	TPES + 6.2 wt.-% APP + 18.7 wt.-% EG + 5 wt.-% AlPi	5.8
TPES-MDH-ZB-GF-EG-APP	TPES + 30 wt.-% $Mg(OH)_2$ + 2.5 wt.-% ZnB + 2.5 wt.-% glass frits + 10 wt.-% EG + 5 wt.-% APP	5.8
PA66-20SID	PA66 + 20 wt.-% Sidistar® T 120	4
PA12-20SID	PA12 + 20 wt.-% SID	4
HDPE3mm	High density poly(ethylene) (Hostalen® GM 5050)	3
HDPE6mm	HDPE	6
HDPE3mm-15MDH	HDPE + 15 wt.-% $Mg(OH)_2$	3
HDPE6mm-15MDH	HDPE + 15 wt.-% $Mg(OH)_2$	6
HDPE3mm-30MDH	HDPE + 30 wt.-% $Mg(OH)_2$	3
PINE	Pine	10
BELMA	Beech Belmadur	10
PINUS	Pinus radiata	10
ACCO	Accoya	10
BayblendFR3005	Flame retarded PCABS (Bayblend® FR 3005)	4
BayblendFR2000	Flame retarded PCABS (Bayblend® FR 2000)	4
BayblendFR3000	Flame retarded PCABS (Bayblend® FR 3000)	4
BayblendFR3030	Flame retarded PCABS (Bayblend® FR 3030)	4
BayblendKU2-1514	Flame retarded PCABS (Bayblend® KU 2-1514)	4
EP	Epoxy resin (Araldite® GY 250/Aradur® 250, 2:1)	5
EP-5NANO	EP + 5 wt.-% layered silicate (Nanomer® I.30E)	5
EP-5NANO-7SID	EP + 5 wt.-% layered silicate + 7 wt.-% SID	5
PVC-5ZnS	Poly(vinyl chloride) + 5 wt.-% ZnS	4
LDPE	Low density poly(ethylene) (LD 615BA)	4
PS	Polystyrene (Lacqrene 1810)	4
EP300K-5EG60	Impact-resistant PP (Moplen) + 5 wt.-% expanded graphite	3
EP300K-5MLG350	EP300K + 5 wt.-% multilayer graphene (BET = 350 $m^2\ g^{-1}$)	3

(*continued on next page*)

Table 2 (*continued*)

Abbreviations	Material	Thickness in mm
PS4	Flame retarded polystyrene (FR 3180)	3
MERANTI	Shorea bracteolata	10
CHIP	Chipboard	10
WOOD	Pine sapwood	5

Table 3
Coefficients of correlations among results derived from the rapid mass calorimeter. PHRR: peak of heat release rate, t_{ig}: time of ignition, THE: total heat evolved, FIGRA: fire growth rate index, MARHE: maximum average rate of heat emission, HRR_{avg}: average heat release rate from time of ignition to time of flameout.

		Rapid Mass Calorimeter					
		PHRR	t_{ig}	THE	FIGRA	MARHE	HRR_{avg}
RAPID MASS CALORIMETER	PHRR	1.00					
	t_{ig}	0.44	1.00				
	THE	0.55	−0.03	1.00			
	FIGRA	**0.92**	0.33	0.47	1.00		
	MARHE	**0.85**	0.16	0.77	0.79	1.00	
	HRR_{avg}	**0.90**	0.49	0.64	0.83	**0.90**	1.00

Table 4
Correlation coefficients of results derived from the cone calorimeter. PHRR: peak of heat release rate, t_{ig}: time of ignition, THE: total heat evolved, FIGRA: fire growth rate index, MARHE: maximum average rate of heat emission, HRR_{avg}: average heat release rate from time of ignition to time of flameout.

		Cone Calorimeter					
		PHRR	t_{ig}	THE	FIGRA	MARHE	HRR_{avg}
CONE CALORIMETER	PHRR	1.00					
	t_{ig}	0.38	1.00				
	THE	0.65	0.05	1.00			
	FIGRA	0.82	0.08	0.43	1.00		
	MARHE	**0.95**	0.28	0.73	0.81	1.00	
	HRR_{avg}	**0.93**	0.36	0.71	0.76	**0.97**	1.00

PTFE. In the rapid mass calorimeter the slope of the HRR curve became larger while the PHRR decreased. This explains the outlier found in that particular example. The PP-MDH-TRGO sample series actually shows strong correlation when divided into two groups, with and without TRGO as an adjuvant. When TRGO was added to a PP-MDH formulation, the rapid mass calorimeter HRR curves were decreased in PHRR with increasing MDH load, but the slope of the curve decreased at a different rate than it did without TRGO. This analysis shows that curve shape and burning behavior strongly influence the FIGRA and the PHRR, which makes them the most important values in describing and comparing rapid mass calorimeter results.

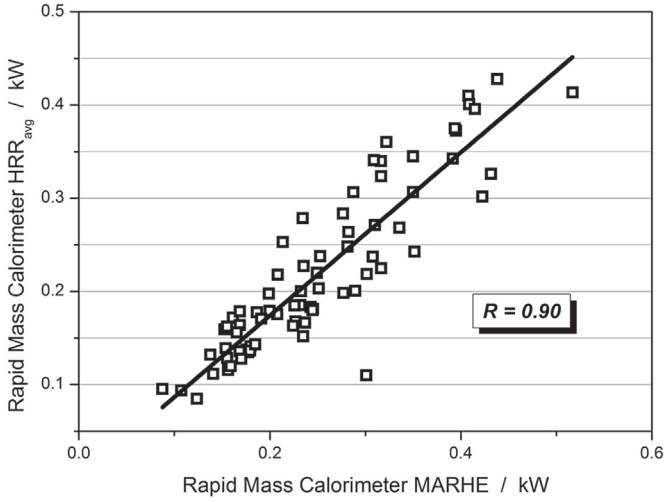

Fig. 1. Correlation between MARHE and HRRavg from the rapid mass calorimeter.

3.2. Correlations between rapid mass calorimeter and cone calorimeter results

Comparing the results of both the cone calorimeter and rapid mass calorimeter method allows a statement about the reliability of results obtained with the rapid mass calorimeter (see Table 5).

Calculation of the average rate of heat emission (ARHE) has the effect that cone calorimeter HRR curves are always reduced to an average curve, which has less pronounced peaks and often only one

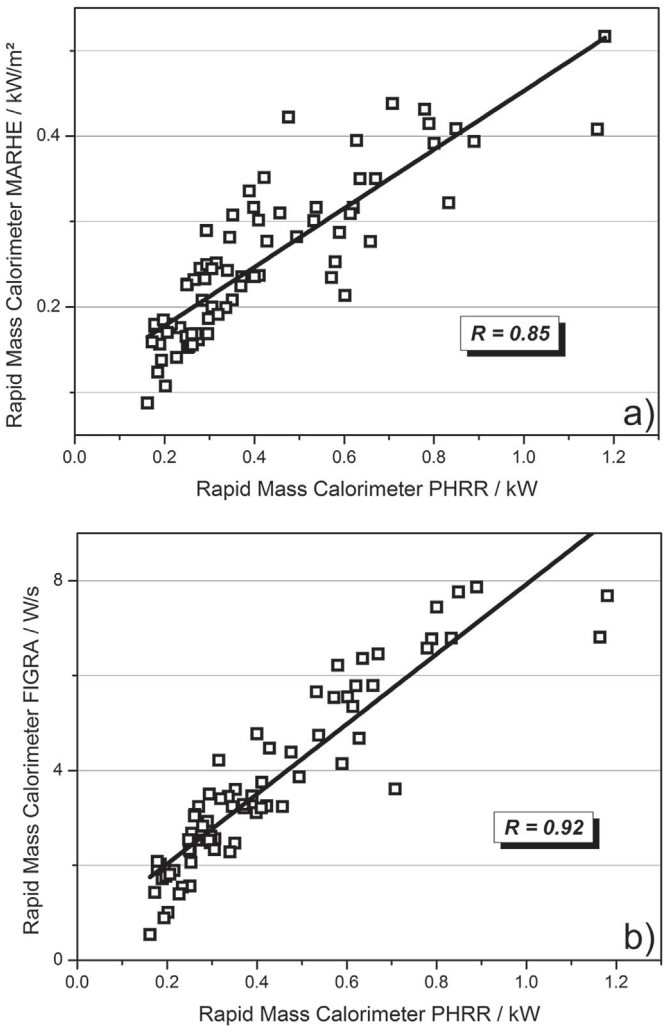

Fig. 2. Relationships between rapid mass calorimeter results for MARHE and PHRR (a) and FIGRA and PHRR (b).

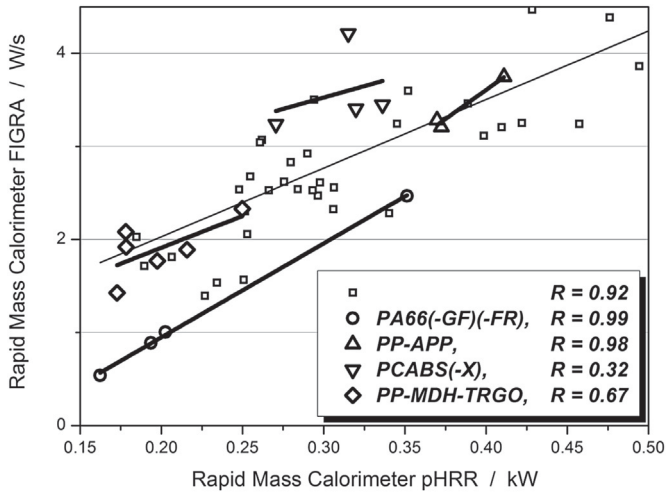

Fig. 3. Correlation between rapid mass calorimeter PHRR and FIGRA for all tested materials, and specifically for PA66(-GF)(-FR), PP-APP, PCABS(-X) and PP-MDH-TRGO.

Table 5
Correlation coefficients for selected measures.

		Rapid Mass Calorimeter					
		PHRR	t_{ig}	THE	FIGRA	MARHE	HRRavg
Cone Calorimeter	PHRR	**0.88**	0.43	0.41	**0.89**	0.68	0.79
	t_{ig}	0.37	0.88	0.02	0.31	0.12	0.42
	THE	0.75	0.04	0.75	0.61	0.82	0.74
	FIGRA	0.63	0.17	0.40	0.72	0.56	0.58
	MARHE	**0.87**	0.34	0.50	**0.88**	0.77	0.81
	HRRavg	0.84	0.41	0.47	0.83	0.72	0.80

maximum, no matter how many local maxima were found in the HRR curve. Due to the fact that the rapid mass calorimeter HRR curves show only one maximum, the strong correlation between MARHE from the cone calorimeter and PHRR as well as FIGRA is explained. Fig. 4 depicts the correlations of the whole set of measured materials compared to single material series. The overall correlation between the MARHE from the cone calorimeter and the PHRR derived from the rapid mass calorimeter is already strong, with a coefficient of R = 0.86. Evaluating a particular sample series provides information about how well the assumption fits that ARHE curves from cone calorimeter results become similar to rapid mass calorimeter HRR curves. In most cases the correlation coefficients grow even stronger. The samples series consisting of glass fiber reinforced PA66 with and without red phosphorus shows a coefficient of R = 0.95, while PCABS with and without PTFE or BDP and the combination of both correlate with each other with a coefficient of R = 0.99. Both series show characteristic HRR curves when measured in the cone calorimeter, which are summarized into ARHE curves showing behavior similar to reduced-scale HRR curves in the rapid mass calorimeter. PP filled with magnesium hydroxide shows strong correlations when split in two groups: one with, and one without the addition of 1 wt.-% of the adjuvant TRGO (R = 0.89 and R = 1.00, respectively).

The HRRavg shows similar behavior as regards to the correlation with the PHRR from rapid mass calorimeter results (Fig. 5). With a coefficient of R = 0.88, only the sample series consisting of the different PP-APP formulations shows a better correlation when compared to the cone calorimeter MARHE. This analysis shows that the rapid mass calorimeter and cone calorimeter results are in very good accordance. The averaging HRR results like MARHE and HRR_{avg} are most important when comparing results of both methods. A more detailed evaluation of the differences in burning behavior and HRR measurement results between the cone calorimeter and the rapid mass calorimeter is elucidated in section 3.3.

3.3. Comparison of heat release rate curve forms from the cone calorimeter and the rapid mass calorimeter

The distinct materials shown in Table 6 were analyzed in detail to provide insight into how the burning behavior and the HRR curve shape change for different sample sizes.

Fig. 6 displays the typical HRR curve form for a glass fiber filled polymer in the cone calorimeter, e.g. PA66-35 GF. The polymer matrix is consumed in the fire until a sufficient amount of glass fiber is left over, forming a protective glass fiber mat on top of the specimen. This impedes the transport of heat from the flame to the pyrolysis zone, resulting in a plateau after the PHRR in the HRR curve. Addition of red phosphorus as a char-inducing flame retardant in PA66 results in a lowering of the PHRR and a significant prolongation of burning time. The HRR curve is typical for charring burning behavior. When the amount of glass fiber was reduced from 35 to 25 wt.-%, a slight deterioration in PHRR and in the height

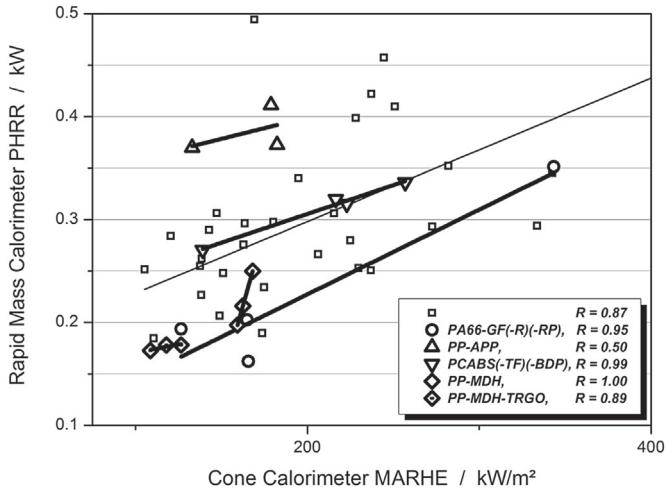

Fig. 4. Correlation between MARHE from the cone calorimeter and PHRR from the rapid mass calorimeter for all measured formulations and the specific systematic sequences.

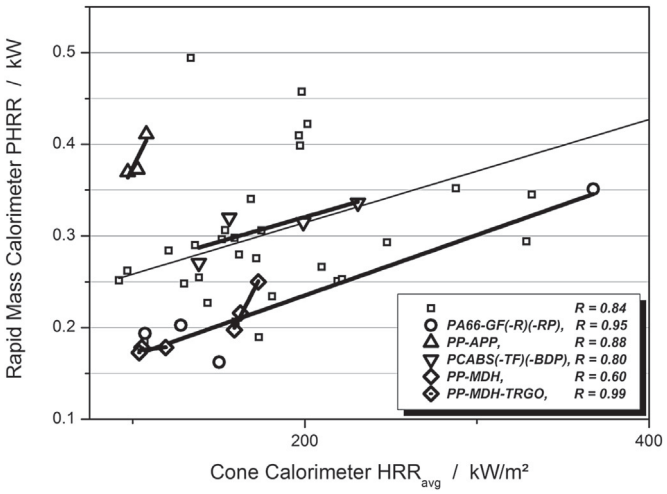

Fig. 5. Correlation between the cone calorimeter HRRavg and PHRR from the rapid mass calorimeter.

of the steady burning phase was observed. In total, the differences of the two formulations flame retarded with red phosphorus are only marginal when looking at the HRR curves in cone calorimeter measurements. Their burning behaviors are similar [19].

Reduced-scale measurements in the rapid mass calorimeter show interesting results, which allow for similar interpretation. The formulation without red phosphorus, PA66-35 GF, shows the highest PHRR and the shortest burning time. However, it shows a shoulder prior to the PHRR, which indicates the effect of the glass fiber mat. In contrast to the cone calorimeter results, the peak occurs after the shoulder because the protection effect is overshadowed by edge burning effects. Fuel transport occurs through the edges of the glass fiber mat. The addition of red phosphorus also results in a different HRR curve than was observed in the cone calorimeter. The shoulder prior to the peak HRR is now more distinct and the overall burning time is greatly prolonged. Reduction of the amount of glass fiber filler, however, increases the PHRR in a similar way as in the cone calorimeter experiments. The shoulder is much less pronounced with 10 wt.-% less inert filler, which leads to a much better differentiation of the two formulations in the rapid mass calorimeter experiments than in the cone calorimeter.

PP-APP formulations show the typical HRR curve behavior when measured in the cone calorimeter, as shown in Fig. 7. The initial peak after ignition, the decrease in HRR and the subsequent formation of the PHRR are characteristic for many intumescent systems. This sample series shows the influence of encapsulation and the reduction of APP loading by 5 wt.-%. Encapsulation alone results in an increased flame retardancy performance, by prolonging not only the overall burning time, but also the time to cracking of the protection layer. The PHRR as well as the height of the initial peak were reduced. Comparing PP-25APP* with PP-20APP* shows that even with reduced APP load the effect of encapsulation ensures a lower PHRR. Nevertheless, the THE of PP-20APP* is the highest of all three formulations.

When measured in the rapid mass calorimeter, the three intumescent PP-APP systems show a different order of fire performance ranking on first glance. Comparing the PHRR of the systems alone leads to the assumption that PP-20APP* shows a higher PHRR and thus worse performance than PP with 25 wt.-% of non-encapsulated APP. PP-25APP and PP-25APP*, however, show a similar ranking in fire performance as in the cone calorimeter when looking at the PHRR. The HRRavg values of the cone calorimeter results are similar to the PHRR values from the rapid mass calorimeter in terms of their relative differences and their order. The highest HRRavg value is found in the PP-20APP* system, followed by the formulation with APP, namely PP-25APP. PP-25APP* shows the lowest HRRavg in the cone calorimeter. This coincides

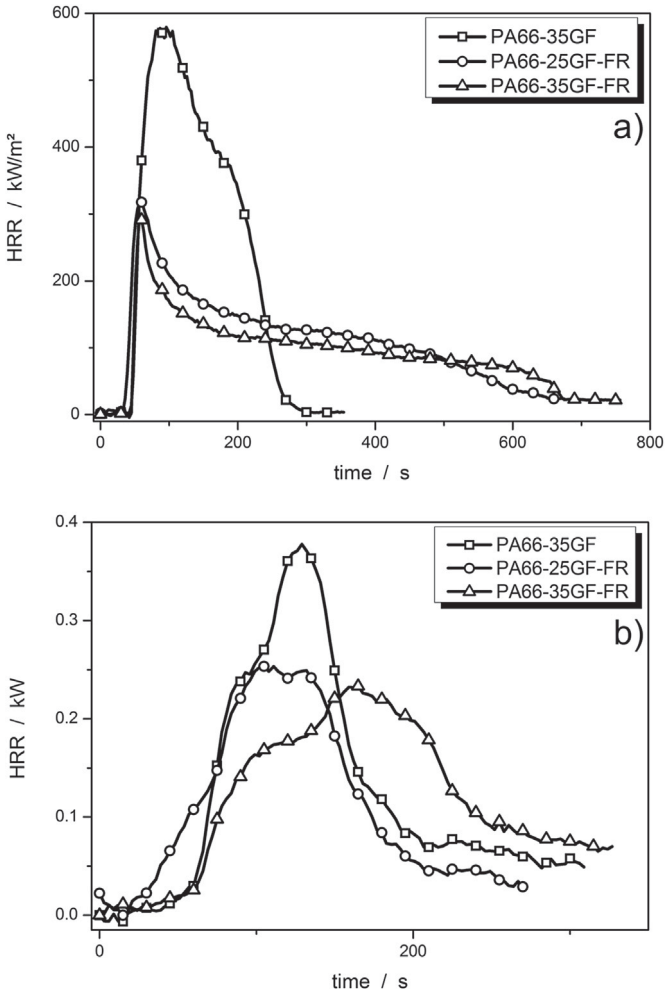

Fig. 6. Typical HRR curve behavior of an intermediate thick inert filler thermoplastic (PA66-35 GF) and added char-inducing flame retardant red phosphorus (PA66-25 GF-FR and PA66-35 GF-FR) in the cone calorimeter (a) and the rapid mass calorimeter (b).

Table 6
Cone calorimeter and rapid mass calorimeter results for the formulations examined in detail.

Sample	Cone Calorimeter			Rapid Mass Calorimeter		
	PHRR/kW/m^2	THE/MJ/m^2	Residue/wt.-%	PHRR/W	THE/kJ	Residue/wt.-%
PA66	1509 ± 10	100 ± 2	0	1102 ± 27	35 ± 1	0
PA66-35 GF	582 ± 3	80 ± 1	34	377 ± 25	15 ± 1	28
PA66-25 GF-FR	322 ± 15	74 ± 1	12	253 ± 5	19 ± 1	41
PA66-35 GF-FR	299 ± 10	66 ± 2	43	233 ± 15	12 ± 1	35
PA66-25 GF-R-FR	326 ± 2	71 ± 1	11	223 ± 9	10 ± 1	21
PP	2349 ± 90	123 ± 2	0	1252 ± 90	63 ± 2	0
PP-25APP	345 ± 14	95 ± 2	16	373 ± 34	20 ± 1	17
PP-25APP*	260 ± 20	93 ± 4	16	370 ± 34	24 ± 2	17
PP-20APP*	288 ± 4	101 ± 1	8	411 ± 38	22 ± 1	17
PP-54MDH	219 ± 2	80 ± 1	14	244 ± 11	15 ± 1	67
PP-54MDH-1TRGO	205 ± 4	80 ± 1	15	151 ± 5	17 ± 1	45
TPES	2346 ± 140	215 ± 4	0	779 ± 6	29 ± 1	0
TPES-50MDH	191 ± 1	151 ± 2	28	198 ± 12	44 ± 2	48
PCABS	607 ± 30	68 ± 1	6	336 ± 15	9 ± 1	7
PCABS-BDP	378 ± 38	60 ± 1	4	320 ± 16	10 ± 1	6
PCABS-PTFE	424 ± 42	64 ± 2	6	315 ± 15	14 ± 1	7
PCABS-PTFE-BDP	294 ± 28	57 ± 1	6	270 ± 15	12 ± 1	7

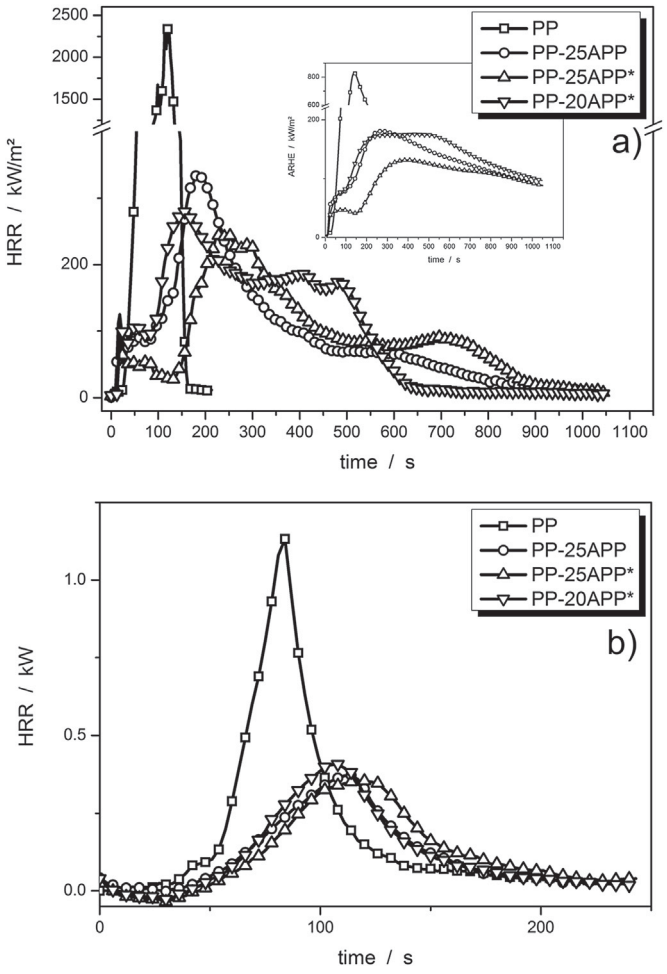

Fig. 7. HRR and ARHE curves of an intumescent system (PP-APP) from the cone calorimeter (a) and HRR curve from the rapid mass calorimeter (b).

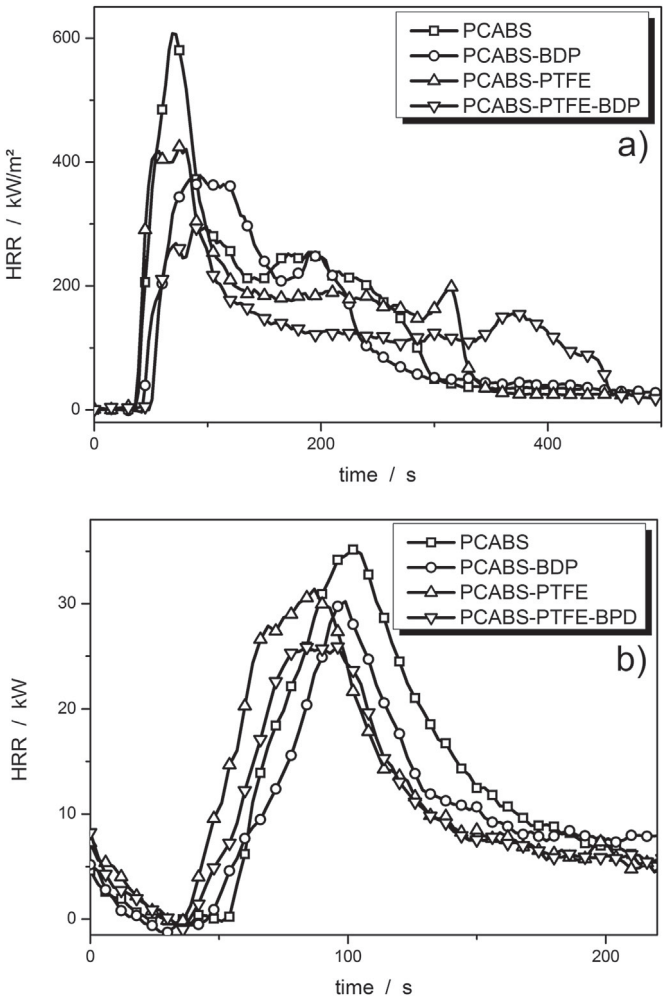

Fig. 8. HRR curves of PCABS, PCABS flame retarded with BDP, PCABS with PTFE as an anti-dripping agent and the combination of both derived from a) cone calorimeter and b) rapid mass calorimeter.

with the PHRR values of the rapid mass calorimeter measurements and serves as proof that the rapid mass calorimeter HRR curves are actual representations of averaged cone calorimeter curves.

PCABS shows a distinct peak at the beginning of the HRR curve in cone calorimeter measurements, after which a second, broader peak of around 250 kW/m^2 is reached. The addition of the anti-dripping agent PTFE lowers the PHRR to 67% and creates a plateau of steady burning between both peaks of around 150 kW/m^2. The time of burning is increased by around 150 s due to the char-inducing effect of PTFE [22]. The flame retardant BDP in PCABS prolongs the time to ignition, decreases the FIGRA and lowers the PHRR to around 63%. Furthermore, it leads to a broadening of the first peak and a reduction in burning time.

Both additives together cause a reduction of PHRR to 50% as well as a decrease in both the height and length of the steadily burning plateau in PCABS. The HRR curves are shown in Fig. 8 [9].

This example demonstrates the combined effect of charring and flame inhibition, exhibiting a characteristic HRR curve with its highest peak in the beginning, a phase of steady burning and a smaller peak shortly before flameout. The trends that were identified in the cone calorimeter forced-flaming tests also occurred in the rapid mass calorimeter when samples 20 mm × 20 mm in size were used. PCABS treated only with BDP has a slightly lower PHRR than PCABS with PTFE while the incorporation of both additives leads to the strongest decrease. Additionally, the HRR curves of the systems containing PTFE show a broadening of the peak, similar to the cone calorimeter tests, where a plateau of steady burning was introduced. This supports the hypothesis that testing under forced-flaming conditions on a smaller scale depicts an average of the characteristics shown by an HRR curve from the cone calorimeter. However, the trends in time to ignition show different results in the rapid mass calorimeter than in the cone calorimeter. In the cone calorimeter tests, time to ignition was prolonged when PTFE, BDP, or both were added. The rapid mass calorimeter scale showed a reduction in t_{ig} when PTFE or BDP was added. Comparison of the ARHE curves from cone calorimeter measurements (Fig. 9) and the heat release rates from the reduced-scale rapid mass calorimeter reveals similarities in their maximums. The non-flame retarded PCABS has the highest MARHE value in the cone calorimeter as well as the highest PHRR observed in the rapid mass calorimeter. The MARHE value from results of PCABS-PTFE is greater than of PCABS-BDP, and the combination of both PTFE and BDP in PCABS has the lowest MARHE. The same order reappears in the PHRR values of reduced-scale measurements in the rapid mass calorimeter. The ARHE also gives clearer insight into the differences in performance due to the rather complicated HRR curves, and is thus a suitable criterion to compare these particular materials.

The PHRR of polypropylene is reduced significantly, by over 90%, when combined with 54 wt.-% of magnesium hydroxide (Fig. 10). Its burning behavior changed such that it yields a characteristic HRR

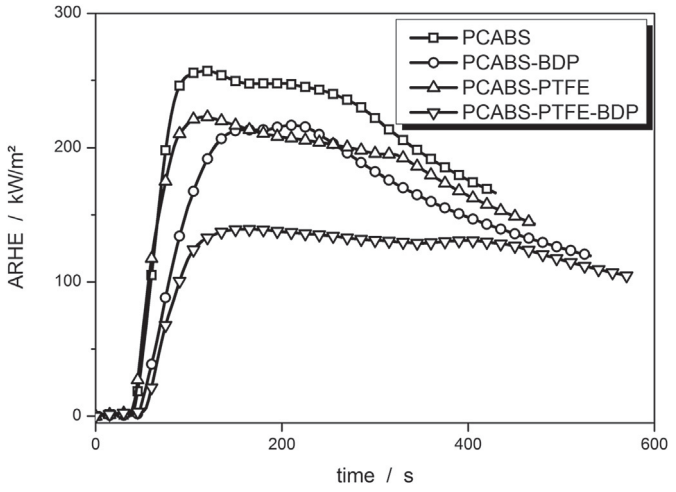

Fig. 9. ARHE curves of the investigated PCABS formulations from the cone calorimeter.

curve. It consists of two peaks of about the same height, occurring at the beginning and at the end of burning, with a stretched local minimum in between. The high amount of mineral filler not only reduces the amount of polymer matrix consumed as fuel by the flame, but also releases water during the burning process, which

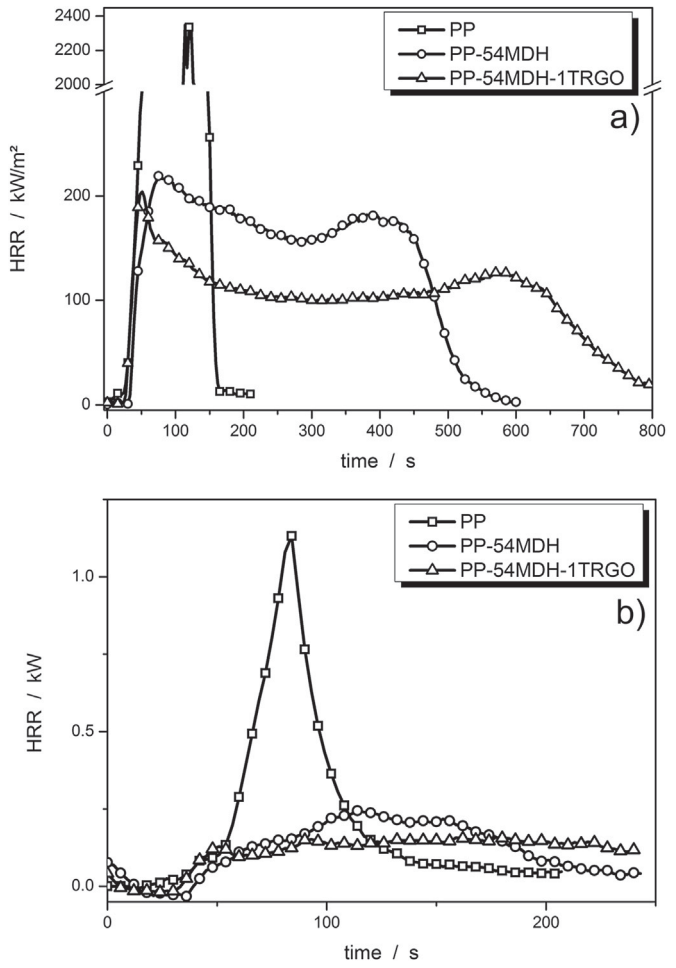

Fig. 10. Characteristic HRR curve obtained with the cone calorimeter (a) showing a peak at the beginning and at the end of burning respectively, and the rapid mass calorimeter (b).

dilutes and cools down the flame. An increase in the HRR shortly before flameout occurs due to the fact that the pyrolysis front has moved so far that the sample can now be considered thermally thin. Addition of only 1 wt.-% TRGO causes only a small reduction in PHRR, but decreases the height of the steady burning phase and increases its duration as well as the burning time in general [25].

The difference in the intensity of the HRR curves between PP and the other two formulations in the rapid mass calorimeter are clearly recognizable. While PP shows a very sharp and intense peak, the flame retarded formulations are strongly reduced in height. In fact, PHRR is reduced to 22 and 14%, respectively. This leads to a small but still distinguishable difference in PHRR between the two formulations, containing and lacking 1 wt.-% of the adjuvant TRGO. This enables even small changes in HRR to be evaluated on the small scale of the rapid mass calorimeter samples. However, the advantages of adding 1 wt.-% of TRGO to the system of 54 wt.-% MDH in PP do not become as clear in the rapid mass calorimeter as they do in the cone calorimeter. A simple calculation was made in order to confirm the conclusion that HRR curves are compressed when going from cone calorimeter samples to the reduced specimen size in the rapid mass calorimeter. The reduction in PHRR between the formulation with only 54 wt.-% MDH and the system with added TRGO in the rapid mass calorimeter is 35%. This equals exactly the reduction of HRRavg between both materials in the cone calorimeter.

TPES shows a dramatic change in burning behavior monitored by the cone calorimeter when 50 wt.-% of MDH are incorporated (Fig. 11). The characteristically strong slope in HRR at the beginning of the burning remains, but as soon as the temperature is reached at which MDH releases water into the gas phase and thus dilutes the flame, the HRR decreases again. The PHRR is reduced drastically to less than 10% and burning time is prolonged significantly from around 200 s to more than 1200 s. In contrast to the PP-MDH systems discussed above, TPES-50MDH does not show a second peak at the end of burning; the HRR curve is more of a classic example of a constant heat release decay when a mineral filler is included.

HRR results from the rapid mass calorimeter for the TPES show a strong slope and an abrupt decay similar to cone calorimeter tests. When 50 wt.-% of the mineral filler are added, curve behavior starts to differ from the tests. Instead of maintaining the strong HRR increase in the beginning, the HRR shows a rather weak slope. However, upon reaching the PHRR, the reduced-size sample undergoes a slow decay in HRR similar to that of the 100 mm × 100 mm specimen. The PHRR is decreased to about 25% and allows the assertion that significant PHRR reductions are observed in the rapid mass calorimeter.

3.4. Comparison of fire performance between the rapid mass calorimeter and cone calorimeter

Following the approach of Lopez-Cuesta et al. [31], sample series consisting of polymeric materials and their flame retarded equivalents were pictured in a performance ratio plot (Fig. 12). R1 stands for the ratio between the PHRR of the flame retarded material to the PHRR of the material in the rapid mass calorimeter, while R2 is calculated by dividing the PHRR of the flame retarded material by the PHRR of the material in the cone calorimeter measurements. All of the data points are located above the ideal correlation line. This means that the PHRR reduction is more apparent in the cone calorimeter than in the rapid mass calorimeter. The only reason for this divergent behavior is the reduced sample size and thus the increase in edge burning effect. To prove this, HDPE with 30 wt.-% of MDH and a thickness of 3 mm, HDPE with 15 wt.-% MDH and a thickness of 6 mm, and their respective non-flame retarded

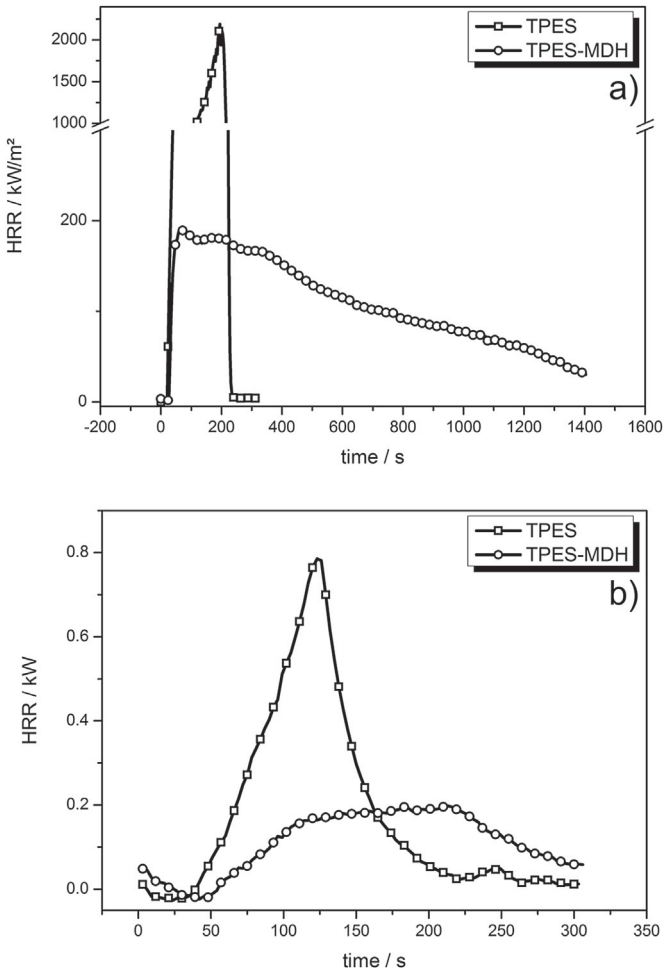

Fig. 11. Cone calorimeter (a) and rapid mass calorimeter (b) HRR curves of TPES and TPES with added mineral filler showing the typical characteristic curve form in the cone calorimeter.

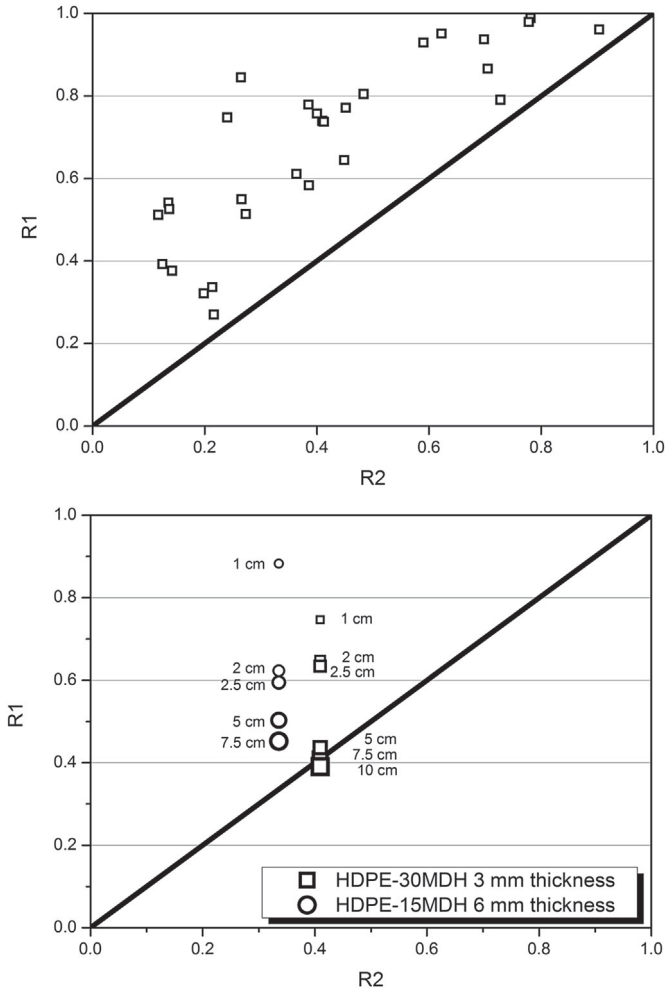

Fig. 12. Ratio correlation of PHRR from both methods. The plot shows the ratio of PHRR of non-flame retarded material to flame retarded material in the rapid mass calorimeter (R1) over the cone calorimeter (R2).

counterparts were varied in size and measured in the rapid mass calorimeter. Calculating the performance ratios of the respective PHRR values reveals that with increasing sample size, the data points approach the line of ideal correlation (Fig. 12). The effects like edge burning, which accompany a reduction in sample size, decreased and the fire performance of a material in the rapid mass calorimeter approximates the performance in the cone calorimeter. Modes of action like flame inhibition and the effect of a protection layer are detectable in the rapid mass calorimeter.

4. Conclusion

The reduced-scale measurements show many similarities with results from the cone calorimeter. The change in length scale while maintaining the same thickness and using another mode of heat release recording has vast consequences for the obtained results. It was demonstrated that the rapid mass calorimeter is both a versatile screening tool and a method to investigate burning behavior. Comparing the correlation coefficients of HRR values from each method shows a more or less strong peculiarity of certain measures, and thus is used to render the character of the rapid mass calorimeter more clearly. Additionally, correlations between the methods, especially regarding specific sample series, yield information about how certain curve forms change when the sample size is reduced. The combination of both the correlation over all formulations as a statistical approach, and over specific systematic series of samples, helps clarify the similarities between the cone calorimeter and the rapid mass calorimeter, and shows how the two tests are related. Performance correlations indicated a less pronounced performance effect of a flame retardant in a polymeric material in the rapid mass calorimeter than in the cone calorimeter. This was proven to depend solely on the sample size, and is not a result of changes in measurement conditions.

Acknowledgements

This research did not receive any specific grant from funding agencies in the public, commercial, or not-for-profit sectors. We would like to acknowledge our sample providers, flame retarded and non-flame retarded, inter alia ELKEM, Bayer MaterialScience (now Convestro), BASF, University Freiburg, TITK (Rudolstadt), and SKZ (Würzburg). Thanks also go to P. Klack for helping set up the rapid mass calorimeter.

References

[1] M.P. Stevens, Polymer additives: Part I. Mechanical property modifiers, J. Chem. Educ. 70 (6) (1993) 444.
[2] M.P. Stevens, Polymer additives: II. Chemical and aesthetic property modifiers, J. Chem. Educ. 70 (7) (1993) 535.

[3] M.P. Stevens, Polymer additives: III. Surface property and processing modifiers, J. Chem. Educ. 70 (9) (1993) 713.
[4] E.D. Weil, S.V. Levchik, Flame retardants for polystyrenes in commercial use or development, J. Fire Sci. 25 (2007) 241–265.
[5] E.D. Weil, S.V. Levchik, Flame retardants in commercial use or development for polyolefins, J. Fire Sci. 26 (2008) 5–43.
[6] P. Hughes, G.V. Jackson, R.N. Rothon, Particle morphology effects on the performance of PMMA filled with aluminium hydroxide in a variety of fire tests, Makromol. Chem. Macromol. Symp. 74 (1) (1993) 179–183.
[7] H. Huang, M. Tian, W. Liang, L. Zhang, Effect of particle size on flame retardancy of Mg(OH)2-filled ethylene vinyl acetate copolymer composites, J. Appl. Polym. Sci. 100 (6) (2006) 4461–4469.
[8] R.E. Lyon, R.N. Walters, Pyrolysis combustion flow calorimetry, J. Anal. Appl. Pyrolysis 71 (1) (2004) 27–46.
[9] B. Schartel, K.H. Pawlowski, R.E. Lyon, Pyrolysis combustion flow calorimeter: a tool to assess flame retarded PC/ABS materials? Thermochim. Acta 462 (1) (2007) 1–14.
[10] S. Rabe, B. Schartel, The Rapid Mass Calorimeter: a route to high throughput fire testing, Fire Mater., (2016) (accepted).
[11] C.A. Wilkie, G. Chigwada, J.W. Gilman, R.E. Lyon, High-throughput techniques for the evaluation of fire retardancy, J. Mater. Chem. 16 (2006) 2023–2029.
[12] J. Lindholm, A. Brink, M. Hupa, Influence of decreased sample size on cone calorimeter results, Fire Mater 36 (1) (2012) 63–73.
[13] V. Babrauskas, in: P.J. DiNenno, D. Drysdale, C.L. Beyler, W.D. Walton, R.L.P. Custer, J.R. Hall Jr., J.M. Watts Jr. (Eds.), Heat Release Rates. The SFPE Handbook of Fire Protection Engineering, third ed., National Fire Protection Association, Inc, 2002, pp. 3–8.
[14] S.J. Ritchie, K.D. Steckler, A. Hamins, T.G. Cleary, J.C. Yang, T. Kashiwagi. The effect of sample size on the heat release rate of charring materials, in: Fire Safety Science – Proceedings of the Fifth International Symposium, Melbourne, (1997). 177–188.
[15] M. Janssens, J. Huczek, A. Faw. Effect of specimen size on test results obtained in the cone calorimeter, in: Proceedings of the BCC Conference on Flame Retardancy, Norwalk, CT, (2008).
[16] Plastics – Simple heat release test, Plastics – Simple Heat Release Test Using a Conical Radiant Heater and a Thermopile Detector, ISO 13927, first ed., 2001.
[17] Reaction-to-fire tests – Heat release, Smoke Production and Mass Loss Rate, ISO 5660–1, third ed., 2015-03.
[18] L.L. Havlicek, R.D. Crane, Practical Statistics for the Physical Sciences, American Chemical Society, Washington, DC, 1988.
[19] B. Schartel, R. Kunze, D. Neubert, Red phosphorus-controlled decomposition for fire retardant PA 66, J. Appl. Polym. Sci. 83 (10) (2002) 2060–2071.
[20] B. Schartel, R. Kunze, D. Neubert, A. Tidjani, ZnS as fire retardant in plasticized PVC, Polym. Int. 51 (3) (2002) 213–222.
[21] B. Schartel, U. Braun, U. Schwarz, S. Reinemann, Fire retardancy of polypropylene/flax blends, Polymer 44 (20) (2003) 6241–6250.
[22] K.H. Pawlowski, B. Schartel, Flame retardancy mechanism of triphenyl phosphate, resorcinol bis(diphenyl phosphate) and bisphenol A bis(diphenyl phosphate) in polycarbonate/acrylonitrile-butadiene-styrene blends, Polym. Int. 56 (11) (2007) 1404–1414.
[23] U. Braun, B. Schartel, Flame retardancy mechanisms of aluminium phosphinate in combination with melamine cyanurate in Glass-Fibre-Reinforced poly(1,4-butylene terephthalate), Macromol. Mater. Eng. 293 (3) (2008) 206–217.
[24] B. Schartel, K.H. Richter, M. Böhning, Synergistic use of talc in Halogen-free Fflame retarded polycarbonate/acrylonitrile-butadiene-styrene blends, ACS Symposium Series 1118, in: A.B. Morgan, C.A. Wilkie, G.L. Nelson (Eds.), Fire and Polymers VI: New Advances in Flame Retardant Chemistry and Science, ACS, Washington, DC, USA, 2012, pp. 15–36. chap. 2.
[25] B. Dittrich, K.A. Wartig, D. Hofmann, R. Mülhaupt, B. Schartel, Flame retardancy through carbon nanomaterials: carbon black, multiwall nanotubes, expanded graphite, multi-layer grapheme and grapheme in polypropylene, Polym. Degrad. Stab. 98 (8) (2013) 1495–1505.
[26] B. Dittrich, K.A. Wartig, R. Mülhaupt, B. Schartel, Flame-retardancy Properties of intumescent ammonium poly(Phosphate) and mineral filler magnesium hydroxide in combination with graphene, Polymers 6 (11) (2014) 2875–2895.
[27] K. Langfeld, A. Wilke, A. Sut, S. Greiser, B. Ulmer, V. Andrievici, P. Limbach, M. Bastian, B. Schartel, Halogen-free fire retardant styrene-ethylene-butylene-styrene-based thermoplastic elastomers using synergistic aluminum diethylphosphinate-based combinations, J. Fire Sci. 33 (2) (2015) 157–177.
[28] U. Braun, V. Wachtendorf, A. Geburtig, H. Bahr, B. Schartel, Weathering resistance of halogen-free flame retardance in thermoplastics, Polym. Degrad. Stab. 95 (12) (2010) 2421–2429.
[29] E. Gallo, B. Schartel, U. Braun, P. Russo, D. Acierno, Fire retardant synergisms between nanometric Fe2O3 and aluminium phosphinate in poly(butylene terephthalate), Polym. Adv. Technol. 22 (12) (2011) 2382–2391.
[30] B. Schartel, G. Schmaucks. Flame retardancy synergism in polymers through different inert fillers' geometry, *Polym. Eng. Sci.* (in press), http://dx.doi.org/10.1002/pen.24485.
[31] R. Sonnier, L. Ferry, C. Longuet, F. Laoutid, B. Friederich, A. Laachachi, J.-M. Lopez-Cuesta, Combining cone calorimeter and PCFC to determine the mode of action of flame-retardant additives, Polym. Adv. Technol. 22 (7) (2011) 1091–1099.

3.3 Exploring the Modes of Action of Phosphorus-Based Flame Retardants in Polymeric Systems

Sebastian Rabe, Yuttapong Chuenban, Bernhard Schartel, *Materials* **2017**, 10, 455.

https://doi.org/10.3390/ma10050455

This article was accepted and published.

First author contribution:

- Conceptualization of the working packages
- Manufacturing of the polyester resin and paraffin specimen
- TG-FTIR and cone calorimeter measurements of the manufactured specimens
- Analysis and interpretation of all results
- Scientific discussion and conclusions
- Outline and writing of the manuscript

Contributions from other authors:

- Yuttapong Chuenban:
    - Manufacturing of the epoxy resin and PMMA resin specimens
    - TG-FTIR and cone calorimeter measurements of the manufacture specimen
    - Contribution to the analysis of the results
- Bernhard Schartel:
    - Writing of the funding application
    - Contribution to the scientific discussion
    - Contribution to the outline of the manuscript

Abstract: Phosphorus-based flame retardants were incorporated into different, easily preparable matrices such as polymeric thermoset resins and paraffin as a proposed model for polyolefins and were investigated for their flame retardancy performance. The favored mode of action of each flame retardant was identified in each respective system and at each respective concentration. Thermogravimetric analysis was used in combination with infrared spectroscopy of the evolved gas to determine the pyrolysis behavior, residue formation and the release of phosphorus species. Forced flaming tests in the cone calorimeter provided insight into burning behavior and macroscopic residue effects. The results were put in relation to the phosphorus content to reveal correlations between phosphorus concentration in the gas phase and flame inhibition performance, as well as between phosphorus concentration in the residue and condensed phase activity. Total heat evolved (fire load) and peak heat release rate were calculated based on changes in the effective heat of combustion and residue, and then were compared with the measured values to address the modes of action of the flame retardants quantitatively. The quantification of flame inhibition, charring, and the protective layer effect measure the non-linear flame retardancy effects as functions of the phosphorus concentration. Overall, this screening approach using easily preparable polymer systems provides great insight into the effect of phosphorus in different flame retarded polymers with regard to polymer structure, phosphorus concentration, and phosphorus species.

materials

MDPI

Article

Exploring the Modes of Action of Phosphorus-Based Flame Retardants in Polymeric Systems

Sebastian Rabe, Yuttapong Chuenban and Bernhard Schartel *

Bundesanstalt für Materialforschung und -prüfung (BAM), 12205 Berlin, Germany; sebastian.rabe@bam.de (S.R.); yuttapong1131@hotmail.com (Y.C.)

* Correspondence: bernhard.schartel@bam.de; Tel.: +49-30-8104-1021

Academic Editor: De-Yi Wang

Received: 20 February 2017; Accepted: 20 April 2017; Published: 26 April 2017

Abstract: Phosphorus-based flame retardants were incorporated into different, easily preparable matrices, such as polymeric thermoset resins and paraffin as a proposed model for polyolefins and investigated for their flame retardancy performance. The favored mode of action of each flame retardant was identified in each respective system and at each respective concentration. Thermogravimetric analysis was used in combination with infrared spectroscopy of the evolved gas to determine the pyrolysis behavior, residue formation and the release of phosphorus species. Forced flaming tests in the cone calorimeter provided insight into burning behavior and macroscopic residue effects. The results were put into relation to the phosphorus content to reveal correlations between phosphorus concentration in the gas phase and flame inhibition performance, as well as phosphorus concentration in the residue and condensed phase activity. Total heat evolved (fire load) and peak heat release rate were calculated based on changes in the effective heat of combustion and residue, and then compared with the measured values to address the modes of action of the flame retardants quantitatively. The quantification of flame inhibition, charring, and the protective layer effect measure the non-linear flame retardancy effects as functions of the phosphorus concentration. Overall, this screening approach using easily preparable polymer systems provides great insight into the effect of phosphorus in different flame retarded polymers, with regard to polymer structure, phosphorus concentration, and phosphorus species.

Keywords: flame retardants; flame inhibition; cone calorimeter; aluminum diethyl phosphinate; polyester; PMMA; epoxy resin; red phosphorus; BDP

1. Introduction

Nowadays, the ever growing numbers of different flame retardants for all kinds of applications, along with their variations in concentration, particle size distribution and so on, create a need for screening methods that allow time and material savings while yielding significant results and enabling reasonable conclusions. Several different approaches have been taken to accelerate fire testing, such as the microscale combustion calorimeter, the rapid cone calorimeter and the rapid mass calorimeter [1–4]. These methods are specifically designed for screening the fire performance of large numbers of samples. However, all of the methods require specific sample preparation, such as extrusion and injection molding, to ensure homogenous implementation of the flame retardant in the thermoplastic. With the acceleration of the actual testing method, the bottleneck shifts towards sample preparation. Thus, here a screening approach is presented that uses cone calorimeter investigations on different thermosets and on paraffin, which is proposed as a model for polyolefins, to address different phosphorous flame retardants in different concentrations.

Phosphorus-based flame retardants have been proposed to replace halogenated flame retarding additives due to their good fire properties and better environmental sustainability [5–7]. They exhibit

all kinds of flame retardant modes of action, such as flame inhibition in the gas phase and char enhancement, and intumescence and formation of inorganic glass in the condensed phase [6,8–16]. In many polymers, aluminum diethyl phosphinate (AlPi) is reported to exhibit high activity in the gas phase by releasing diethylphosphinic acid [17–20]. Often only a small fraction of it remains in the condensed phase to induce some char or residue formation [21]. Phosphate-based flame retardants are reported to act in the condensed phase as acid precursors, leading to char formation by esterification and dehydration [22–24]. Nevertheless, if the phosphate esters are released into the gas phase instead of reacting with the decomposing polymer, they show high flame inhibiting effects [25,26]. Thus, phosphate flame retardants such as bisphenol-A bis(diphenyl phosphate) (BDP), triphenyl phosphate (TPP) and resorcinol bis(diphenyl phosphate) (RDP) have different flame inhibition effectiveness, due to variations in decomposition behavior and releasability [25,27]. Despite its flammability hazard, red phosphorus is used as a flame retardant as well. It can act in both the gas phase and the condensed phase [8,16,28]. Indeed, phosphorous flame retardants often act in the condensed phase and in the gas phase at the same time [8,10,26,29]. It was also demonstrated that the existence and efficiency of the mode of action as well as its effect on the performance of the flame retardant depends not only on its chemical structure, but also strongly on its interaction with the polymeric matrix in which it is incorporated [8,11,15,26,30].

In this work, two AlPi flame retardants with different particle size distributions were used, as well as BDP and red phosphorus. Thus, it was possible to investigate and compare a range of different phosphorus sources with different phosphorus content and particle sizes. To achieve easier and faster sample preparation, the flame retardants were incorporated into resins, which are cured under laboratory conditions and into paraffin. Here, epoxy-, polyester- and acrylate-based resins were used by simply mixing them with the additive and molding in small amounts in the laboratory. It has to be noted, however, that the used epoxy resin cannot be seen as an example for all epoxy resins, since burning behavior and behavior of the flame retardants in the respective resin may be different. The group of polyolefins was replaced by paraffin. The relatively fast compounding aims to shift the bottleneck in the testing process away from sample preparation. Furthermore, the results obtained by means of these easily compounded polymeric systems are explained using general model assumptions.

2. Materials and Methods

2.1. Thermogravimetric Analysis Coupled with FTIR

Thermogravimetric analysis was conducted on a TG 209 F1 Iris (Netzsch Instruments, Selb, Germany). Specimens were provided in 5 mg portions of powder in a ceramic crucible, which were pyrolyzed under nitrogen at a heating rate of 10 K/min. Pyrolysis was performed in the absence of oxygen to simulate the oxygen-lean conditions in a laminar flame. To analyze and identify the gases during pyrolysis, the TGA was coupled via a transfer line with a Tensor 27 infrared spectrometer (Bruker Optics, Ettlingen, Germany). The gas cell and transfer line were operated at a temperature of 270 °C to ensure transport of the pyrolysis gases without condensation effects [31].

2.2. Cone Calorimeter

Forced flaming combustion tests were performed using a cone calorimeter (FTT, East Grinstead, UK) in accordance with ISO 5660. Specimens 100 × 100 × 3 mm^3 in size were conditioned for 48 h at 23 °C and 50% relative humidity, wrapped in an aluminum tray, and irradiated with 50 kW/m^2 at a distance of 35 mm from the cone heater [32] to ensure sufficient spacing for the greatest possible residue formation. Samples were measured in triplicate when the first two measurements deviated by more than 10% in any result.

2.3. Elemental Analysis

Elemental analysis was performed by Mikroanalytisches Laboratorium Kolbe (Mühlheim an der Ruhr, Germany).

2.4. Materials

2.4.1. Flame Retardants

Aluminum diethylphosphinate (AlPi) was used in two different varieties, Exolit OP935 and Exolit OP1230 (Clariant). Exolit OP935 is a fine-grained AlPi developed especially for adhesive applications, and is established as an effective flame inhibitor in epoxy, acrylic and TPE resins [18,33]. The highly stable Exolit OP 1230 is widely used for high-temperature polyamides, as well as in polyamide-AlPi mixtures [34–36]. Both flame retardants contain around 23.5 wt % phosphorus. Red phosphorus (Exolit RP607, Clariant) is typically used in thermoplastics for electronics applications [28]. As it is the most concentrated source of phosphorus as a flame retardant, its application concentration generally lies below 10 wt %, and it is usually applied as encapsulated material. Bisphenol-A bis(diphenyl phosphate) (BDP) is an oligomeric aryl phosphate ester designed for use in engineering resins such as PC/ABS [5,6]. Since BDP contains only around 9 wt % of phosphorus, a higher BDP load must be considered in the material. BDP was used in concentrations of 10, 20, 25 and 35 wt % to reach the effective range of phosphorus concentration. All other investigated flame retardants were concentrated at 5, 10, 15 and 20 wt %.

2.4.2. Resin Systems

Epoxy resins have become important materials for electronics and lightweight construction, especially as fiber reinforced composites [37,38]. Bisphenol-A diglycidyl ether (DGEBA, Araldit MY740, Bodo Möller Chemie GmbH, Offenbach, Germany) and isophorone diamine (IPDA, Merck KGaA, Darmstadt, Germany) was used as an example for an epoxy resin [39]. IPDA and the respective flame retardant were added to DGEBA and stirred until a homogenous mixture was obtained. Forty grams of the mixture was poured into a 100 × 100 × 6 mm^3 aluminum mold and cured for 30 min at 80 °C and for 70 min at 120 °C. The aluminum frame was stabilized with weights to prevent deformation during curing. The edges of the finished specimens had to be ground down in order to obtain a flat surface. The rest of the mixture was also cured as described above, followed by grinding to obtain powder for TGA-FTIR measurements.

As an acrylate thermoset, a pre-accelerated PMMA resin with an incorporated, UV-induced curing agent was used (S. u. K. Hock GmbH, Regen, Germany). The respective flame retardant was added to the methyl methacrylate resin and stirred until homogeneity was achieved. The mixture was then poured into aluminum molds and cured at room temperature and irradiated by a daylight spectrum lamp for 12 h. Systems with red phosphorus could not be produced because the curing process was hindered so that complete hardening could not be achieved.

For preparation of the polyester system, the flame retardant was added to a mixture of polyester resin L800 and the curing agent methyl ethyl ketone peroxide (MEKP) (S. u. K. Hock GmbH, Regen, Germany). The mixture was then poured into aluminum molds and cured at room temperature for 8 h. The edges of the molds were also weighed down to prevent deformation during curing. Red phosphorus prevented the resin from curing, so that a polyester formulation with RP as flame retardant could not be manufactured.

To represent the group of polyolefins, paraffin pellets were melted at 75 °C and combined with the flame retardant. The hot mixture was poured into the aluminum molds and cooled down to room temperature. It was not possible to implement BDP into paraffin because the two phases were immiscible. BDP accumulated as a bubble underneath the paraffin in the mold. All produced materials were given a label according to Table 1.

Table 1. Nomenclature of the produced flame retarded polymeric materials with *x* = concentration of the flame retardant, 5, 10, 15 or 20 wt % for Exolit OP935, OP1230 and RP607 and 10, 20, 25 and 35 wt % for BDP respectively.

	Exolit OP935	**Exolit OP1230**	**Exolit RP607**	**BDP**
DGEBA/IPDA	EP-*x*-ExOP935	EP-*x*-ExOP1230	EP-*x*-ExRP	EP-*x*-BDP
PMMA-resin	PMMA-*x*-ExOP935	PMMA-*x*-ExOP1230	—	PMMA-*x*-BDP
Polyester-resin	Pes-*x*-ExOP935	Pes-*x*-ExOP1230	—	Pes-*x*-BDP
Paraffin	P-*x*-ExOP935	P-*x*-ExOP1230	P-*x*-ExRP	—

3. Results and Discussion

3.1. Thermogravimetric Analysis Results

All investigated systems, with and without flame retardant, were investigated via thermogravimetric analysis in the absence of oxygen. Mass and DTG curves are displayed in Figure 1 and results are listed in Table 2.

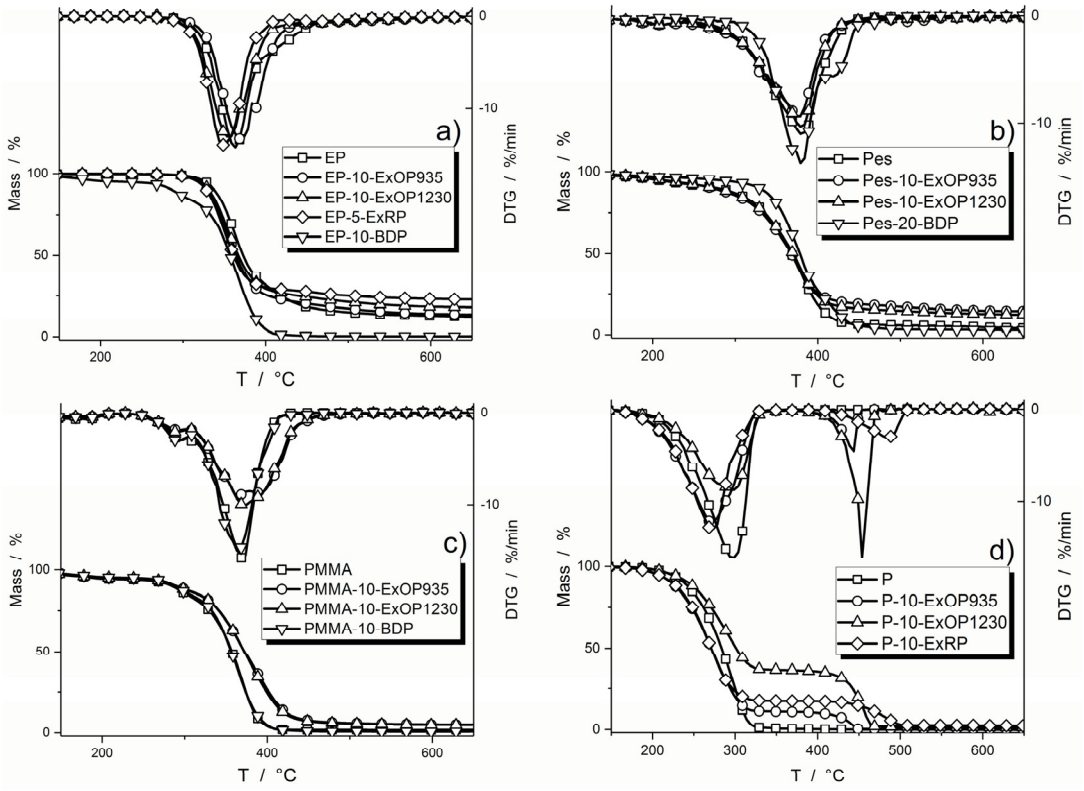

Figure 1. Thermogravimetric (TG) and derivative thermogravimetric (DTG) results for selected flame retarded and non-flame retarded specimens with: epoxy resin (**a**); polyester resin (**b**); PMMA resin (**c**); and paraffin (**d**) as polymer matrix.

Table 2. Results from thermogravimetric analysis (TGA). $T_{5\%\ ML}$ is the temperature at which 5 wt % of the mass is lost, T_{DTGmax} is the temperature of the maximum of the mass loss rate. The residue was determined at 800 °C.

Material	$T_{5\%\ ML}$	T_{DTGmax}	Residue
	°C	°C	wt %
EP	326 ± 1	360 ± 2	10.7 ± 0.1
EP-10-ExOP935	320 ± 1	355 ± 1	12.1 ± 0.3
EP-10-ExOP1230	320 ± 2	353 ± 1	12.1 ± 0.3
EP-5-ExRP	318 ± 1	349 ± 1	17.0 ± 0.2
EP-10-BDP	265 ± 1	365 ± 1	3.0 ± 0.1
Pes	204 ± 1	380 ± 2	2.9 ± 0.1
Pes-10-ExOP935	211 ± 1	378 ± 1	14.0 ± 0.4
Pes-10-ExOP1230	210 ± 1	382 ± 2	11.7 ± 0.2
Pes-20-BDP	277 ± 2	380 ± 2	2.6 ± 0.1
PMMA	192 ± 1	370 ± 2	1.7 ± 0.1
PMMA-10-ExOP935	229 ± 2	368 ± 1	4.6 ± 0.2
PMMA-10-ExOP1230	228 ± 1	370 ± 2	4.5 ± 0.1
PMMA-10-BDP	246 ± 2	364 ± 1	0.7 ± 0.1
P	223 ± 1	296 ± 1	0.1 ± 0.1
P-10-ExOP935	207 ± 1	274 ± 1	0.2 ± 0.1
P-10-ExOP1230	225 ± 2	454 ± 3	1.4 ± 0.2
P-10-ExRP	207 ± 1	273 ± 1	2.1 ± 0.2

The start of the decomposition $T_{5\%\ ML}$ (at which 5 wt % of the material was lost) for epoxy resin formulations shifted towards lower temperatures when flame retardants were added. EP-10-ExOP935 and EP-10-ExOP1230 showed decomposition behavior similar to the pure epoxy resin. The temperature of the maximum mass loss rate, T_{DTGmax}, was shifted to temperatures 5 and 7 °C lower, respectively. With the non-flame retarded epoxy resin producing 10.7 wt % of residue, replacement of 10 wt % of the resin with AlPi flame retardants would still produce 9.6 wt % residue. Since residue formation increased to 12.1 wt %, 2.5 wt % of the residue results from the incorporation of the flame retardant. Epoxy resin with 5 wt % of red phosphorus flame retardant added began decomposition at an even lower temperature, exhibiting a lower T_{DTGmax}, and an increase in residue of around 6.8 wt %. This means that carbonaceous char was produced. Besides the drastic lowering of the temperature at the start of decomposition, incorporation of 10 wt % of BDP in the epoxy resin resulted in a second decomposition step prior to the main one. It also formed much less residue than the other epoxy formulations, leading to the conclusion that this amount of BDP prevents residue production in epoxy resin. The temperature of maximum decomposition was shifted to temperatures 5 °C higher.

For the polyester system, the beginning of decomposition shifted to temperatures only slightly higher for Pes-10-ExOP935 and Pes-10-ExOP1230, but the effect was stronger when BDP was added. Ten weight percent of Exolit OP935 promoted the production of residue, increasing the amount by 11.4 wt %. Carbonaceous char was formed. For 10 wt % of Exolit OP1230 in polyester resin, the residue formation was promoted by 9.1 wt % compared to the non-flame retarded polyester resin. Pes-20-BDP produced only 0.3 wt % more residue. The temperatures of maximum decomposition did not alter much with the addition of a respective flame retardant.

In the PMMA resin, the starting temperature for decomposition shifted to higher temperatures with the addition of flame retardants. Incorporation of 10 wt % Exolit OP935 or OP1230 increased the temperature of 5 wt % mass loss by around 37 °C, whereas BDP raised it by more than 50 °C. There are no differences in decomposition observed between Exolit OP935 and OP1230. Ten weight percent of either flame retardant in PMMA resin increased the amount of residue by 3 wt %, consisting of inorganic ash. The amount of residue of PMMA-10-BDP was insignificant. Only for 10% BDP was a relevant shift of T_{DTGmax} by 6% to lower temperatures observed.

For paraffin, all of the flame retarded formulations showed a two-step decomposition process, clearly visible in both the mass loss and the mass loss rate curves (Figure 1d). The AlPi flame retardant Exolit OP935 as well as the red phosphorus caused a decrease in the temperature at which

decomposition begins. Furthermore, both flame retardants caused a shift in the maximum of the mass loss rate to temperatures 22 to 23% lower. In the DTG curves it becomes clear that the formulation with 10 wt % of Exolit OP1230 showed the highest mass loss rate in the second step of decomposition. It was even higher than what is considered the main decomposition step for the other formulations, changing the T_{DTGmax} to 454 °C. The residues produced by all paraffin formulations are negligible. These results clarified that the phosphorus-based flame retardants only slightly promote the formation of a residue, especially at relatively low concentrations of up to 10 wt %, and thus are mainly released into the gas phase. The varied particle size distribution in Exolit OP935 and Exolit OP1230 had no significant influence on the thermal decomposition properties.

3.2. FTIR Spectra of the Gaseous Phase

To confirm that phosphorus species were released into the gas phase, the pyrolysis gases evolved from TGA measurements were introduced into an IR cell. It was possible to identify various volatile phosphorus species. The FTIR spectra of the investigated formulations are shown in Figure 2. These experiments simply serve as a way to enable a discussion about the gas phase activity due to the release of phosphorus species.

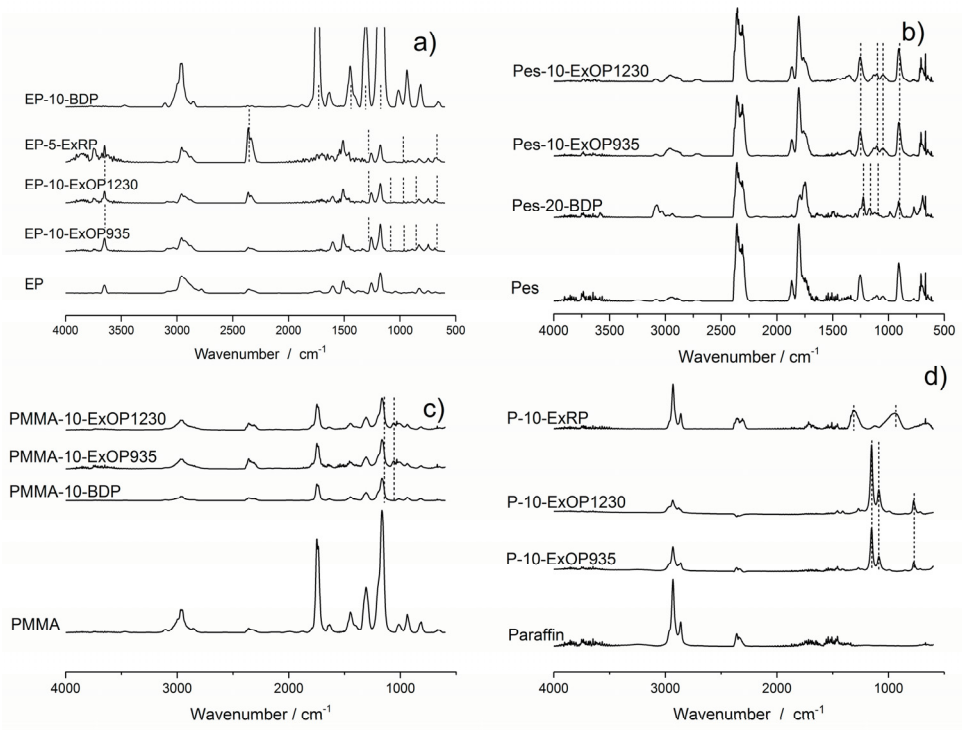

Figure 2. Fourier transform infrared (FTIR) spectra at the respective main decomposition step of flame retardants in: epoxy (**a**); polyester (**b**); PMMA (**c**); and paraffin (**d**) systems. Dotted lines were included as an aid to highlight smaller peaks from phosphorus species.

The AlPi flame retardants Exolit OP935 and OP1230 showed peaks at wavenumbers 854, 3650 and 1265 cm^{-1} in the epoxy resin, indicating the P–O, P–OH and P=O-stretch of diethylphosphinic acid. At 1078 cm^{-1}, a weak peak expressed the PO^{2-} anion of the AlPi molecule, whereas the peak at 952 cm^{-1} signified the production of ethene by a P–C bond break in AlPi. A phosphinate peak was found at 670 cm^{-1} [21,40,41]. Red phosphorus showed peaks at 670, 922, 1256 and 2375 cm^{-1}, which are representative for PO_4^{3-}, P–OP, P=O and P–OH vibrations. In the EP-10-BDP formulation, several peaks corresponding to phenolic derivatives of bisphenol-A were found at 1261, 1173, 1490 and 1620 cm^{-1}, which represent aromatic phosphate esters.

In the polyester resin, Exolit OP935 and 1230 showed peaks at 1105 and 1053 cm^{-1}, which display PO^{2-} vibration. The peak at 1257 cm^{-1} is attributed to P=O. A peak for a P–O–P vibration was found at 910 cm^{-1}. In BDP, those vibrations occurred at 1165, 1087, 1230 and 910 cm^{-1}.

Peaks related to phosphorus species are less pronounced in the flame retarded PMMA resin formulations. The strong release of methyl methycrylate, verified by the characteristic peaks such as the C–H stretch at around 2950 cm^{-1}, the C=O stretch at 1700 cm^{-1}, the C=C stretch at 1600 cm^{-1} and the C–O stretch at around 1200 cm^{-1}, concealed most of the phosphorus-related peaks. Only the peaks at 1056 and 1168 cm^{-1} suggest the existence of PO^{2-} species in the gas phase. However, Exolit OP935 and OP1230 incorporated into paraffin showed strong PO^{2-} peaks at 1156 and 1085 cm^{-1}, as well as a peak at 775 cm^{-1} which is attributed to diethylphosphinic acid. Red phosphorus in paraffin did not exhibit phosphorus-related peaks at the first decomposition step. However, at the second decomposition step, phosphorus was released as mixtures of undefined low-oxidized phosphorus oxides indicated by broad peaks at around 1300 and 950 cm^{-1}. Earlier work showed that phosphorus was released as P_4 molecules, breaking down to P_2 molecules with increasing temperature [16].

The results from the FTIR experiments demonstrated that phosphorus species are traceable in the gaseous phase and thus are released during pyrolysis of the formulations. This is the premise of the following investigations into the extent to which phosphorus compounds and the concentration of phosphorus in the gas phase are attributed to flame inhibition, and whether the remaining phosphorus in the residue has any effect on other modes of action in flame retardancy.

3.3. Forced Flaming Fire Behavior: Cone Calorimeter

3.3.1. Comparison of Heat Release Rates

Forced flaming fire tests were conducted in the cone calorimeter. At first, it was interesting to see the differences between the investigated flame retardants at the same concentration in different matrices. The heat release rate (HRR) curves are displayed in Figure 3. The results of all cone calorimeter measurements are summarized in Table 3.

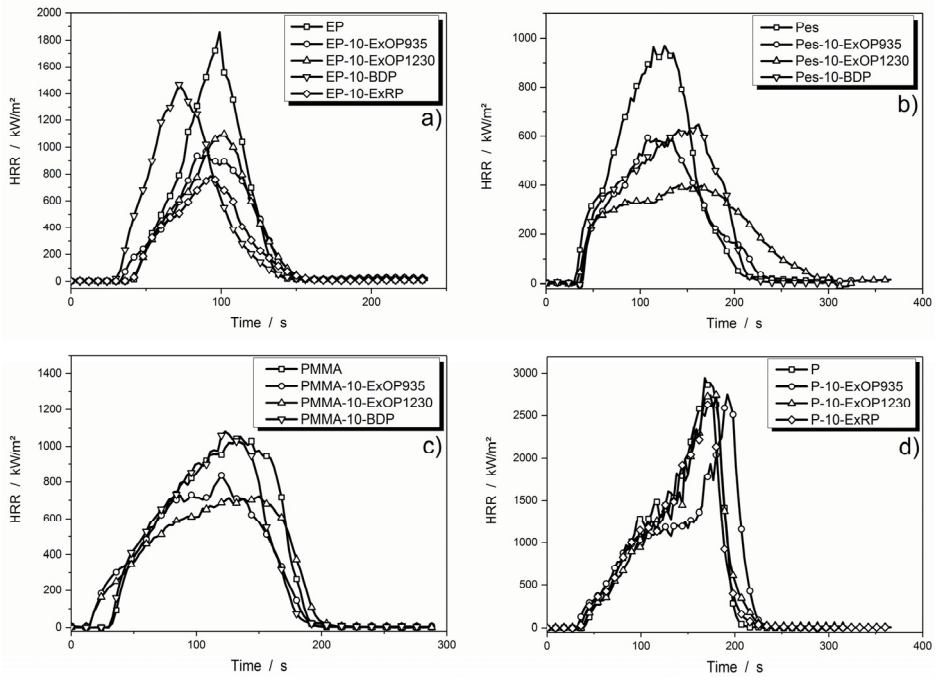

Figure 3. Cone calorimeter heat release rate (HRR) curves of flame retardants in: DGEBA/IPDA (**a**); Pes-resin (**b**); PMMA resin (**c**); and paraffin (**d**) with a concentration of 10 wt %.

Table 3. Cone calorimeter results.

System	t_{ig}	PHRR	THE	EHC	Residue at End of Test
	s	kW/m^2	MJ/m^2	MJ/kg	wt %
EP	39 ± 1	1858 ± 41	81.3 ± 0.1	24.7 ± 0.1	0.5 ± 0.0
EP-5-ExOP935	30 ± 1	1632 ± 4	71.1 ± 2.1	21.6 ± 0.4	4.3 ± 0.3
EP-10-ExOP935	32 ± 1	969 ± 57	59.0 ± 1.3	19.2 ± 0.3	6.3 ± 0.3
EP-15-ExOP935	30 ± 1	864 ± 9	57.0 ± 0.3	18.3 ± 0.0	8.6 ± 0.3
EP-20-ExOP935	30 ± 0	817 ± 25	52.3 ± 0.1	17.7 ± 0.1	11.3 ± 0.6
EP-5-ExOP1230	31 ± 2	1105 ± 52	71.6 ± 0.3	19.9 ± 1.4	4.9 ± 0.1
EP-10-ExOP1230	32 ± 1	1097 ± 50	61.1 ± 0.1	19.0 ± 0.0	6.3 ± 0.2
EP-15-ExOP1230	30 ± 0	1007 ± 16	58.9 ± 0.8	18.2 ± 0.2	8.6 ± 0.2
EP-20-ExOP1230	31 ± 2	861 ± 2	54.0 ± 0.3	18.0 ± 0.1	10.8 ± 0.0
EP-5-ExRP	29 ± 1	964 ± 16	51.1 ± 1.9	15.7 ± 0.3	6.3 ± 0.1
EP-10-ExRP	33 ± 1	786 ± 24	47.2 ± 1.0	15.4 ± 0.4	8.0 ± 0.1
EP-15-ExRP	34 ± 2	673 ± 125	42.4 ± 0.9	13.5 ± 0.4	8.7 ± 0.5
EP-20-ExRP	32 ± 2	873 ± 56	50.1 ± 0.4	16.6 ± 0.3	9.9 ± 1.5
EP-10-BDP	25 ± 3	1468 ± 44	74.0 ± 4.1	22.7 ± 1.4	5.0 ± 0.3
EP-20-BDP	26 ± 1	688 ± 3	49.0 ± 0.7	16.9 ± 0.1	14.9 ± 1.1
EP-25-BDP	22 ± 2	660 ± 1	45.0 ± 0.3	15.5 ± 0.1	15.8 ± 1.7
EP-35-BDP	28 ± 1	628 ± 3	42.5 ± 0.6	15.3 ± 0.3	17.3 ± 0.4
Pes	26 ± 1	1017 ± 16	94.3 ± 2.9	19.9 ± 0.9	0.1 ± 0.1
Pes-5-ExOP935	33 ± 2	854 ± 38	85.5 ± 0.4	19.1 ± 0.1	4.1 ± 0.2
Pes-10-ExOP935	32 ± 1	599 ± 6	64.5 ± 1.3	15.7 ± 0.1	7.7 ± 0.5
Pes-15-ExOP935	36 ± 2	577 ± 29	70.9 ± 0.0	16.5 ± 0.2	8.5 ± 0.3
Pes-20-ExOP935	34 ± 1	521 ± 15	60.9 ± 3.2	14.7 ± 0.6	8.6 ± 0.5
Pes-5-ExOP1230	31 ± 2	969 ± 33	89.8 ± 0.1	19.8 ± 0.1	3.7 ± 0.3
Pes-10-ExOP1230	32 ± 5	428 ± 27	69.4 ± 2.2	14.9 ± 2.0	8.5 ± 0.1
Pes-15-ExOP1230	30 ± 2	603 ± 37	73.4 ± 4.0	13.9 ± 2.3	9.4 ± 0.4
Pes-20-ExOP1230	33 ± 1	456 ± 8	61.2 ± 1.7	14.4 ± 0.4	10.0 ± 0.1
Pes-10-BDP	35 ± 1	727 ± 80	77.8 ± 1.4	16.9 ± 0.3	1.1 ± 0.4
Pes-20-BDP	32 ± 1	629 ± 63	66.5 ± 0.7	11.3 ± 3.2	2.1 ± 0.5
Pes-25-BDP	37 ± 6	570 ± 17	59.6 ± 0.6	11.7 ± 1.7	3.5 ± 0.5
Pes-35-BDP	34 ± 5	538 ± 49	55.9 ± 1.4	12.1 ± 0.4	4.8 ± 0.3
PMMA	32 ± 1	1051 ± 41	106.9 ± 0.6	25.1 ± 0.5	0.1 ± 0.0
PMMA-5-ExOP935	26 ± 1	836 ± 1	93.7 ± 2.5	22.8 ± 0.7	1.2 ± 0.2
PMMA-10-ExOP935	25 ± 1	792 ± 21	88.8 ± 0.5	22.8 ± 0.2	2.5 ± 0.1
PMMA-15-ExOP935	24 ± 1	740 ± 37	83.8 ± 0.3	20.9 ± 0.1	3.8 ± 0.0
PMMA-20-ExOP935	22 ± 1	615 ± 33	81.8 ± 1.0	21.0 ± 0.4	5.7 ± 0.5
PMMA-5-ExOP1230	23 ± 1	852 ± 20	97.0 ± 1.0	23.2 ± 1.8	1.5 ± 0.1
PMMA-10-ExOP1230	22 ± 0	722 ± 16	89.2 ± 1.1	22.6 ± 0.4	2.9 ± 0.0
PMMA-15-ExOP1230	24 ± 2	678 ± 63	86.6 ± 3.0	21.6 ± 0.6	3.4 ± 0.1
PMMA-20-ExOP1230	26 ± 2	620 ± 4	82.8 ± 0.6	21.4 ± 04	4.8 ± 0.5
PMMA-10-BDP	29 ± 0	1079 ± 25	108.4 ± 0.3	24.7 ± 2.3	0.5 ± 0.1
PMMA-20-BDP	31 ± 1	994 ± 38	97.4 ± 0.9	23.4 ± 0.4	0.6 ± 0.0
PMMA-25-BDP	28 ± 1	868 ± 48	91.5 ± 1.9	21.7 ± 0.1	0.7 ± 0.1
PMMA-35-BDP	28 ± 1	928 ± 19	93.0 ± 0.2	22.3 ± 0.4	0.8 ± 0.1
P	40 ± 3	2996 ± 24	210.1 ± 2.9	44.1 ± 0.5	0.1 ± 0.0
P-5-ExOP935	32 ± 1	1935 ± 167	198.8 ± 7.1	42.3 ± 0.7	0.0 ± 0.0
P-10-ExOP935	27 ± 2	1593 ± 96	189.9 ± 27.1	41.4 ± 1.0	0.0 ± 0.2
P-15-ExOP935	23 ± 1	1371 ± 101	183.8 ± 1.3	39.4 ± 0.1	2.1 ± 0.3
P-20-ExOP935	23 ± 2	1130 ± 69	187.6 ± 3.7	38.9 ± 0.4	1 ± 0.6
P-5-ExOP1230	37 ± 2	2872 ± 318	197.2 ± 1.5	44.0 ± 0.2	0.1 ± 0.1
P-10-ExOP1230	42 ± 6	2868 ± 123	209.9 ± 2.9	43.3 ± 0.3	1.3 ± 0.8
P-15-ExOP1230	29 ± 1	2559 ± 223	195.8 ± 3.5	42.4 ± 0.7	2.9 ± 0.3
P-20-ExOP1230	27 ± 4	2257 ± 67	188.6 ± 12.6	40.7 ± 1.6	4.3 ± 1.0
P-5-ExRP	33 ± 1	2945 ± 13	212.5 ± 10.9	43.2 ± 0.2	0.5 ± 0.5
P-10-ExRP	34 ± 1	2781 ± 150	201.1 ± 1.6	41.4 ± 0.1	0.5 ± 0.0
P-15-ExRP	29 ± 3	2559 ± 219	191.8 ± 1.5	40.4 ± 0.6	0.2 ± 0.1
P-20-ExRP	35 ± 4	2519 ± 35	189.9 ± 2.6	38.5 ± 0.7	0.3 ± 0.6

Except for paraffin, the systems clearly showed improvements in terms of flame retardancy, such as reduction in peak heat release rate (PHRR) and total heat evolved (THE). In the epoxy resin, the formulation with 10 wt % of BDP was the least effective; it lowered the PHRR but shortened the time to ignition. Ten weight percent of Exolit OP935 and OP1230 further reduced PHRR, with OP935 showing slightly better performance. However, their efficiency at 10 wt % was similar. Compared to the residue analysis results from TGA, the increase in residue was much more evident in the cone calorimeter, with an increase of 10% for the highest investigated flame retardant load. Red phosphorus induced the largest reduction in HRR, although an even greater reduction was expected because of the high phosphorus content. This suggests that not only the phosphorus content of a flame retardant is responsible for its performance, but also the way the phosphorus is incorporated. Compared to the results from the thermogravimetric analysis, the residue produced is not as distinct, especially not for red phosphorus. At the same time, THE is reduced by almost 50% for EP-15-ExRP. This allows the conclusion that gas phase activity is mainly responsible for the high THE reduction. However, the residue produced by BDP increased strongly with higher flame retardant load. This suggests that there is a clear tendency for condensed phase activity of BDP. In the epoxy resin, 15 wt % of red phosphorus as well as 35 wt % of BDP showed the best HRR and THE reduction.

Polyester resin showed a PHRR of 900 to 1000 kW/m^2 without any flame retardant. The flame retardants Exolit OP935 and BDP caused a similar reduction in PHRR to around 600 kW/m^2, even though BDP has lower phosphorus content. The performance of 10 wt % Exolit OP1230 in polyester resin exceeded those of the other polyester formulations, as the PHRR was reduced further, to around 400 kW/m^2. In the PMMA resin, the formulation with 10 wt % of BDP had about the same performance as the non-flame retarded resin. Residue formation of the polyester resin formulations did not show salience; amounts increased with increasing flame retardant load, but remained below 10 wt %. It was found that Exolit OP1230 resulted in the greatest HRR and THE reduction, especially at 20 wt %.

When Exolit OP935 or 1230 were incorporated into PMMA resin, the PHRR decreased but the time to ignition was shortened. Exolit OP1230 showed slightly lower PHRR but a longer time of burning. Residue formations were in great accordance with results from thermogravimetric analysis, and demonstrated that all flame retardants work mainly via gas phase activity. Incorporation of BDP did not deliver satisfying results in HRR and THE reduction and was thus considered the worst additive for these purposes.

Forced flaming heat release tests on paraffin and the respective flame retarded formulations did not differ substantially as a pure system or with 10 wt % flame retardant load. Only the system with 10 wt % of Exolit OP935 showed prolongation of the small plateau of steady burning and a slight shift of the PHRR to later times. Observation of the burning process of the formulations including red phosphorus showed a peculiarity—at the end of the burning process the flame became very bright and smoke production increased. Red phosphorus did not contribute significantly to inhibiting the burning process. Rather, it burned away at the end of the burning process. Reductions in PHRR were thus due to fuel replacement by the flame retardant. No significant residue was formed. Only at high concentrations of the AlPi flame retardants were 2 to 4 wt % of residue measured. However, it was observed that they formed towards the end of the burning, when the flame was about to extinguish; thus, they were not able to affect the burning behavior through condensed phase activity. Overall, 20 wt % of Exolit OP935 reduced PHRR from 2972 to 1130 kW/m^2 and THE from 210 to 188 MJ/m^2, and is thus considered to be the best suited additive in paraffin.

One of the most important characteristics when it comes to the fire performance of a flame retardant in a polymeric system is the change in PHRR. The reduction in PHRR signifies several other phenomena: reduction in the effective heat of combustion, reduction in released fuel due to an increased amount of residue, and the effect of a protective layer are all reflected by this measure. To illustrate the correlation between PHRR reduction and phosphorus content in a flame retardant, they were plotted in Figure 4.

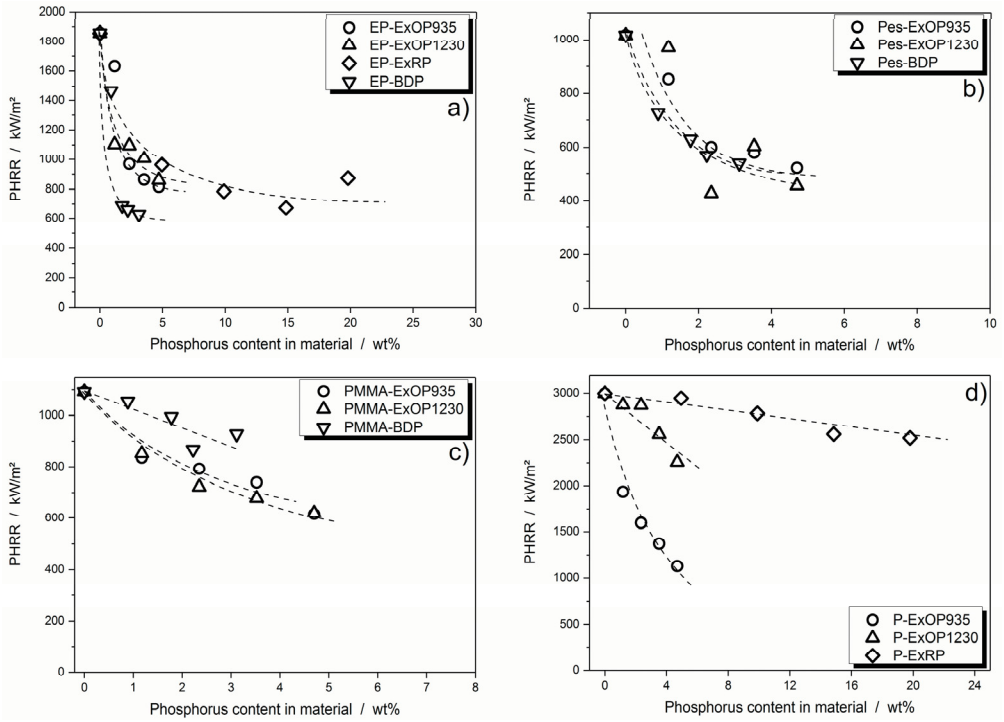

Figure 4. Peak of heat release rate (PHRR) of epoxy resin (**a**), polyester resin (**b**), PMMA resin (**c**) and paraffin (**d**) systems plotted against amount of phosphorus in the bulk material. The dotted lines are included as guides for the eye analogous to the findings from Brehme et al. for comparable materials [31].

The DGEBA/IPDA epoxy resin showed a very pronounced leveling off of flame retardancy effectiveness for all investigated flame retardants. This leveling off set in at around 10 wt % phosphorus content for RP, whereas the AlPi flame retardants Exolit OP935 and OP1230 already displayed this effect at a lower phosphorus content. For BDP, which had the lowest phosphorus content of all investigated flame retardants, the reduction in PHRR was highest, but leveled off at around 700 to 600 kW/m^2 at even low phosphorus concentrations (Figure 4a).

The leveling off of PHRR reduction effectiveness was also visible in the polyester resin. However, since the absolute reduction in PHRR was not as high as in the epoxy resin, the leveling off was not as pronounced. The PHRR reduction was more or less the same for all three incorporated flame retardants (Figure 4b). Deviations in the Exolit OP1230 polyester system may derive from slight variations in curing time.

Flame retardants in the PMMA resin tended to level off in effectiveness in terms of PHRR reduction. However, the decay in effectiveness was more gradual, especially since the pure reduction in PHRR was less significant than in the epoxy resin. BDP in the PMMA resin even seemed to have a linear decay in PHRR with increasing phosphorus content (Figure 4c).

Flame retardants in paraffin did not exhibit leveling off, but rather a linear decay in PHRR. Red phosphorus did not lead to a significant reduction in PHRR. Exolit OP935 was the most effective flame retardant, reducing the PHRR from 3000 to around 1000 kW/m^2 with a phosphorus content of only 4.7 wt % (Figure 4d). It would now be interesting to establish how much of the flame retardant performance actually resulted from gas phase activity, namely flame inhibition.

3.3.2. Flame Inhibition Dependency on Phosphorus Content Released into Gas Phase

To investigate gas phase activity, it was first necessary to determine the amount of phosphorus released into the gas phase. This was calculated by subtracting the measured phosphorus content remaining in the residue from the total amount of phosphorus in the sample. Concentration of

phosphorus inside the residue was measured via elemental analysis. For visualization purposes, phosphorus release is depicted in a bar graph for every formulation in Figure 5.

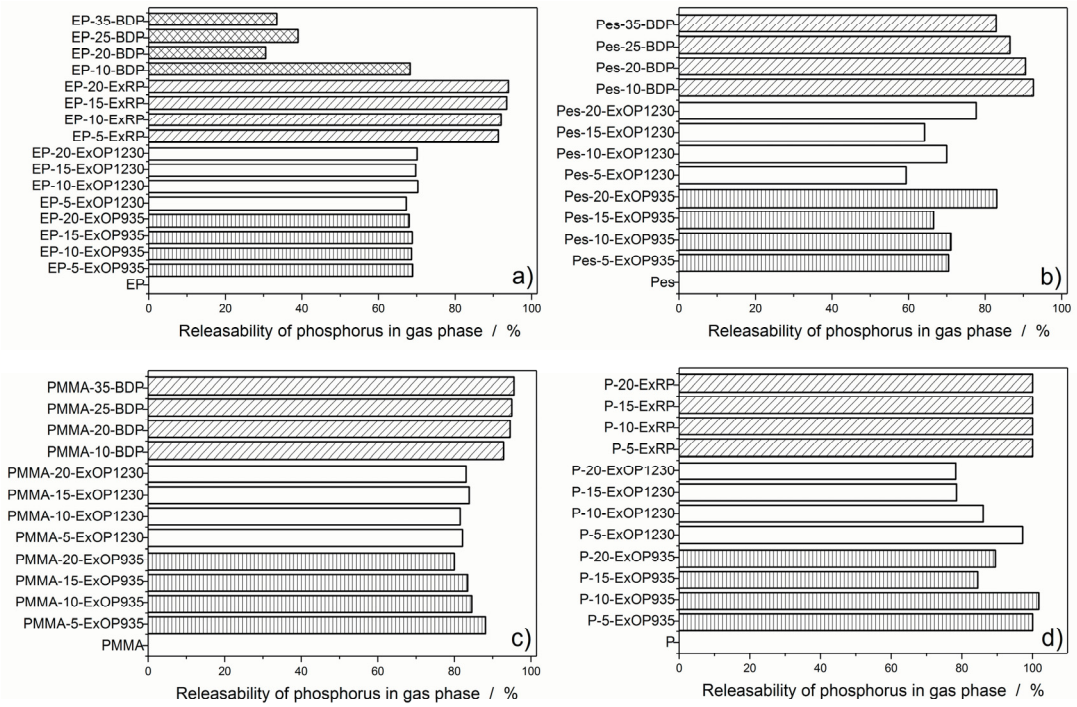

Figure 5. Bar graphs of the percentage of phosphorus released in the gas phase during combustion for epoxy resin (**a**); polyester resin (**b**); PMMA resin (**c**); and paraffin (**d**) formulations.

In the epoxy resin, there were no differences in phosphorus release between Exolit OP935 and OP1230. At any flame retardant load in the sample, around 70% of the phosphorus was released into the gas phase. Phosphorus release at 10 wt % flame retardant load was similar to that of the AlPi flame retardants at any concentration, but with increasing BDP load, this amount was significantly reduced to less than half of the phosphorus released into the gas phase. Red phosphorus released over 90% of its phosphorus into the gas phase and showed a slight increase with increasing flame retardant load (Figure 5a).

Exolit OP935 in polyester resin had a higher phosphorus release than Exolit OP1230. The highest release of phosphorus was also at the highest flame retardant load. By contrast, formulations with BDP had the highest phosphorus release at 10 wt % of BDP load, which gradually decreased to around 80% with increasing amounts of BDP (Figure 5b).

In the PMMA resin, Exolit OP935 showed the maximum phosphorus release at the lowest amount of flame retardant. This decreased with increasing flame retardant load. The phosphorus release of Exolit OP1230 was constant at around 80 to 85% at all investigated flame retardant loads. For BDP the phosphorus release was at a very high level, at around 90 to 95% with increasing load in the matrix (Figure 5c).

Exolit OP935 and OP1230 in paraffin both showed decreasing phosphorus release with increasing flame retardant load. However, this effect was more significant with Exolit OP1230. The highest phosphorus release into the gas phase was at 10 wt % of flame retardant load. Formulations with RP left no residue at all; thus, all phosphorus was released into gas phase during burning (Figure 5d). It was observed that, towards the end of the burning process, the flame turned very bright. It is assumed that the red phosphorus was burning separately, resulting in this bright flame, and thus did not take part in any pyrolysis reaction with the matrix. This is supported by monitoring the effective heat of combustion (EHC) during the test. As seen in Figure 6, the EHC is split into two areas, the first

one attributed to the burning of the paraffin matrix at around 40 MJ/kg. After reaching the PHRR at around 200 s, the EHC curve features a second, lower plateau at approximately 20 MJ/kg with a final decay, which is associated with the burning of red phosphorus. This is in analogy to the different burning phases observed for example in polymer blends [42]. Contrarily, the EHC of 20 wt % AlPi incorporated in paraffin features a constant EHC throughout the entire period of burning. This shows, that the decomposition temperatures of red phosphorus and the paraffin matrix were not overlapping and thus did not ensure an active flame retardancy.

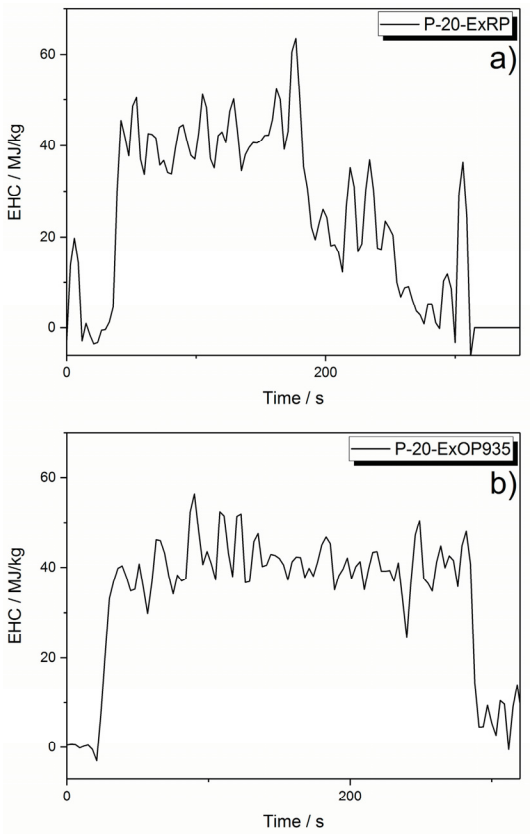

Figure 6. Effective heat of combustion: for P-20-ExRP exhibiting a two-part progression (**a**); and for P-20-ExOP935 as an example for a constant EHC (**b**).

Overall, it is demonstrated that phosphorus release is controlled by the polymer matrix, the phosphorus species itself and the concentration of phosphorus in the specimen. To learn about the way flame inhibition is influenced by the amount of phosphorus release into the gas phase, the effective heat of combustion (EHC) is plotted versus phosphorus concentration in the gas phase (Figure 7). The EHC measured by the cone calorimeter includes the effective heat of the combustion of the volatiles multiplied by the combustion efficiency of the flame, and thus is a measure for the efficiency of a flame retardant in terms of flame inhibition and gas phase activity in general.

As seen in Figure 7a especially, the curve progression of EHC levels off with increasing phosphorus content in the gas phase. The model curve in Figure 8 is proposed as a basis for the following discussion and is based on findings in previous works [31,43], in which the EHC first dwindles in a linear fashion (I), up to a certain level where the effectiveness in EHC reduction levels off (II). This effect is very prominent in epoxy resin, and less pronounced in the polyester system. The phase is described as (III) in Figure 8, which depicts an increase in EHC with even higher amounts of phosphorus in the gas phase. This converse effect occurs due to increased burning of the phosphorus species without exhibiting any flame inhibiting effect.

In epoxy resin, RP showed a higher reduction in EHC than the AlPi flame retardants Exolit OP935 and OP1230. More phosphorus was released into the gas phases, contributing strongly to EHC reduction. However, BDP displayed a similar EHC reduction while releasing less phosphorus into the gas phase, and the leveling off set in at around 15 MJ/kg. This demonstrated that not only the pure amount of phosphorus but also the nature of the phosphorus species had an influence on the flame inhibition [23]. At higher concentrations, all formulations showed a leveling off of the EHC reduction in the same range (Figure 7a). EHC was reduced by around 55–65% before an increase in phosphorus content in the gas phase ceased to have a beneficial effect.

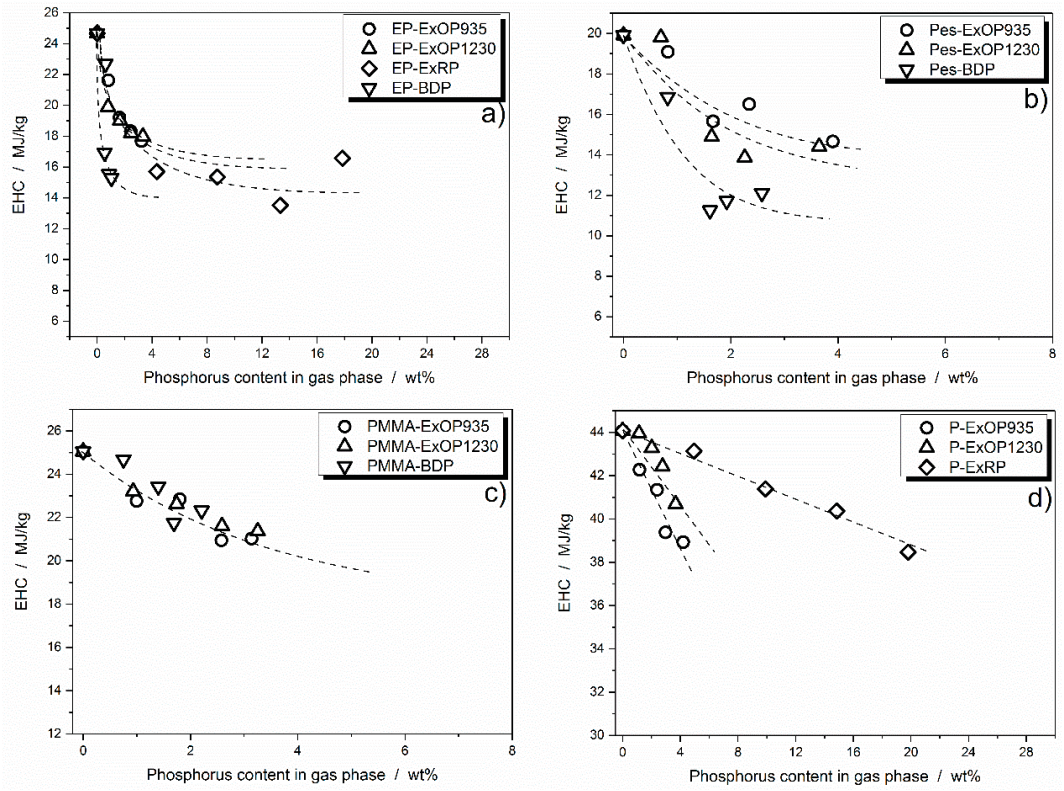

Figure 7. Effective heat of combustion plotted versus the actual amount of phosphorus released into the gas phase during combustion in: DGEBA/IPDA (**a**); polyester resin (**b**); PMMA resin (**c**); and paraffin (**d**).

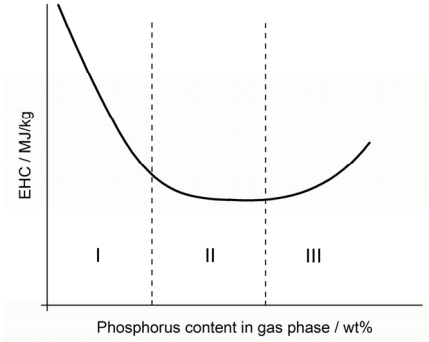

Figure 8. Proposed model for the dependency of effective heat of combustion on the phosphorus content released into the gas phase based on previous work by Brehme et al. [31]. The curve progression follows a linear decrease of EHC (I) and leads to a leveling off of EHC reduction (II). Further phosphorus increase is proposed to have a negative impact on efficiency, thus the increase in EHC (III).

In the polyester resin, BDP showed higher efficiency than Exolit OP935 and OP1230, reducing the EHC to around 11 MJ/kg (Figure 7b). Nevertheless, in this system, too, it became clear that, with increasing phosphorus concentration in the gas phase, the reduction in EHC, i.e., the effectiveness of a flame retardant in terms of gas phase activity, reached its limit. For the polyester resin, the minimum EHC was found to be at around 50 to 65% of the non-flame retarded formulation, depending on which flame retardant is used.

In contrast, formulations with PMMA resin as the polymer matrix showed no clear differences in EHC reduction behavior, and a slight tendency toward leveling off is possible (Figure 7c).

Paraffin differed from the other investigated systems in that no leveling off in EHC reduction was apparent. All three of the flame retardants used exhibited approximately linear behavior with increased concentrations in the gas phase, as also observed for the decrease in PHRR with increasing phosphorus load (Figure 7d). From these investigations, it can be concluded that, for the two systems epoxy resin and polyester resin, there is a maximum concentration of phosphorus at which flame inhibition has its highest efficiency as a mode of action. After that point, a higher load of flame retardant and thus phosphorus concentration will more likely contribute to condensed phase activity. Furthermore, the polymeric matrix in which the flame retardants are used can alter their efficiency significantly. The PMMA systems showed a slight tendency towards a non-linear EHC reduction with increasing phosphorus content and for paraffin, no tendency toward leveling off was observed. Rather, it was found that paraffin does not seem to be qualified as a suitable polymeric matrix to investigate phosphorus-based flame retardants in polyolefinic polymers.

Additionally, the effective heat of combustion depending on phosphorus content in the gas phase was checked by comparing the different polymeric matrices flame retarded with the same flame retardant. This enables to make a statement about which flame retardant is most effective in which system. Since all systems exhibit different initial values for the non-flame retarded equivalent, the EHC had to be normalized in order to compare the effectiveness. The results of the comparisons are shown in Figure 9.

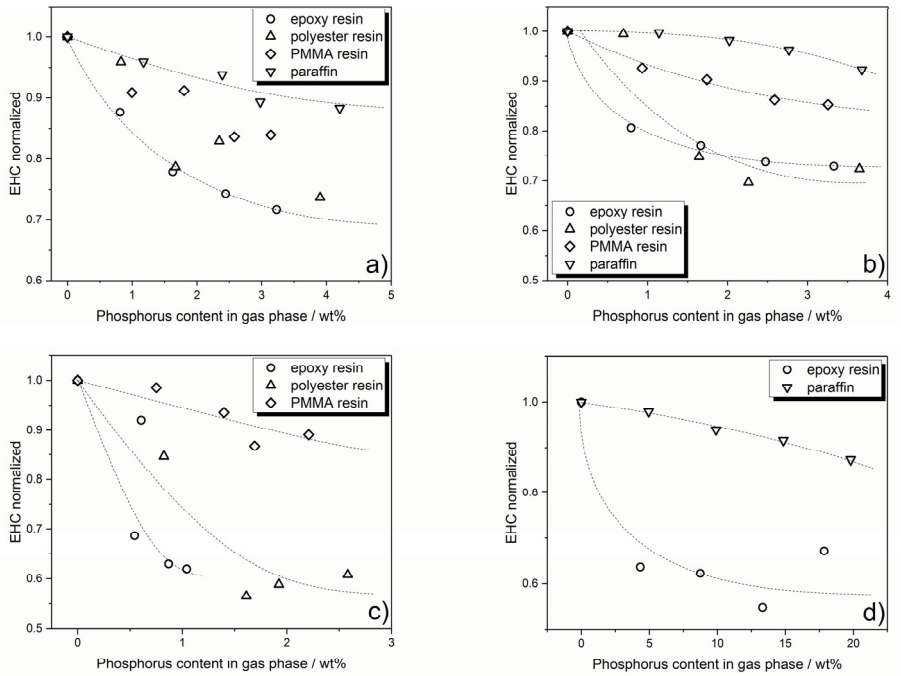

Figure 9. Effective heat of combustion versus the phosphorus content in the gas phase for the different polymeric systems flame retarded with: Exolit OP935 (**a**); Exolit OP1230 (**b**); BDP (**c**); and red phosphorus (**d**). Dotted lines are included as a guide to the eyes.

In order to compare the differences occurring with varying particle size distributions, both AlPi flame retardants Exolit OP935 and Exolit OP1230 are compared in the four different polymer matrices. Exolit OP935 is least efficient in paraffin, achieving only a reduction in EHC to 90%. In PMMA, a reduction to 85% is observed, followed by a reduction to around 75% in polyester resin. Exolit OP935 performs best in epoxy resin, when it comes to reduction in EHC.

Exolit OP1230 shows only a minor effect in paraffin, reducing the EHC to 95% at the highest loading. In PMMA resin, the efficiency is higher. The EHC is reduced up to 85%. In epoxy resin and polyester resin, Exolit OP1230 exhibits equally good EHC reduction, making both the ideal matrix for this flame retardant.

This comparison showed that there are slight differences in effectiveness depending on the polymer matrix resulting from different particle size distributions of Exolit OP935 and Exolit OP1230. Due to incorporation of BDP into the polymeric systems (Figure 9c), the EHC was reduced to around 60% in the epoxy resin at around 1 wt % of phosphorus in the gas phase. In the polyester resin, a higher phosphorus content in the gas phase was observed, reducing the EHC to around 55% at 1.5 wt % of released phosphorus. In the PMMA resin, only a reduction to around 85% was achieved.

Red phosphorus was incorporated into epoxy resin and paraffin. Both systems exhibit a totally different behavior. As shown in Figure 6, the EHC of the separately burning red phosphorus is lower than the EHC of the paraffin matrix. The mean EHC depicted here is decreasing with higher flame retardant load, because the duration of burning red phosphorus increases. It is not a result of an active flame inhibiting effect. In the epoxy system, red phosphorus shows a maximum reduction of EHC to around 55% while releasing 13 wt % of phosphorus into the gas phase.

This matrix comparison for each flame retardant showed, that the effectiveness with increasing flame retardant load and thus phosphorus content is highly dependent on the polymer matrix. All systems, except for paraffin, exhibit a more or less distinctive non-linear leveling off behavior. In addition, modifications such as the particle size distributions may play a minor role in whether a flame retardant is more effective in one or another polymeric matrix. Furthermore, paraffin was shown to be unsuitable to simulate the fire behavior of a polyolefinic polymer matrix.

3.3.3. Dependency of Condensed Phase Activity on Phosphorus Content

Phosphorus remaining in the residue after burning reacted during pyrolysis to contribute to condensed phase activity. The residue at the end of the cone calorimeter measurement is plotted versus the phosphorus content remaining in the residue in Figure 10. This plot gives information about the influence of increasing phosphorus content in the residue on residue formation.

We propose that the curves resulting from all of the measured formulations take S-shapes, or are assumed to take an S-shape, as depicted in Figure 11. This is because the buildup of a protective layer is ever more significant with increasing amounts of flame retardant, in this case phosphorus content. The point of inflection of the sigmoidal curves, described by area II in Figure 11, is considered to be the amount of phosphorus needed to induce formation of a protective layer. After this inflection point, the amount of residue flattens again and results in a continuous increase with increasing phosphorus content (Figure 11 III).

In epoxy resin, the curve of residue increase for the BDP formulations has its point of inflection at a relatively low phosphorus concentration in the residue. This means that a protective layer effect, and thus the level of decomposition, started to influence the burning behavior after the inflection point, found at around 7 wt % of phosphorus in the residue. This is in accordance with previous results, in which BDP was shown to be a good precursor for condensed phase activity [6]. Depending on the step height of the sigmoidal curve, the degree of decomposition changes, up to a point, where the material is incompletely pyrolyzed [44–46]. For BDP in epoxy resin, this step height is observed from around 5 wt % to 15 wt % of residue. For Exolit OP935 and OP1230, the highest concentration of phosphorus in the investigated samples was at around 13 wt %. Up to this point, it is observed that the slope of the curve gradually increases. It is imaginable, that with higher flame retardant load, and thus higher

concentrations of phosphorus found in the residue, the curve will exhibit a point of inflection as well, and continue as a sigmoidal curve. Red phosphorus incorporated in epoxy resin released more than 90% of phosphorus into the gas phase during burning. Nevertheless, the concentration of phosphorus in the residue increased with higher flame retardant load. Since this increase was not as significant as for the AlPi flame retardants, the point of inflection will occur at a much higher concentration of phosphorus in the residue (Figure 10a).

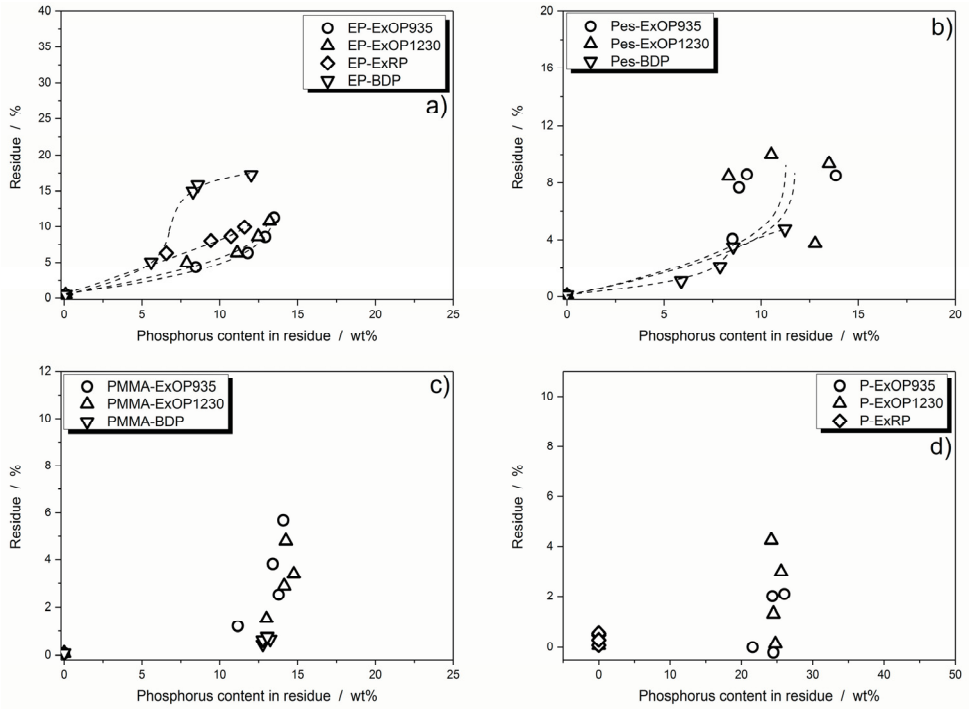

Figure 10. Residue plotted against the phosphorus content in the residue: DGEBA/IPDA (**a**); polyester (**b**); PMMA (**c**); and paraffin (**d**) system.

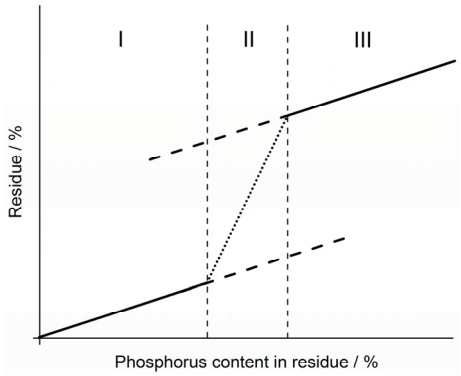

Figure 11. Proposed progression of residue formation with increasing phosphorus in the residue. The curve is divided into: an approximately linear phosphorus-residue relation (I); an area of inflection of the curve (II); and a continuous increase of residue with phosphorus content after the inflection point (III) [45].

BDP in the polyester resin had a similar effect as in the epoxy resin, exhibiting the sigmoidal curve progression at relatively low concentrations of phosphorus in the residue. However, the amount of residue was relatively low as well, with only 4 wt % at the highest phosphorus concentration measured. The area of inflection in this system lies at around 7 wt % to 9 wt % of phosphorus in the residue.

Since the height of the curve increases only slightly during the inflection, by around 2%, the change in decomposition level was much less than in the epoxy resin system. Residue formation was much higher for Exolit OP935 and OP1230, but the amount of phosphorus remaining in the residue varied moderately, as was the case for the amount of phosphorus released into the gas phase (Figure 10b).

In the PMMA resin, BDP formed almost no residue at all. Only 1 wt % was built up at around 13 wt % of phosphorus in the residue. For Exolit OP 935 and OP1230 a residue formation of 5 wt % was observed at a phosphorus concentration of around 14 wt % in the residue, which was the highest flame retardant load investigated (Figure 10c). In paraffin, the AlPi flame retardants Exolit OP935 and OP1230 exhibited a very high concentration of phosphorus in the residue. The phosphorus concentration stagnated at around 24 wt %, while the amount of residue formation increased up to 4 wt %. Formulations with red phosphorus did not form any residue from which a sample could be taken for elemental analysis. Thus, it was assumed that all of the phosphorus content was released into the gas phase (Figure 10d). In the PMMA resin and paraffin system, a trend such as the one proposed in Figure 11 was not recognizable. In fact, the phosphorus concentration in the residue was observed to be constant in the range of 0 to 20 wt % of flame retardant load. However, it is conceivable, that with even higher load, the amount of phosphorus in the residue will increase additionally to the amount of residue.

For the epoxy and polyester resin formulations, it was observed that with increasing flame retardant load, the amount of phosphorus remaining in the residue increased as well, up to a point where the concentration of phosphorus stagnated. Because of the increase in residue formation, it was assumed that this is the point where the effect of a change in decomposition level, up to the presence of incompletely pyrolyzed polymer due to a protective layer effect contributes more and more to the overall flame retardancy performance.

Residue pictures of flame retarded epoxy resin formulations reveal the influence of a protective layer on burning performance (Figure 12). Whereas residues from EP-15-ExOP935 and EP-15-ExOP1230 show beginnings of a closed residue surface that can serve as a protective layer, the residue of 15 wt % of RP in the epoxy resin is loose and brittle with no significant sign of a protective layer. In contrast to those examples, the completely closed surface of the residue of EP-25-BDP is evidence of a protective layer effect on burning performance, which prevented the complete combustion of some of the material.

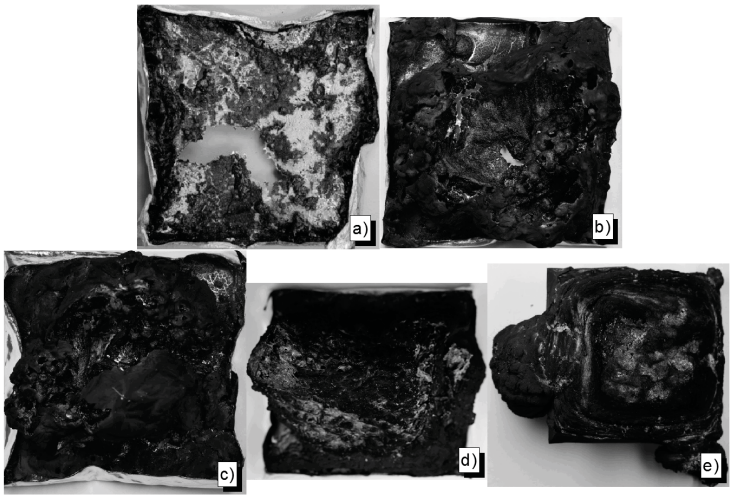

Figure 12. Residue pictures: EP (**a**); EP-15-ExOP935 (**b**); EP-15-ExOP1230 (**c**); EP-15-ExRP (**d**); and EP-25-BDP (**e**).

Exolit OP935 and OP1230 in polyester resin produced a residue that was very compact and had a closed surface, even though it was very light (Figure 13). However, due to the strong deformation during burning, the residue broke and a significant effect of a protective layer was lost. Pes-25-BDP,

on the other hand, did not produce significant residue, but only a small, but compact and shiny char of 3.5 wt %. This demonstrates that the main flame retardancy effect has to come from gas phase activity, namely flame inhibition. In the next segment, this effect is quantified, along with charring and protection layer effects.

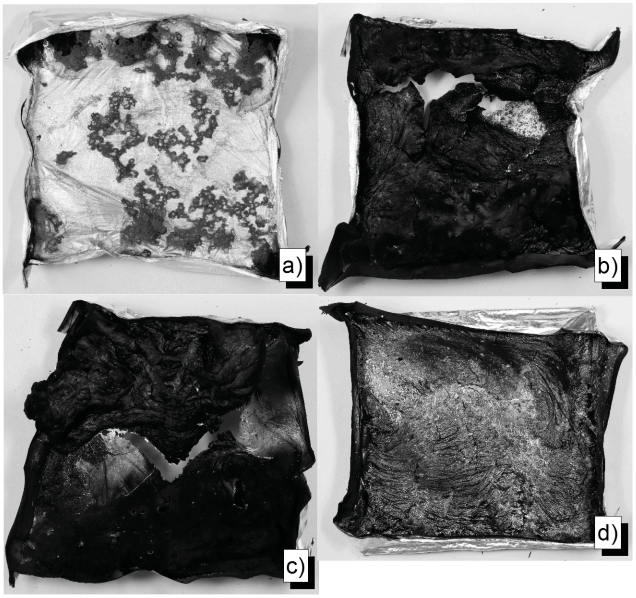

Figure 13. Residue pictures: Pes (**a**); Pes-15-ExOP935 (**b**); Pes-15-ExOP1230 (**c**); and Pes-25-BDP (**d**).

3.4. Quantification of Cone Calorimeter Results

Flame retardancy effects have been quantified for various flame retarded polymeric materials in previous works [46,47]. Equations (1) and (2) were used to calculate the theoretical values for PHRR and THE.

$$HRR \sim \chi \cdot (1 - \mu) \cdot h_c^0 \quad (1)$$

$$THE \sim \chi \cdot (1 - \mu) \cdot h_c^0 \cdot m_0 \quad (2)$$

In these equations, χ is the combustion efficiency, h_c^0 is the heat of complete combustion of the fuel gases, μ is the char yield and m_0 the mass of the specimen. The main premise is that the reduction of the effective heat of combustion $\chi \cdot h_c^0$ is influenced by flame inhibition, and this is displayed along with the effect of fuel reduction $(1 - \mu)$ and the altered density due to addition of a flame retardant. By measuring the formed residue as well as the reduction of EHC and the change in sample weight, a value for THE can be calculated. Comparing this calculated THE with the measured THE almost always shows perfect accordance. The values of measured and calculated reduction are expressed as percentages in Table 4, in which the non-flame retarded material is always set to 100%. Together with the effect of a protection layer, all three modes of action are displayed in the reduction of PHRR. The reduction in PHRR is calculated using Equation (1); however, this does not include the protective layer effect. Thus, the difference between calculated and measured PHRR reduction is a quantitative measure for a protective layer effect. To provide a better understanding of the approach, the calculation of the percentage of protective layer effect in EP-35-BDP is presented. The char yield of EP-35-BDP amounted to 17.3 wt %. Since the pure epoxy resin produced 0.5 wt % of char, the effective char yield resulting from addition of 35 wt % of BDP amounts to 16.9%. This equates to a fuel reduction $(1 - \mu)$ to 83.1% of the fuel released from pure epoxy resin. The effective heat of combustion $\chi \cdot h_c^0$ was measured in the cone calorimeter and was reduced to 62.0% of the EHC from pure epoxy resin. Multiplication of both values (0.831×0.620) leads to a calculated PHRR of 51.5% of the PHRR from pure epoxy resin. However, the measured PHRR was 33.8% of the PHRR from pure epoxy resin, which means

that this further reduction has to be the result of other effects than fuel reduction and flame inhibition, which is mainly a protective layer effect. While more than those indices play a role in reducing the PHRR, it is considered to be one approximation to monitor protective layer effect. The change in steady state burning phase would be more accurate, but hardly any of our materials exhibited such a phase. The efficiency of a protective layer is also different, when the measurement method changes, leading to deviant behaviors in the cone calorimeter, UL94 and LOI tests.

Table 4. Quantification of the reduction in THE and PHRR due to the flame retardancy modes of action: charring, gas phase action, and residual protection layer for all of the examined systems.

Material	$(1-\mu)$	$\emptyset \cdot h_c^0$	m_0	Cal. THE	THE	Cal. PHRR	PHRR	Prot. Layer
	%	%	%	%	%	%	%	%
EP	100.0	100.0	100.0	100.0	100.0	100.0	100.0	0.0
EP-5-ExOP935	96.1	87.7	103.8	87.5	87.5	84.3	87.9	−4.3
EP-10-ExOP935	94.2	77.9	98.9	72.5	72.6	73.3	52.2	28.9
EP-15-ExOP935	91.9	74.3	102.7	70.1	70.1	68.3	46.5	31.9
EP-20-ExOP935	89.2	71.7	100.7	64.4	64.4	63.9	44.0	31.2
EP-5-ExOP1230	95.6	80.6	105.5	81.3	88.2	77.1	59.5	22.8
EP-10-ExOP1230	94.1	77.1	103.6	75.2	75.2	72.5	59.0	18.6
EP-15-ExOP1230	91.8	73.8	107.0	72.5	72.5	67.8	54.2	20.0
EP-20-ExOP1230	89.7	72.9	101.7	66.5	66.5	65.4	46.3	29.2
EP-5-ExRP	94.2	63.7	104.8	62.9	62.9	60.0	51.9	13.5
EP-10-ExRP	92.4	62.3	101.0	58.1	58.1	57.5	42.3	26.5
EP-15-ExRP	91.8	54.8	103.7	52.2	52.1	50.3	36.2	27.9
EP-20-ExRP	90.5	67.2	101.4	61.7	61.6	60.8	47.0	22.7
EP-10-BDP	95.4	92.0	103.7	91.1	91.0	87.8	79.0	10.0
EP-20-BDP	85.5	68.6	102.8	60.3	60.3	58.7	37.0	36.9
EP-25-BDP	84.6	63.0	104.0	55.4	55.4	53.3	35.5	33.3
EP-35-BDP	83.1	62.0	101.4	52.3	52.3	51.5	33.8	34.4
Pes	100.0	100.0	100.0	100.0	100.0	100.0	100.0	0.0
Pes-5-ExOP935	96.0	95.9	101.3	93.3	90.7	92.1	84.0	8.8
Pes-10-ExOP935	92.4	78.7	96.6	70.2	68.4	72.7	58.9	18.9
Pes-15-ExOP935	91.6	82.9	102.3	77.6	75.2	75.9	56.8	25.2
Pes-20-ExOP935	91.5	73.6	98.9	66.6	64.6	67.4	51.2	24.0
Pes-5-ExOP1230	96.4	99.5	102.4	98.2	95.2	95.9	95.3	0.5
Pes-10-ExOP1230	91.6	74.8	102.4	70.2	73.7	68.6	42.1	38.6
Pes-15-ExOP1230	90.8	69.7	101.1	63.9	77.8	63.2	59.3	6.2
Pes-20-ExOP1230	90.1	72.4	101.3	66.1	64.9	65.3	44.8	31.3
Pes-10-BDP	99.0	84.6	100.3	84.0	82.5	83.8	71.5	14.7
Pes-20-BDP	98.0	56.5	100.3	55.5	70.5	55.4	61.8	-11.7
Pes-25-BDP	96.6	58.9	99.3	56.5	63.2	56.9	56.0	1.4
Pes-35-BDP	95.4	60.8	98.9	57.3	59.3	58.0	52.9	8.8
PMMA	100.0	100.0	100.0	100.0	100.0	100.0	100.0	0.0
PMMA-5-ExOP935	98.9	90.9	97.5	87.6	87.6	89.9	79.6	11.4
PMMA-10-ExOP935	97.6	91.2	93.4	83.1	83.1	89.0	75.4	15.2
PMMA-15-ExOP935	96.3	83.6	97.4	78.4	78.4	80.5	70.4	12.6
PMMA-20-ExOP935	94.4	83.9	96.5	76.4	76.5	79.2	58.6	26.0
PMMA-5-ExOP1230	98.6	92.6	99.4	90.8	90.7	91.3	81.1	11.1
PMMA-10-ExOP1230	97.2	90.3	95.0	83.4	83.4	87.8	68.7	21.7
PMMA-15-ExOP1230	96.7	86.3	97.1	80.9	81.0	83.4	64.5	22.6
PMMA-20-ExOP1230	95.3	85.3	95.2	77.4	77.4	81.3	59.0	27.4
PMMA-10-BDP	99.6	104.6	97.6	101.7	101.4	104.2	102.6	1.5
PMMA-20-BDP	99.5	93.5	97.9	91.1	91.1	93.0	94.6	-1.7
PMMA-25-BDP	99.4	86.8	99.2	85.6	85.6	86.3	82.6	4.3
PMMA-35-BDP	99.3	89.1	98.3	87.0	87.0	88.5	88.3	0.2
P	100.0	100.0	100.0	100.0	100.0	100.0	100.0	0.0
P-5-ExOP935	100.1	95.9	98.2	94.2	94.7	96.0	64.6	32.7
P-10-ExOP935	100.1	93.2	96.3	90.4	90.4	93.9	53.2	43.4
P-15-ExOP935	98.0	89.4	99.1	86.8	87.5	87.5	45.8	47.7
P-20-ExOP935	98.1	88.3	103.3	89.5	89.3	86.6	37.7	56.5
P-5-ExOP1230	99.9	99.7	94.5	94.1	93.9	99.7	95.9	3.8
P-10-ExOP1230	98.7	98.2	102.9	99.8	99.9	97.0	95.7	1.3
P-15-ExOP1230	97.1	96.3	98.0	91.6	93.2	93.5	85.4	8.6
P-20-ExOP1230	95.8	92.3	102.2	90.4	89.8	88.5	75.3	14.9
P-5-ExRP	99.6	97.9	103.1	100.5	101.1	97.5	98.3	-0.8
P-10-ExRP	99.5	93.9	102.5	95.8	95.7	93.5	92.8	0.7
P-15-ExRP	99.8	100.7	100.1	91.5	91.3	91.4	85.4	6.5
P-20-ExRP	99.8	87.3	104.2	90.8	90.4	87.1	84.1	3.5

For most of the specimens investigated, the effect of a protective layer was quite low. In the case of BDP in epoxy resin, the share of flame retardancy performance coming from a protective layer mode of action increased with increasing BDP load. This confirms the previous conclusions and complies with the conclusions from observing the residue pictures. Both AlPi flame retardants gave similar results in the epoxy resin, reducing the PHRR to around 45% at a flame retardant load of 20 wt %. They worked mainly in the gas phase. Red phosphorus, at a load of 20 wt %, was calculated to have the lowest protective layer effect of all tested flame retardants in epoxy resin, while achieving a satisfactory reduction in PHRR.

The ratio between PHRR reduction and the share in effectiveness that does not come from a protective layer effect was especially good in the polyester resin-BDP system. The PHRR was reduced to around 53%, and only 9% of this reduction is due to a protective layer effect. Twenty weight percent of ExOP1230 showed a slightly better PHRR reduction than ExOP935, but the share of the protective layer effect was also higher, at 39% compared to 26%.

BDP incorporated in the PMMA resin had the worst performance of any BDP formulation. At a load of 20 wt %, the PHRR was reduced to only 88%. Practically no protective layer effect could be detected. Both AlPi flame retardants showed about the same PHRR reduction at 20 wt % load, and the share in protection layer effect was similar as well.

In paraffin, a reduction of PHRR of around 64% was achieved with 20 wt % of Exolit OP935. However, 59% of the flame retardant effect was due to a protective layer. Those calculated values are not in accordance with the observations made during burning. No protective layer was formed during the forced flaming combustion tests in the cone calorimeter. Rather, the residue formed right before the flames extinguished.

According to the results depicted in Table 4, BDP and red phosphorus are the most effective flame retardants in epoxy resin. Up to a load of 25 wt %, the flame inhibition efficiency of BDP reaches its maximum. For red phosphorus, 15 wt % were concluded to be the optimal concentration in this system. In the polyester resin, Exolit OP1230 at a load of 10 to 20 wt % was most efficient. In the PMMA resin, the AlPi flame retardants showed their best performance at 20 wt %, while the incorporation of BDP did not result in satisfactory results even at high loads of 35 wt %. Differences in both tested AlPi flame retardants were most pronounced in paraffin. Twenty weight percent of Exolit OP935 in paraffin was concluded to be the best combination.

4. Conclusions

The use of easily preparable thermosets for investigating flame retardant modes of action, particularly flame inhibition in this work, was shown to be an effective method. Commercially available resins as well as paraffin were used to replace the time-consuming extrusion and injection molding of specimens. Although some flame retardants could not be implemented in certain matrices due to interferences with the curing process, much was learned from thermogravimetric analysis, infrared spectroscopy and burning behavior under forced flaming conditions. The dependence of EHC reduction and residue formation on phosphorus content in the gas phase and on residue, respectively, was revealed and investigated for each polymer matrix. Additionally, the performance in terms of EHC of a single flame retardant was compared among the different polymeric matrices. It was found that paraffin is not a suitable matrix for the rapid incorporation and investigation of modes of action of flame retardants and failed as a model for polyolefinic systems. The other polymer matrices gave great insight into the leveling off of flame inhibition efficiency of phosphorus-based flame retardants. Furthermore, the effect of particle size distribution was observed by comparing Exolit OP935 and Exolit OP1230 in epoxy resin and polyester resin, respectively. It was found that the finer grained Exolit OP935 is most effective in epoxy resin, whereas incorporation of Exolit OP1230 does not exhibit a large difference in epoxy resin and polyester resin. To investigate and explain the behavior of residue formation with increasing phosphorus content in the residue, a thesis for a crucial phosphorus concentration inducing a protective layer effect was proposed and proven in certain formulations, such

as for BDP in epoxy or polyester resin. It was proposed that, for these specific formulations, there is a critical phosphorus concentration, at which the level of degradation changes significantly, up to the retention of incompletely pyrolyzed polymer due to a protective layer. The results were quantified with simple calculations and it was shown that they are in great accordance with observed and measured outcomes. However, it has to be mentioned that flame retardant behavior and performance in a polymeric system is not easy to generalize. There are noticeable trends when it comes to the changes in effectiveness and flame retardant mode of action of varying loads of BDP in epoxy resin, for example, but they do not allow predictions of behavior for a different epoxy-based polymeric system. These systems do not give a statement about the fire behavior of any epoxy-, acrylate- or polyester-based polymer, besides the ones studied. Overall, several new relations between polymer matrix, phosphorus species, phosphorus concentration and results under forced flaming conditions were clarified.

Author Contributions: Sebastian Rabe conceptualized the working packages for this project and the scientific work. Sebastian Rabe carried out specimen preparation, experiments and data evaluation as well as the scientific discussion. Sebastian Rabe wrote this publication. Yuttapong Chuenban performed sample preparation, experiments, and data evaluation, and contributed to the interpretation of the results. Bernhard Schartel acquired the project and conceived the basic idea of the project. Bernhard Schartel supervised the work and contributed to the scientific discussion of the results and the conclusions. Bernhard Schartel collaborated on the writing of this publication.

Conflicts of Interest: The authors declare no conflict of interest.

References

1. Lyon, R.E.; Walters, R.N. Pyrolysis combustion flow calorimetry. *J. Anal. Appl. Pyrolysis* **2004**, *71*, 27–46. [CrossRef]
2. Wilkie, C.A.; Chigwada, G.; Gilman, J.W.; Lyon, R.E. High-throughput techniques for the evaluation of fire retardancy. *J. Mater. Chem.* **2006**, *16*, 2023–2029. [CrossRef]
3. Rabe, S.; Schartel, B. The Rapid Mass Calorimeter: A route to high throughput fire testing. *Fire Mater.* **2016**. [CrossRef]
4. Rabe, S.; Schartel, B. The rapid mass calorimeter: Understanding reduced-scale fire test results. *Polym. Test.* **2017**, *57*, 165–174. [CrossRef]
5. Weil, E.D.; Levchik, S.V. Flame retardants for plastics and textiles. In *Practical Applications*, 2nd ed.; Carl Hansen Verlag: Munich, Germany, 2015.
6. Levchik, S.V. A review of recent progress in phosphorus-based flame retardants. *J. Fire Sci.* **2006**, *24*, 345–364. [CrossRef]
7. Levchik, S.V.; Weil, E.D. Developments in phosphorus flame retardants. In *Advances in Fire Retardant Materials*; Horrocks, A.R., Price, D., Eds.; Woodhead Publishing Ltd.: Cambridge, UK, 2008; pp. 41–66.
8. Brauman, S.K. Phosphorus fire retardants in polymers. 1. General mode of action. *J. Fire Retard. Chem.* **1977**, *4*, 18–37.
9. Hastie, J.W. Molecular basis of flame inhibition. *J. Res. Natl. Stand. Sec. A* **1973**, *77A*, 733–754. [CrossRef]
10. Brehme, S.; Schartel, B.; Goebbels, J.; Fischer, O.; Pospiech, D.; Bykov, Y.; Döring, M. Phosphorus Polyester Versus Aluminium Phosphinate in Poly(butylene terephthalate) (PBT): Flame Retardancy Performance and Mechanisms. *Polym. Degrad. Stab.* **2011**, *96*, 875–884. [CrossRef]
11. Schartel, B. Phosphorus-based flame retardancy mechanisms—Old hat or a starting point for future development? *Materials* **2010**, *3*, 4710–4745. [CrossRef]
12. Levchick, S.V. Introduction to flame retardancy and polymer flammability. In *Flame Retardant Polymer Nanocomposites*; Morgan, A.B., Wilkie, C.A., Eds.; John Wiley & Sons: Hoboken, NJ, USA, 2007; Chapter 1; pp. 1–29.
13. Bourbigot, S.; Le Bras, M.; Duquesne, S.; Rochery, M. Recent Advances for Intumescent Polymers. *Macromol. Mater. Eng.* **2004**, *289*, 499–511. [CrossRef]
14. Camino, G.; Lomakin, S. Intumescent materials. In *Fire Retardant Materials*; Horrocks, A.R., Price, D., Eds.; Woodhead Publishing: Cambridge, UK, 2001; Chapter 10; pp. 318–336.
15. Brauman, S.K. Phosphorus fire retardance in polymers. 2. Retardant-polymer substrate interactions. *J. Fire Retard. Chem.* **1977**, *4*, 38–58.

16. Braun, U.; Schartel, B. Effect of Red Phosphorus and Melamine Polyphosphate on the Fire Behavior of HIPS. *J. Fire Sci.* **2005**, *23*, 5–30. [CrossRef]
17. Braun, U.; Schartel, B. Flame Retardancy Mechanisms of Aluminium Phosphinate in Combination with Melamine Cyanurate in Glass-Fibre.Reinforced Poly(1,4-butylene terephthalate). *Macromol. Mater. Eng.* **2008**, *293*, 206–217. [CrossRef]
18. Langfeld, K.; Wilke, A.; Sut, A.; Greiser, A.; Ulmer, B.; Andrievici, V.; Limbach, P.; Bastian, M.; Schartel, B. Halogen-free fire retardant styrene–ethylene–butylene–styrene-based thermoplastic elastomers using synergistic aluminum diethylphosphinate-based combinations. *J. Fire Sci.* **2015**, *33*, 157–177. [CrossRef]
19. Gallo, E.; Schartel, B.; Braun, U.; Russo, P.; Acierno, D. Fire Retardant Synergisms between Nanometric Fe_2O_3 and Aluminium Phosphinate in Poly(butylene terephthalate). *Polym. Adv. Technol.* **2011**, *22*, 2382–2391. [CrossRef]
20. Gallo, E.; Schartel, B.; Acierno, D.; Russo, P. Flame Retardant Biocomposites: Synergism between Phosphinate and Nanometric Metal Oxides. *Eur. Polym. J.* **2011**, *47*, 1390–1401. [CrossRef]
21. Braun, U.; Bahr, H.; Sturm, H.; Schartel, B. Flame retardancy mechanisms of metal phosphinates and metal phosphinates in combination with melamine cyanurate in glass-fiber reinforced poly(1,4-butylene terephthalate): The influence of metal cation. *Polym. Adv. Technol.* **2008**, *19*, 680–692. [CrossRef]
22. Lyons, J.W. Mechanisms of Fire Retardation with Phosphorus Compound: Some Speculations. *J. Fire Flam.* **1970**, *1*, 302–311.
23. Braun, U.; Balabanovich, A.I.; Schartel, B.; Knoll, U.; Artner, J.; Ciesielski, M.; Döring, M.; Perez, R.; Sandler, J.K.W.; Altstädt, V.; et al. Influence of the Oxidation State of Phosphorus on the Decomposition and Fire Behaviour of Flame-Retarded Epoxy Resin Composites. *Polymer* **2006**, *47*, 8495–8508. [CrossRef]
24. Hergenrother, P.M.; Thompson, C.M.; Smith, J.G., Jr.; Connell, J.W.; Hinkley, J.A.; Lyon, R.E.; Moulton, R. Flame retardant aircraft epoxy resins containing phosphorus. *Polymer* **2005**, *46*, 5012–5024. [CrossRef]
25. Perret, B.; Pawlowski, K.H.; Schartel, B. Fire Retardancy Mechanisms of Arylphosphates in Polycarbonate (PC) and PC/Acrylonitrile-Butadiene-Styrene: The Key Role of Decomposition Temperature. *J. Therm. Anal. Calorim.* **2009**, *97*, 949–958. [CrossRef]
26. Pawlowski, K.H.; Schartel, B. Flame retardancy mechanisms of triphenyl phosphate, resorcinol bis(diphenyl phosphate) and bisphenol-A bis(diphenylphosphate) in polycarbonate/acrylonitrile-butadiene-styrene blends. *Polym. Int.* **2007**, *56*, 1404–1414. [CrossRef]
27. Wawrzyn, E.; Schartel, B.; Ciesielski, M.; Kretzschmar, B.; Braun, U.; Döring, M. Are Novel Aryl Phosphates Competitors for Bisphenol A bis(diphenyl phosphate) in Halogen-free Flame-retarded Polycarbonate/Acrylonitrile-butadiene-styrene Blends? *Eur. Polym. J.* **2012**, *48*, 1561–1574. [CrossRef]
28. Schartel, B.; Kunze, R.; Neubert, D. Red phosphorus-controlled decomposition for fire retardant PA 66. *J. Appl. Polym. Sci.* **2002**, *83*, 2060–2071. [CrossRef]
29. Schartel, B.; Balabanovich, A.I.; Braun, U.; Knoll, U.; Artner, J.; Ciesielski, M.; Döring, M.; Perez, R.; Sandler, J.K.W.; Altstädt, V.; et al. Pyrolysis of epoxy resins and fire behavior of epoxy resin composites flame-retarded with 9,10-dihydro-9-oxa-10-phosphaphenanthrene-10-oxide additives. *J. Appl. Polym. Sci.* **2007**, *104*, 2260–2269. [CrossRef]
30. Schartel, B.; Perret, B.; Dittrich, B.; Ciesielski, M.; Krämer, J.; Müller, P.; Altstädt, V.; Zang, L.; Döring, M. Flame Retardancy of Polymers: The Role of Specific Reactions in the Condensed Phase. *Macromol. Mater. Eng.* **2016**, *301*, 9–35. [CrossRef]
31. Brehme, S.; Köppl, T.; Schartel, B.; Altstädt, V. Competition in aluminium phosphinate-based halogen-free flame retardancy of poly(butylene terephthalate) and its glass-fibre composites. *E-Polymers* **2014**, *14*, 193–208. [CrossRef]
32. Schartel, B.; Bartholmai, M.; Knoll, U. Some comments on the use of cone calorimeter data. *Polym. Degrad. Stab.* **2005**, *88*, 540–547. [CrossRef]
33. Liu, X.Q.; Liu, J.Y.; Sun, S.; Chen, J. A New Type of Flame Retarded Epoxy Resin Based on Metal Phosphinates. *Polym. Polym. Compos.* **2012**, *20*, 151–154.
34. Braun, U.; Schartel, B.; Fichera, M.A.; Jäger, C. Flame retardancy mechanisms of aluminium phosphinate in combination with melamine polyphosphate and zinc borate in glass-fibre reinforced polyamide 6,6. *Polym. Degrad. Stab.* **2017**, *92*, 1528–1545. [CrossRef]
35. Braun, U.; Bahr, H.; Schartel, B. Fire retardancy effect of aluminium phosphinate and melamine polyphosphate in glass fibre reinforced polyamide 6. *E-Polymers* **2010**, *10*, 443–456.

36. Seefeldt, H.; Duemichen, E.; Braun, U. Flame retardancy of glass fiber reinforced high temperature polyamide by use of aluminium diethylphosphinate: Thermal and thermo-oxidative effects. *Polym. Int.* **2013**, *62*, 1608–1616.
37. Ellis, B. *Chemistry and Technology of Epoxy Resin*; Blackie Academic & Professional: London, UK, 1993.
38. Pham, H.Q.; Marks, M.J. *Epoxy Resins*; Wiley-VCH: Weinheim, Germany, 2005.
39. Täuber, K.; Marsico, F.; Wurm, F.R.; Schartel, B. Hyperbranched poly(phosphoester)s as flame retardants for technical and high performance polymers. *Polym. Chem.* **2014**, *5*, 7042–7053. [CrossRef]
40. Sut, A.; Greiser, S.; Jäger, C.; Schartel, B. Interactions in multicomponent flame-retardant polymers: Solid-state NMR identifying the chemistry behind it. *Polym. Degrad. Stab.* **2015**, *121*, 116–125. [CrossRef]
41. Duquesne, S.; Fontaine, G.; Cérin-Delaval, O.; Gardelle, B.; Tricot, G.; Bourbigot, S. Study of the thermal degradation of an aluminium phosphinate-aluminium trihydrate combination. *Thermochim. Acta* **2013**, *551*, 175–183. [CrossRef]
42. Sonnier, R.; Viretto, A.; Dumazert, L.; Gallard, B. A method to study the two-step decomposition of binary blends in cone calorimeter. *Combust. Flame* **2016**, *169*, 1–10. [CrossRef]
43. Levchik, G.F.; Levchik, S.V.; Camino, G.; Weil, E.D. Fire retardant action of red phosphorus in Nylon 6. In *Fire Retardancy of Polymers the Use of Intumescence*; Le Bras, M., Camino, G., Bourbigot, S., Delobel, R., Eds.; The Royal Society of Chemistry: London, UK, 1998; pp. 304–315.
44. Wang, X.; Xing, W.; Feng, X.; Yu, B.; Song, L.; Hu, Y. Functionalization of graphene with grafted polyphosphamide for flame retardant epoxy composites: Synthesis, flammability and mechanism. *Polym. Chem.* **2014**, *5*, 1145–1154. [CrossRef]
45. Eckel, T. The most important flame retardant plastics. In *Plastics Flammability Handbook*; Troitzsch, J, Ed.; Hanser: Munich, Germany, 2004; pp. 158–172.
46. Brehme, S.; Köppl, T.; Schartel, B.; Fischer, O.; Altstädt, V.; Pospiech, D.; Döring, M. Phosphorus Polyester—An Alternative to Low-Molecular-Weight Flame Retardants in Poly(Butylene Terephthalate)? *Macromol. Chem. Phys.* **2012**, *213*, 2386–2397. [CrossRef]
47. Pappalardo, S.; Russo, P.; Acierno, D.; Rabe, S.; Schartel, B. The synergistic effect of organically modified sepiolite in intumescent flame retardant polypropylene. *Eur. Polym. J.* **2016**, *76*, 196–207. [CrossRef]

Summary

Due to the ever-increasing number of additives, adjuvants, synergists, and fillers, together with variations in concentration, particle size distribution and other modifications, methods for accelerated assessment of flame retarded polymeric materials are strongly needed. This work presents two novel approaches to assess the rapid screening of flame retardants in polymeric materials. Furthermore, flame retardants exhibit varying behavior in different polymer matrices and at different concentrations. The mode of action of a flame retardant ought to be quickly investigated to find the optimal conditions for the desired application. These two premises, the need for rapid flame retardant performance screening and the desire for a quick and reliable mode of action evaluation, are the foundation of the presented work.

High throughput performance screening of flame retardants in polymeric systems was realized by establishing an expedient measurement setup based on a commercially available mass loss calorimeter. The resulting rapid mass calorimeter combines the advantages of both state-of-the-art methods for this kind of assessment, namely the cone calorimeter and the pyrolysis combustion flow calorimeter. By reducing the size of a cone calorimeter specimen from ten by ten to two by two centimeters in surface area, the measurement time was drastically reduced while maintaining the possibility to assess macroscopic effects in fire behavior. The aim of this work was, besides developing a reliable screening method with the rapid mass calorimeter, to investigate the change in burning behavior with varying specimen size and to evaluate the significance of the obtained results by analyzing correlations with existing fire tests. The rapid mass calorimeter was shown to be a useful tool for the rapid screening of flame retarded polymeric materials by producing significant results while overcoming the challenge of sample size reduction.

Furthermore, a screening method for the rapid investigation of modes of action of flame retardants in polymeric systems is presented. Here, the use of easily preparable polymeric resins in the laboratory in small scale, as opposed to extrusion and injection molding, aims to shift the

bottleneck of the whole process away from sample preparation. Four different phosphorus-based flame retardants were used in four different polymeric systems at varying concentrations, providing a great data pool to investigate miscellaneous dependencies of the mode of action of a flame retardant. The role of phosphorus in these experiments was examined by measuring the amount of phosphorus which remained in the residue after burning. An interesting relationship between the amount of formed residue and the phosphorus content in the residue was found for some flame retardant – matrix – combinations. Additionally, the amount of phosphorus which was released into the gas phase during burning was calculated and the relationship between a flame inhibiting effect and phosphorus content in the gas phase was studied. For most formulations, a leveling off effect was found with increasing phosphorus concentration, hinting at a limited effectiveness of phosphorus-based flame retardants for higher concentrations in terms of gas phase activity. Quantification of the flame retardancy effects clarified the respective contributions of the modes of action to the overall performance of a flame retardant. In conclusion, this approach presented a valuable method for identifying and quantifying the main mode of action of a phosphorus-based flame retardant in a polymeric matrix.

Zusammenfassung

Aufgrund der stetig steigenden Zahl an Additiven, Hilfsmitteln, Synergisten, Füllstoffen usw., die in Konzentration, Partikelgrößenverteilung oder anderen Modfikationen variiert werden können, sind Methoden zur beschleunigten Beurteilung flammgeschützter Polymerwerkstoffe heutzutage dringend nötig. Flammschutzmittel zeigen unterschiedliches Verhalten in unterschiedlichen Polymermatrizen und variierenden Konzentrationen. Daher muss auch hier eine Methode gefunden werden, um die Wirkmechanismen eines Flammschutzmittels in Abhängigkeit der genannten Variablen zu untersuchen, um letztendlich die optimalen Bedingungen für die gewünschte Anwendung zu ermitteln. Diese beiden Ausgangspunkte, der Bedarf an einer schnellen Screeningmethode nach Flammschutzmitteleffektivität und der Wunsch nach einer schnellen Untersuchung der Wirkmechanismen von Flammschutzmitteln, sind die Grundlage der vorliegenden Arbeit.

Ein Hochdurchsatzverfahren zur Beurteilung der Effektivität von Flammschutzmitteln in Polymerwerkstoffen wurde mit Hilfe eines Messaufbaus realisiert, der auf dem kommerziell verfügbaren mass loss calorimeter basiert. Das daraus hervorgehende rapid mass calorimeter vereint die Vorteile beider heutzutage etablierter Messmethoden, namentlich cone calorimeter und pyrolysis combustion flow calorimeter. Indem die Probengröße einer cone calorimeter-Probe von zehn mal zehn mm² auf zwei mal zwei mm² in der Oberfläche reduziert wurde, konnte die benötigte Messzeit drastisch verringert werden, während die Möglichkeit zur Untersuchung makroskopischer Brandeffekte erhalten werden konnte. Neben dem Ziel, eine verlässliche und reproduzierbare Messmethode mit dem rapid mass calorimeter zu entwickeln, wurde das Brandverhalten der in der Größe reduzierten Proben im Detail analysiert. Die Aussagekraft der mit dem rapid mass calorimeter erhaltenen Resultate wurde durch Korrelationsuntersuchungen mit bereits existierenden Brandtests analysiert.

Des Weiteren wird eine Methode zur schnellen Untersuchung der Wirkungsweisen von Flammschutzmitteln in Polymerwerkstoffen vorgestellt. Dabei war es unter anderem das Ziel,

den Flaschenhals des gesamten Prozesses von der Probenherstellung wegzubewegen, indem einfach im Labormaßstab herzustellende Polymerharze verwendet werden. Vier verschiedene phosphorbasierte Flammschutzmittel wurden in vier verschiedene polymere Systeme mit variierenden Konzentrationen integriert. Diese Menge an Daten ermöglicht es, verschiedenste Abhängigkeiten der Wirkmechanismen von Flammschutzmitteln zu untersuchen. Die Rolle des in den Flammschutzmitteln enthaltenen Phosphors wurde durch Ermitteln des Phosphorgehalts im Brandrückstand untersucht. Dabei wurden für einige Flammschutzmittel - Polymerharz - Kombinationen interessante Beziehungen gefunden. Zusätzlich wurde die Menge an während des Brandes in die Gasphase austretenden Phosphors berechnet. Dies ermöglichte die Untersuchung der Flammenvergiftung in Abhängigkeit von der Phosphorkonzentration in der Gasphase. Für die meisten Formulierungen wurde dabei eine abklingende Effektivität bei höheren Konzentrationen festgestellt, was auf eine eingeschränkte Wirksamkeit hinweist. Um die Beiträge der einzelnen Flammschutzeffekte zur gesamten Leistung des Flammschutzmittels zu ermitteln, wurden die Ergebnisse quantifiziert. Alles in Allem stellt dieser Teil der vorgelegten Arbeit eine Herangehensweise dar, die es erlaubt, die wichtigsten Wirkungsweisen von Flammschutzmitteln in Polymeren auf schnellem Wege zu identifizieren und zu quantifizieren.

References

1. Alaee M, Wenning RJ. The significance of brominated flame retardants in the environment: current understanding, issues and challenges. *Chemosphere*. 2002;46:579-582.

2. de Wit CA. An overview of brominated flame retardants in the environment. *Chemosphere*. 2002:583-624.

3. Schartel B. Phosphorus-based Flame Retardancy Mechanisms - Old Hat or a Starting Point for Future Development? *Materials*. 2010;10:4710-4745.

4. Braun U, Schartel B, Fichera MA, Jäger C. Flame retardancy mechanisms of aluminium phosphinate in combination with melamine polyphosphate and zinc borate in glass-fibre reinforced polyamide 6,6. *Polymer Degradation and Stability*. 2007;8:1528-1545.

5. Levchik SV, Weil ED. A review of recent progress in phosphorus-based flame retardants. *Journal of Fire Science*. 2006;5:345-364.

6. Pawlowski KH, Schartel B. Flame retardancy mechanisms of aryl phosphates in combination with boehmite in bisphenol A polycarbonate/acrylonitrile-butadiene-styrene blends. *Polymer Degradation and Stability*. 2008;3:657-667.

7. Lewin M. Synergism and Catalysis in Flame Retardancy of polymers. *Polymers for Advanced Technologies*. 2001;12:215-222.

8. Weil ED. Synergists, adjuvants and antagonists in flame-retardant systems. In: Grand AF, Wilkie CA, eds. *Fire retardancy of polymeric materials*. Vol 1. 1st ed. New York: Marcel Dekker, Inc.; 2000.

9. Lewin M. Synergistic and catalytic effects in flame retardancy of polymeric materials - an overview. *Journal of Fire Sciences* ;1:3-19.

10. Lyon RE. Plastics and Rubber. In: Harper CA, ed. *Handbook of Building Materials for Fire Protection*. New York: McGraw-Hill; 2004.

11. Braumann SK. Phosphorus fire retardance in polymers. 2. Retardant-Polymer Substrate Interactions. *Journal of Fire Retardant Chemistry*. 1977:18-58.

12. Braun U, Balabanovich AI, Schartel B, Knoll U, Artner J. Influence of the oxidation state of phosphorus on the decomposition and fire behaviour of flame-retarded epoxy resin composites. *Polymer*. 2006;26:8495-8508.

13. Wilkie CA. How Important is Synergy? Paper presented at: 27th Annual Conference on Recent Advancs in Flame Retardancy of Polymeric Materials FLAME, 2016; Stamford, CT, USA.

14. Green J. Phosphorus-Containing Flame Retardants. In: Grand AF, Wilkie CA, eds. *Fire Retardancy of Polymeric Materials*. 1st ed. New York: Marcel Dekker, Inc.; 2000.

15. Bourbigot S, Le Bras M, Duquesne S, Rochery M. Recent Advances for Intumescent Polymers. *Macromolecular Materials and Engineering*. 2004;6:499-511.

16. Le Bras M, Camino G, Bourbigot S, Delobel R, eds. *Fire Retardancy of Polymers - The Use of Intumescence*. Vol 1. 1 ed. Cambridge: The Royal Society of Chemistry; 1998.

17. Wang Q, Shi W. Synthesis and thermal decomposition of a novel hyperbranched polyphosphonate ester used for flame retardant systems. *Polymer Degradation and Stability*. 2006;6:1289-1294.

18. Täuber K, Marsico F, Wurm FR, Schartel B. Hyperbranched poly(phosphoester)s as flame retardants for technical and high performance polymers. *Polymer Chemistry*. 2014;5:7042-7053.

19. Schartel B. Development of fire-retarded materials - Interpretation of cone calorimeter data. *Fire and Materials*. 2007;31:327-354.

20. Lyon RE, Walters R. *A Microscale Combustion Calorimeter*. Washington, DC: Federal Aviation Administration; 2002. DOT/FAA/AR-01/117.

21. Lyon RE, Walters RN. Pyrolysis combustion flow calorimetry. *Journal of Analytical and Applied Pyrolysis*. 2004;1:27-46.

22. Lyon RE, Walters RN, Inventors. Microscale combustion calorimeter. US 5981290 A. Nov. 9., 1999.

23. *Standard Test Method for Determining Flammability Characteristics of Plastics and Other Solid Materials Using Microscale Combustion Calorimetry*. West Conshohocken: ASTM; 2007. ASTM D 7307-07.

24. Zhuge J, Chen X, KS A, Manica DP. Microscale combustion calorimeter - application and limitation. *Fire and Materials*. 2016;8:987-998.

25. Schartel B, Pawlowski KH, Lyon RE. Pyrolysis combustion flow calorimeter: A tool to assess flame retarded PC/ABS materials? 2007;1:1-14.

26. Davis RD, Lyon RE, Takemori MT, Eidelman N. High Throughput Techniques for Fire Resistant Materials Development. In: Wilkie CA, Morgan AB, eds. *Fire Retardancy of Polymeric Materials*. 2nd ed. Boca Raton, Fl, USA: Tayler & Francis Group; 2009.

27. Wilkie CA, Chigwada G, Gilman JW, Lyon RE. High-throughput techniques for the evaluation of fire retardancy. 2006;21:2023-2030.

28. Plastics - Thermogravimetry (TG) of polymers - General principles. *ISO 11358:1997(E)*. 1st ed; 1997.

29. Brehme S, Köppl T, Schartel B, Altstädt V. Competition in aluminium phosphinate-based halogen-free flame retardancy of poly(butylene terephtalate) and its glass-fibre composites. *e-Polymers*. 2014;3:193-208.

30. Standard Test Method for Determining Flammability Characteristics of Plastics and Other Solid Materials Using Microscale Combustion Calorimetry. *ASTM D7309-11*. 2nd ed; 2011.

31. Plastics - Determination of burning behaviour by oxygen index - Part 2: Ambient-temperature test. *DIN EN ISO 4589-2:2006-06*. 2nd ed; 2006.

32. Reaction-to-fire tests - Heat Release, Smoke Production and Mass Loss Rate. *ISO 5660-1*. 3rd ed; 2015.

33. Babrauskas V. Development of the Cone Calorimeter - A Bench-scale Heat Release Rate Apparatus Based on Oxygen Consumption. *Fire and Materials*. 1984;2:81-95.

34. Babrauskas V, Peacock RD. Heat release rate: The single most important variable in fire hazard. *Fire Safety Journal*. 1992;3:255-272.

35. Madrigal J, Hernando C, Guijarro M, Díez C, Marino E. Evaluation of Forest Fuel Flammability and Combustion Properties with an Adapted Mass Loss Calorimeter Device. *Journal of Fire Sciences*. 2009;4:323-342.

36. Plastics - Simple Heat Release Test using a Conical Radiant Heater and a Thermopile Detector. *ISO 13927*. 1st ed; 2001.

37. Weil ED, Hirschler MM, Patel NG, Said MM, Shakir S. Oxygen Index: Correlations to Other Fire Tests. *Fire and Materials*. 1992:159-167.

38. Rychly J, Costa L. Modelling of Polymer Ignition and Burning Adopted for Cone Calorimeter Measurements: The Correlation between the Rate of Heat Release and Oxygen Index. *Fire and Materials*. 1995;19:215-220.

39. Sonnier R, Ferry L, Longuet C, et al. Combining cone calorimeter and PCFC to determine the mode of action of flame-retardant additives. *Polymers Advanced Technologies*. 2011;7:1091-1099.

Index of figures

List of publications, presentations and posters

Rabe S, Schartel B. The rapid mass calorimeter: A route to high throughput fire testing. *Fire & Materials*. 2017. DOI 10.1002/fam.2420.

Rabe S, Schartel B. The rapid mass calorimeter: Understanding reduced-scale fire test results. *Polymer Testing*. 2016;57:165-174.

Rabe S, Chuenban Y, Schartel B. Exploring the Modes of Action of Phosphorus-Based Flame Retardants in Polymeric Systems. *Materials*. 2017;10:455.

Pappalardo S, Russo P, Acierno D, Rabe S, Schartel B. The synergistic effect of organically modified sepiolite in intumescent flame retardant polypropylene. *European Polymer Journal*. 2016;76:196-207.

Rabe S, Schartel B. Poster: High-Throughput Evaluation of Flame Retarded Polymeric Materials with the Rapid Mass Calorimeter. 15th European Meeting on Fire Retardancy and Protection of Materials. 22 June – 25 June 2015, Berlin, Germany.

Rabe S, Schartel B. Presentation: Rapid mass calorimeter: High throughput fire performance screening. 27th Conference on Recent Advances in Flame Retardancy of Polymeric Materials, FLAME. 23 May – 25 May 2016, Stamford (CT), USA.